PREPARATION METHOD AND CHARACTERIZATION OF Au MODIFIED TiO_2 FOR PHOTOCATALYTIC H_2 PRODUCTION WITH SIMULATED SOLAR ENERGY

By

Karnnapus Dangsakol

A Thesis Submitted in Partial Fulfillment of the Requirements for the Degree

MASTER OF ENGINEERING

Department of Chemical Engineering

Graduate School

SILPAKORN UNIVERSITY

2011

วิธีการเตรียมและคุณลักษณะของไททาเนียมไดออกไซด์ที่ดัดแปลงด้วยทองสำหรับการผลิตไฮโดรเจนด้วยกระบวนการเร่งปฏิกิริยาด้วยแสงโดยใช้พลังงานแสงอาทิตย์จำลอง

โดย

นายกานต์นภัส แดงสกล

วิทยานิพนธ์นี้เป็นส่วนหนึ่งของการศึกษาตามหลักสูตรปริญญาวิศวกรรมศาสตรมหาบัณฑิต

สาขาวิชาวิศวกรรมเคมี

ภาควิชาวิศวกรรมเคมี

บัณฑิตวิทยาลัย มหาวิทยาลัยศิลปากร

ปีการศึกษา 2554

The Graduate School, Silpakorn University has approved and accredited the Thesis title of "Preparation method and characterization of Au modified TiO_2 for photocatalytic H_2 production with simulated solar energy" submitted by Mr. Karnnapus Dangsakol as a partial fulfillment of the requirements for the degree of Master's of Chemical Engineering.

.....
(Assistant Professor Panjai Tantatsanawong ,Ph.D.)
Dean of Graduate School
...../...../.....

The Thesis Advisor

Tarawipa Puangpetch, Ph.D.

The Thesis Examination Committee

..... Chairman
(Assistant Professor Okorn Mekasuwandumrong, D.Eng.)
...../...../.....

..... Member
(Assistant Professor Siriporn Jongpatiwut, Ph.D.)
...../...../.....

..... Member
(Suwimol Wongsakulphasatch, Ph.D.)
...../...../.....

..... Member
(Tarawipa Puangpetch, Ph.D.)
...../...../.....

53404207 : MAJOR : CHEMICAL ENGINEERING
KEY WORDS : PHOTOCATALYTIC H_2 PRODUCTION/Au MODIFIED TiO_2
KARNNAPUS DANGSAKOL : PREPARATION METHOD AND CHARACTERIZATION OF Au MODIFIED TiO_2 FOR PHOTOCATALYTIC H_2 PRODUCTION WITH SIMULATED SOLAR ENERGY. THESIS ADVISOR : TARAWIPA PAUNGPETCH, Ph.D.. 107 pp.

Photocatalytic H_2 production over TiO_2 prepared by solvothermal, sol-gel, and flame spray pyrolysis methods with Au modification were tested under simulated solar light irradiation. Due to the most suitable balance among these properties: nanocrystallite size, crystallinity, specific surface area, pore size and pore size distribution in mesoporous range, of the TiO_2 prepared by solvothermal method, it exhibited the highest photocatalytic H_2 production efficiency as compared to the TiO_2 prepared by the other methods and the commercial TiO_2 (Degussa P-25). Morover, the preparated parameters of the solvothermal method: solvent type, solvothermal temperature, Ti concentration and calcination temperature significantly affected the properties of TiO_2 based photocatalyst. In addition, Au cocatalyst modified method affected photocatalytic H_2 production. Photodeposition and doping methods provided the Au modified TiO_2 with the same photocatalytic activity. The best Au modified TiO_2 exhibited the H_2 production rate of 13,786 $\mu mol.h^{-1}.g_{cat}^{-1}$.

Department of Chemical Engineering Graduate School, Silpakorn University Academic Year 2011
Student's signature .....
Thesis Advisors' signature .....

53404207 : สาขาวิชาวิศวกรรมเคมี
คำสำคัญ : การผลิตไฮโดรเจนด้วยกระบวนการเร่งปฏิกิริยาด้วยแสง/ ไททาเนียมไดออกไซด์ที่ดัดแปลงด้วยทอง

กานต์นภัส แดงสกล : วิธีการเตรียมและคุณลักษณะของไททาเนียมไดออกไซด์ดัดแปลงด้วยทองสำหรับการผลิตไฮโดรเจนด้วยกระบวนการเร่งปฏิกิริยาด้วยแสงโดยใช้พลังงานแสงอาทิตย์จำลอง. อาจารย์ที่ปรึกษาวิทยานิพนธ์ : ดร. ธรวิภา พวงเพ็ชร. 107 หน้า.

การผลิตไฮโดรเจนด้วยกระบวนการเร่งปฏิกิริยาด้วยแสงโดยใช้พลังงานแสงอาทิตย์จำลองของไททาเนียมไดออกไซด์ที่ดัดแปลงด้วยทองโดยเตรียมด้วยวิธีโซลโวเทอร์มอล โซล-เจล และเฟรมสเปรย์ไพโรไลซิส เนื่องจากการเตรียมด้วยวิธีโซลโวเทอร์มอลทำให้ได้ไททาเนียมไดออกไซด์ที่มีความสมดุลระหว่างคุณสมบัติเหล่านี้ คือ ขนาดผลึกนาโน ความเป็นผลึก พื้นที่ผิว ขนาดรูพรุน และการกระจายตัวของขนาดรูพรุนในช่วงเมโซพอรัส จึงทำให้ได้ไททาเนียมไดออกไซด์ที่มีประสิทธิภาพในการผลิตไฮโดรเจนสูงกว่าไททาเนียมไดออกไซด์ที่เตรียมจากวิธีอื่นและไททาเนียมไดออกไซด์ทางการค้า (P-25) นอกจากนี้ยังพบอีกว่า ชนิดของตัวทำลาย อุณหภูมิในการเตรียม ความเข้มข้นของปริมาณไททาเนียมตั้งต้น และอุณหภูมิในการแคลไซน์ในการเตรียมด้วยวิธีโซลโวเทอร์มอลนั้นมีผลต่อคุณสมบัติของไททาเนียมไดออกไซด์ การเติมทองลงบนไททาเนียมไดออกไซด์ด้วยวิธีวิธีโฟโตดิโพสิชั่นและการโดปจะให้ไททาเนียมไดออกไซด์ประสิทธิภาพที่ใกล้เคียงกัน และสูงกว่าการเติมทองที่เตรียมแบบการเคลือบฝัง ไททาเนียมไดออกไซด์ที่ดัดแปลงด้วยทองที่ดีที่สุดสามารถผลิตไฮโดรเจน 13,786 ไมโครโมลต่อชั่วโมงต่อน้ำหนักตัวเร่งปฏิกิริยา

ภาควิชาวิศวกรรมเคมี บัณฑิตวิทยาลัย มหาวิทยาลัยศิลปากร ปีการศึกษา 2554
ลายมือชื่อนักศึกษา.....
ลายมือชื่ออาจารย์ที่ปรึกษาวิทยานิพนธ์ .....

ACKNOWLEDGEMENTS

The author would like to express his sincere gratitude and appreciation to his advisor, Dr. Tarawipa Puangpetch, for providing valuable advice, encouragement and beneficial discussion througout this thesis. In addition, without the supports for characterization from Dr. Supakij Suttiruengwong, Department of Materials Science and Engineering, Faculty of Engineering and Industrial Technology, Silpakorn university and Dr. Cheewita Suwanchawalit, Department of Chemistry, Faculty of Science, Silpakorn university, this research would never have been achieved.

The author also appreciates for the kind cooperation from Assistant Professor Okorn Mekasuwandumrong as the chairman, and Assistant Professor Siriporn Jongpatiwut and Dr. Suwimol Wongsakulphasatch as the members of the thesis committee.

Furthermore, the author wishes to thank the members of Department of Chemical Engineering, Faculty of Engineering and Industrial Technology, Silpakorn university, for their sincere assistance.

Finally, the auther really would like to express his sincere gratitude to his parents for their love, understanding, and support throughout his life.

TABLE OF CONTENTS

LIST OF TABLES

LIST OF FIGURES

Figures Page

Figures Page

CHAPTER 1

INTRODUCTION

Photocatalytic H_2 production from organic wastes reforming using colloidal semiconductors under sun light irradiation has received much attention because this technology can be not only the direct H_2 production but also the solution of environmental problem reduction. If the large scale hydrogen production from this technology is successfully achieved, the world will benefit from this hydrogen in the terms of energy and superior environment [1 - 8].

TiO_2 is an ideal based photocatalyst for photocatalytic H_2 production due to its suitable-potential level of the band structure, high chemical resistance, high photostability, non-toxicity and relatively low cost [9 - 14]. Particularly, nanoparticle is essential in the activity enhancement of the photocatalyst because it provides high surface area, low particle weight and fast charge-transference decreasing electron-hole recombination. Moreover, nanosize tends to increase the light-absorption, reduce the light-scattering, and well disperse in the liquid media [8, 15, 16]. Two recent methods to prepare nanoparticle are solvothermal [17 - 28] and flame spray pyrolysis methods [29 - 36] due to the good properties of the received nanoparticle as high specific surface area, high crystallinity and size homogeneity, which are considered as an important properties of the photocatalytic activity [5, 6, 27, 37]. However, different methods or different conditions can affect crystal structure, cystal defect, phase composition, surface morphology, surface chemical, etc. and hence photocatalytic activity [4, 6, 15]. So the first purpose of this work is to study the effect of preparation method on characteristic of TiO_2 to find out the suitable TiO_2 based photocatalyst for photocatalytic H_2 production. The studied method are solvothermal and flame spray pyrolysis methods comparing to sol-gel method, which is the most preparation technique for TiO_2 in the present.

The second purpose is due to the following mention. TiO_2 is well known that it has wide band gab about 3.2 eV [6], which only UV light can be utilized for H_2 production. Since the UV light only accounts for about 3% of solar radiation while the visible light contributes about 44% [4], the inability to utilize visible light of TiO_2

limits the efficiency of the solar photocatalytic H_2 production over TiO_2 based photocatalyst. So far, modification of TiO_2 for visible-driven photocatalysts is limited and H_2 production rate is still low under visible light [38 - 58], which is not satisfactory for practical application. Hence, it is needed to develop TiO_2 photocatalysts that exhibited high photocatalytic activity under visible light.

Recently, the use of gold metal as cocatalyst is an effective way to reduce the band gap energy of the wide band gap photocatalysts [33, 34, 35, 59] as it shows a characteristic surface plasmon band in the visible region due to the collective excitation of electrons in the gold nanoparticles and it can strongly attach to the based photocatalyst surface [60, 61]. Moreover, it remarkably enhances photoactivity for H_2 production [62, 63], providing H_2 evolution sites of photocatalyst with decreasing the activation energy for gas evolution and extending for lifetime of excited electron-hole by its role is electron trap because of high electronegativity (EN) and high electron affinity (EA) [63]. Besides, it is a noble metal that does not undergo corrosion under photocatalytic conditions [64] and does not promote the backward reaction between H_2 and O_2 to produce water on the gold cocatalyst when compared to platinum cocatalyst [62]. The photodeposited gold metal onto the based photocatalyst surface [65 - 68] and gold doping [30, 33, 63, 69] are interesting in TiO_2 modification more than impregnation method since it provids highly uniform**,** well dispersion, small size of nanometal and strong interaction between matal and based photocatalyst, resulting in the photocatalytic activity enhancement. However, the different modification methods bring to different characteristic of cocatalyst metal that influence photocatalytic activity, such as electrochemical properties of cocatalyst, nanometal size, amount of H_2 active site, interaction between the activesite and H_2 molecule and interaction between cocatalyst metal and based photocatalyst [65, 67]. Thereby, the second purpose of this work is to investigate the suitable modification method of gold cocatalyst on TiO_2 based photocatalyst.

Objectives of the Research

The purpose of this work are (1) to investigate the suitable preparation method for TiO_2 based photocatalysts that provided the good photocatalytic activity in H_2 production with simulated solar energy, and (2) to investigate the suitable Au cocatalyst modification method on TiO_2 base photocatalysts for photocatalytic activity enhancement.

Scope of the Research

1 Photocatalyst preparation

- Step 1, TiO_2 based photocatalyst is prepared by sol-gel, solvothermal and flame spray pyrolysis methods.

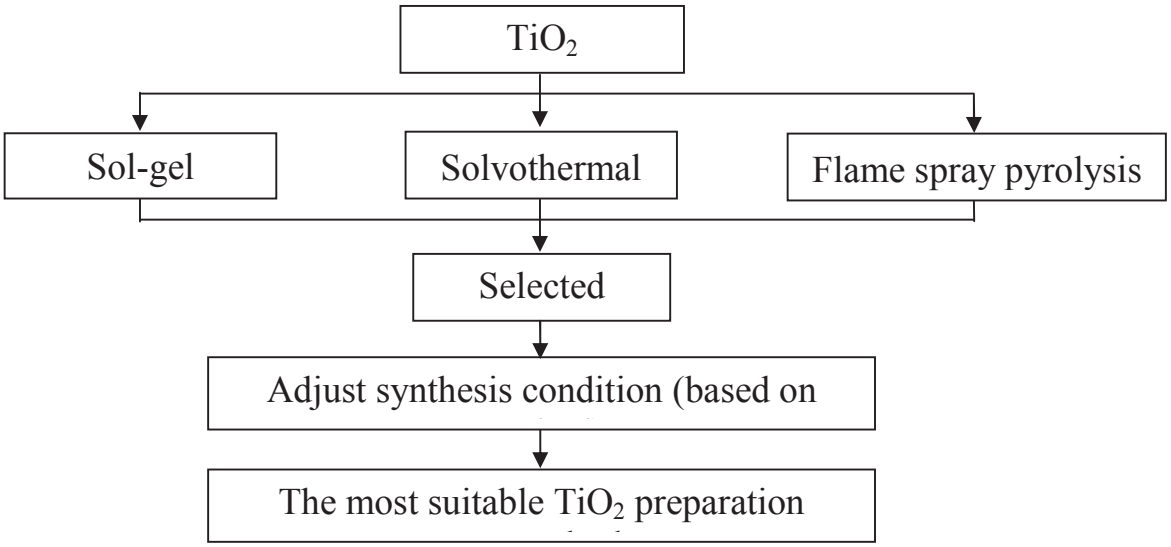

- Step 2, TiO_2 from step 1 is modified with Au cocatalyst by impregnation, photodeposition and doping methods.

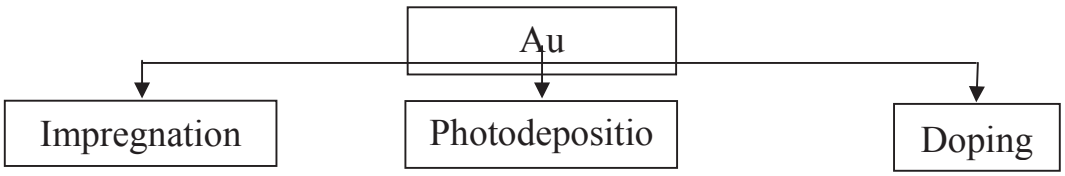

2 Photocatalyst characterization

2.1 The bulk crystal structure and chemical phase composition is determined by X-ray diffraction (XRD)

2.2 The crystallite size is observed using transmission electron microscopy (TEM).

2.3 The surface area of photocatalyst, average pore size diameter and pore size distribution are determined by physisorption of nitrogen using the BET method.

2.4 Diffuse reflection spectra are measured using UV-vis spectrophotometer to estimate bandgaps of photocatalysts.

2.5 The relative amounts of Ti^{3+} surface defects of the TiO_2 based photocatalyst samples are determined by electron spin resonance spectroscopy (ESR).

2.6 The actual amounts of Au cocatalysts are determined by inductively coupled plasma (ICP).

2.7 The relative amounts of active gold metals on the TiO_2 based photocatalyst samples are calculated from H_2 chemisorption.

3 Photocatalytic H_2 production testing

Reaction testing of Au modified TiO_2 photocatalyst is made to investigate the photocatalytic activity for H_2 production from formic acid aqueous solution under solar simulation.

CHAPTER 2

LITERATURE REVIEWS

2.1 TiO_2 preparation by solvothermal method

The solvothermal method employ chemical reactions in several organic media such as Ethanol [21,74], Buthanol[19], Ethylene glycol [19,27,72], 1,4-butandiol [17-19,22], Glycerol [19] and toluene [22,23] under self produced pressures at low temperatures (usually under 300 ^{o}C). Generally, the solvothermal treatment could be useful to control grain size, particle morphology, crystalline phase, and surface chemistry by regulating the solution composition, reaction temperature, pressure, solvent properties, additives, and ageing time. So far, there are several conditions to synthesized TiO_2 for photocatalytic application of TiO_2 as shown in Table 2.1. On the other hand, in case of reaction in 1,4-butanediol, irregular aggregates of nanometer particles are observed for all reaction holding period investigated. It was concluded that nanocrystalline anatase titania prepared in 1,4-butanediol crystallized directly from the solution. On the other hand, for the reaction in toluene, crystalline anatase titania was obtained from solid state transformation of precipitated amorphous product. This difference in morphology suggests that the colloidal stability of the precipitate in toluene is different from that in 1,4-butanediol. The results can be explained by the difference in the dielectric constant of the organic solvents, which affect the colloidal stability and morphology of the product. Moreover, M. Kang [17] found that the solvothermal TiO_2 have a higher the surface charge and the activation energies for desorption of water molecules more than sol-gel method, which were adsorbed on and in particles. From this result, it could be suggested that solvothermal TiO_2 particles were more stable in water (well dispersed in water) and very hydrophilic property.

Table 2.1 Several conditions for TiO_2 synthesis by solvothermal method

Solvent	**Temperature (°C)**	**Holding Time (h)**	**Surface area (m^2/g)**	**Crystallite size (nm)**	**Photocatalytic application**	**Ref.**
1,4-butadiol	300	5/6	122	20-50	$CHCl_3$ decomposition	17
1,4-butadiol	300	1	120	30-50	Methanol decomposition	18
Butanol	300, 350	1	96, 102	12, 7	Methyl Orange decomposition	19
1,4-butadiol	300, 350	1	99, 122	8, 6	Methyl Orange decomposition	19
Glycerol	300, 350	1	107, 111	6, 6	Methyl Orange decomposition	19
Ethylene glycol	160-180	120	120	-	H_2 production	19
Ethanol	200	10	140	-	Acetaldehyde decomposition	21
1,4-butadiol	200-300	0-4	100-150	9-15	Ethylene decomposition	22
Toluene	200-300	0-4	143-204	9-13	Ethylene decomposition	22
Toluene	300-350	0.5-8	51-126	9-15	Ethylene decomposition	23
Ethylene glycol	110	48	91	6-24	H_2 production	27
Ethanol + Acetic acid	200	8	-	15	Dye-sensitized solar cell	28
Ethylene glycol + water	180	8	484	<10	Methyl Orange decomposition	72
Ethanol	160	6	420	5	Phenol decomposition	73

2.2 TiO_2 preparation by flame spray pyrolysis method

In the past two decades flame aerosol synthesis of novel materials has experienced significant growth in both industry and academia. Recent research is focused on the development of new materials in the nanosized range to be used in various applications, such as catalysis, sensors, bio (orthopaedic, dental and nutritional products), phosphors and electroceramics (fuel cells, batteries, superconductors and ferrites) [32]. Several studies indicate that this scalable synthesis method can result in novel and metastable phases of mixed metal oxides of high purity, which may not be easy accessible by conventional wet- or solid-state processes [36,70]. Especially for photocatalytic applications this synthesis method is emerging as an attractive fast and single-step production route for high surface area materials, often with unprecedented structural and photocatalytic properties. The large variety of possible organometallic precursors especially for the liquid-fed aerosol flame synthesis makes this technique very versatile for photocatalystsynthesis. The main advantage of FSP is the formationof generally homogeneous, nanosized particles through control of the precursor solvent composition [31]. FSP has been used for the synthesis of TiO_2 photocatalysts with different condition as shown in Table 2.2. Futhermore, they exhibited high photocatalytic activity in the several photocatalytic application (Table 2.2). However, characteristic of TiO_2 synthesis by FSP depend on condition suach as type of precursor, liquid precursor flow rate, precursor concentration, type of solvent and flow rate of dispersed gas. Increasing the precursor concentration and the feed flow rate as well as the reduction of O_2 dispersing gas during the FSP synthesis would increase the supplied fuel energy to the spray and/or particle concentration so that larger particle size can be obtained, which have been reported by [30,77]. Moreover, H. Chang et al. [76] suggested mechanism for the generation and growth of TiO_2 nanoparticles in the FSP as shown in Figure 2.1, which exhibited to effect temperature in flame and concentration of precursor. Nevertheless, effect of type of organic solvent also influence to physical properties of TiO_2 nanoparticles. G.L. Chiarello et al. [33] reported that the surface area of the FSP synthesised TiO_2 photocatalysts linearly decreases with increasing the combustion heat of the organic solvent/fuel employed. With increasing the combustion heat, the

flame temperature becomes higher, with a consequent increase in the rate of particles growth. Thus, larger particles are obtained, possessing lower specific surface area. The quantitative phase analysis of samples from carboxylic acids solutions, revealed a higher rutile content with increasing the combustion enthalpy of the Ti-precursor solvents, thus for higher flame temperature. However, the use of xylene, the solvent with the highest combustion enthalpy value, led to a higher anatase content in sample. This points to a different TiO_2 formation mechanism in the flame when xylene, an apolar solvent, is used instead of carboxylic acids because, when carboxylic acids are mixed with Ti-isopropoxide the formation of titanium carboxylate and isopropanol can occur, a reaction which is not possible when the same titanium precursor is dissolved in xylene. Therefore, depending on the organic solvent/fuel, TiO_2 synthesis by FSP can start from different titanium precursors, undergoing different oxidation mechanisms in the flame. Furthermore, using xylene as solvent, the sample showed less diffuse scattering with respect to the other FSP samples, indicating a higher crystallinity and a lower content of crystal defects. This may be ascribed to the much higher flame temperature produced by the xylene fuel.

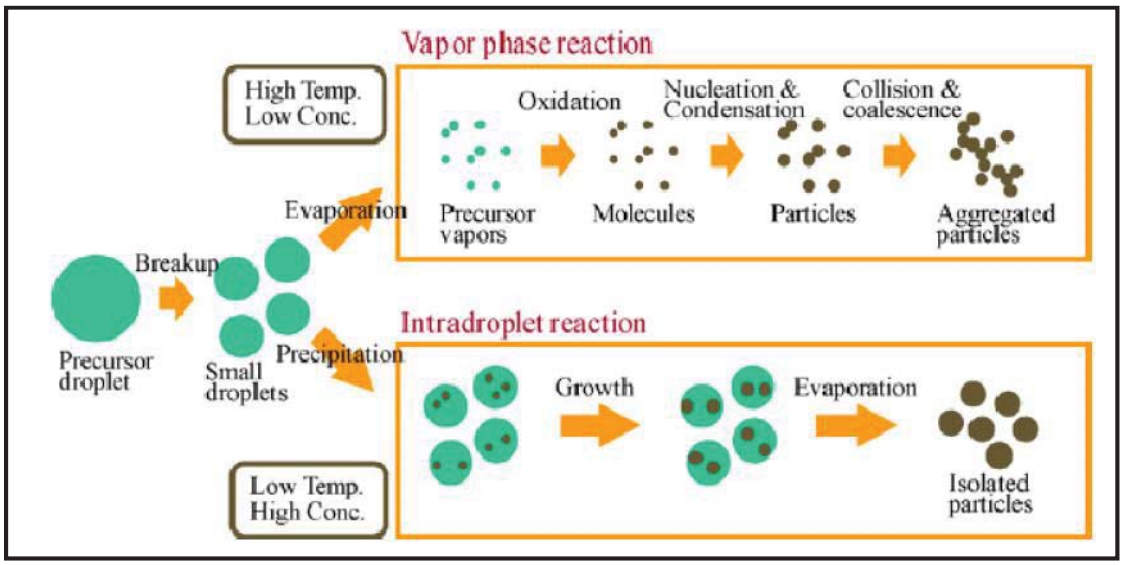

Figure 2.1 Mechanism for the generation and growth of TiO_2 nanoparticles in the FSP [76]

Table 2.2 Several conditions for TiO_2 synthesis by flame spray pyrolysis method

Solvent	Precursor concentration (mol/l)	precursor flow rate (ml/min)	O_2 dispersed flow rate (l/min)	Surface area (m^2/g)	Crystallite size (nm)	Photocatalytic application	Ref.
Xylene + Acetonitrile	0.65	3-7	5	-	7-20	Sucrose mineralisation	30
Propionic acid	0.15	3.1	6	66	5-10	H_2 production	33
Propionic acid + Methanol	0.15	3.1	6	68	-	H_2 production	33
Xylene	0.15	3.1	6	54	-	H_2 production	33
Xylene + Pyridine	0.15	3.1	6	106	-	H_2 production	33
Xylene + Acetonitrile	-	4	5	70	10-25	H_2 production	34
Xylene + Acetonitrile	0.65	5	5	89	16	Oxalic acid mineralisation	74
Xylene	0.15	3.1	6	106	5-10	H_2 production	75

2.3 Using Au cocatalyst in photocatalytic H_2 production

A. Iwase et al. [62] reported that loading of fine Au particles improved photocatalytic activity for water splitting in some titanate, niobate and tantalate photocatalysts because the fine Au particles play an important role in the creation of active sites for H_2 evolution and the enhancement of charge seperation. Moreover, the backward reaction between H_2 and O_2 to produce water on the Au cocatalyst was negligible in comparision with that on a Pt cocatalyst, which is suitable in overall water splitting. Recently, T.Puangpetch et al. [63] presented that Au loaded $SrTiO_3$ exhibited the highest photocatalytic H_2 production rate when comparison with Ag, Pt, Ni, Fe and Ce under both UV and visible irradiation. They explained that Au has higher electonegativity (EN) and electron affinity (EA) than the other metal. The higher EN of metal cacatalyt, as compared to that of the based photocatalyst, resulting

in a more easy photoexcited electron transfer from conduction band of based photocatalyst to the matel cocatalyst. Whereas, high EA promoted the stability of the photogererated electrons until the proton reduction reaction takes place on the metal cocatalyst surface. Moreover, Au has a high ionic radius, resulting in a high H-OH breaking ability. So that, water can be easily reduced to H_2 on the Au metal surface. Presently, C.G. Silva et al. [64] used Au in modification of TiO_2 for photocatalytic H_2 production under visible light. It can be prepared strongly anchored on the titania surface and it exhibits a characteristic surface plasmon band in the visible region due to the collective excitation of electrons in the gold nanoparticles. They demonstrated that gold can have an additional role as light harvester besides gas evolution center. We have found that, using excitation wave lengths corresponding to gold plasmon band, gold nanoparticles absorb photons and inject electrons into the semiconductor conduction band as shown in Figure 2.2. This photoinduced electron injection into the conduction band of as emiconductor is unusual for a metal, but the nanometric size of the gold particles and the operation of quantum size effects should be responsible for the occurrence of this mechanism. Electrons in the titania conduction band and holes in certaingold nanoparticles have adequate potential to generate hydrogen and oxygen from water, respectively. In adition, O. Rosseler et al. [59] proved that using Au modified TiO_2, it can reduces the wide band gab of TiO_2 and enhances visible light absorption as shown in Table 2.3 and Figure 2.3. Hence, Au is a promissing in modification of wide band gap photocatalyst for reponse to visible light. However, this properties depend on method in modification of Au, which have been reported by V.R. Gonzalez et al. [78].

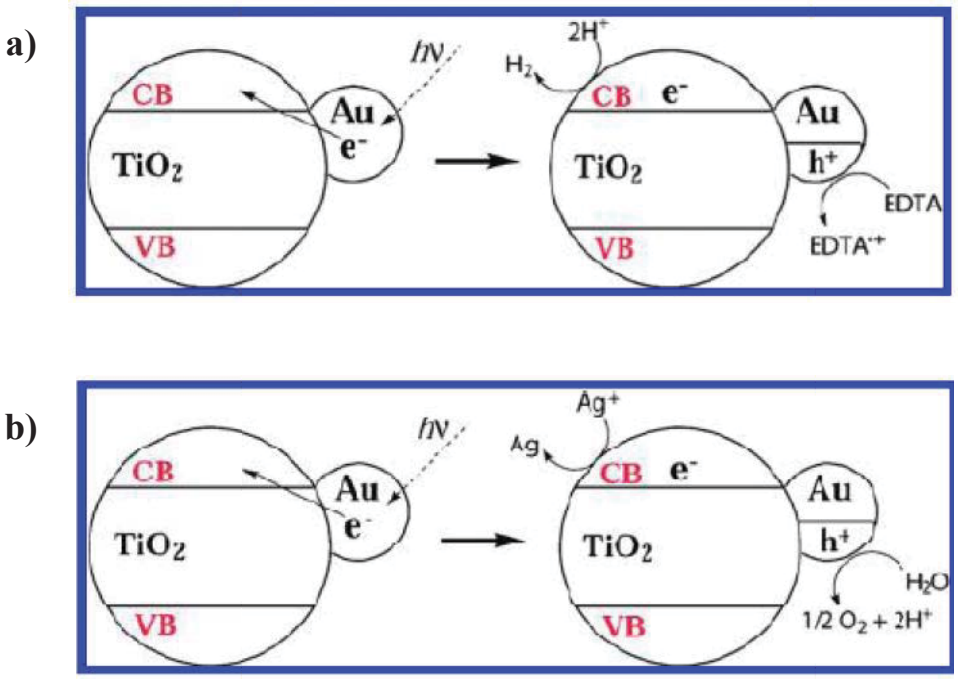

Figure 2.2 Mechanism of the photocatalytic activityof Au/TiO_2 forming H_2 (a) or O_2 (b) upon excitation of the gold surfaceplasmon band [64]

Table 2.3 Band gap and cut-off wavelength absorption of the different Au/TiO_2 photocatalyst [59]

Photocatalyst	Band gap (eV)	Maximum wavelength absorption (nm)
P25	3.23	385
TiO_2 Brij56	3.02	411
1.4 wt.% Au/P25	2.69	461
2 wt.% Au/P25	2.76	450
0.3 wt.% Au/TiO_2 Brij56	2.91	427
1.4 wt.% Au/TiO_2–Brij56	2.56	485
2 wt.% Au/TiO_2 anatase–Brij56	2.73	455

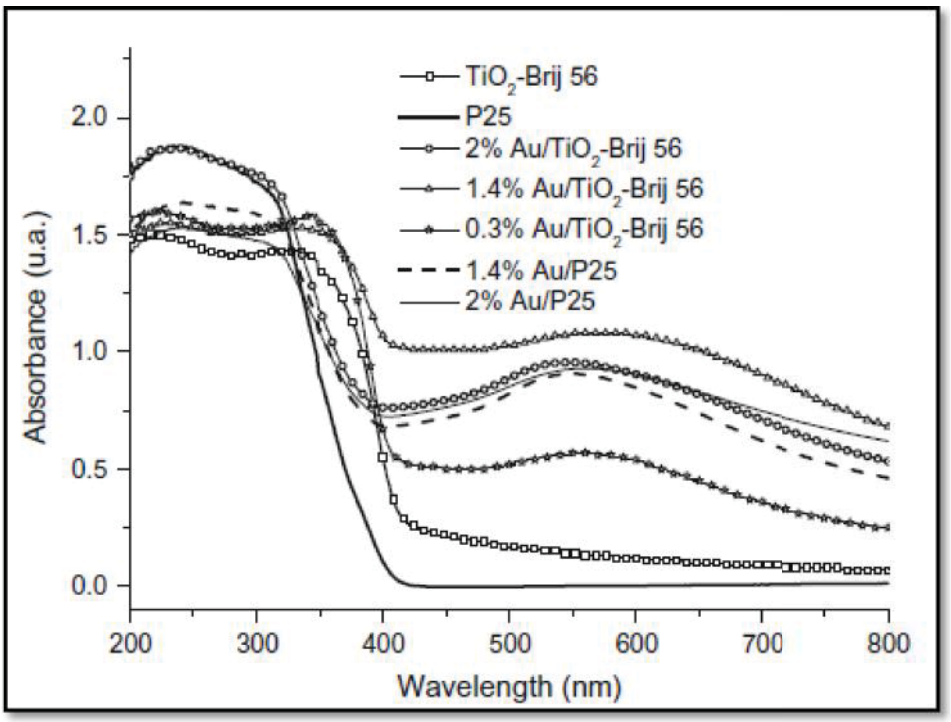

Figure 2.3 Light absorption properties of Au/TiO_2 photocatalysts [59]

2.4 Metal cocatalyst photodeposition

Metal photodeposition method is photoreducing of metal ions on based photocatalyst surface. G.R. Bamwenda et al. [65] proved that the photodeposition of Au and Pt have higher efficiency in photocatalytic H_2 production than deposition-precipitation, impregnation and physical mixing because Au and Pt particles are well dispersed on TiO_2 and small metal particles in the rang 1-10 nm for Au/TO_2 and in the rang 1-6 for Pt/TiO_2. In addition, the exposed nanosize or surface area of gold has only a small influence on the rate of hydrogen generation. However, the final Au and Pt loadings obtained during photodeposition depend on the type and concentration of hole scavengers and the illumination time and intensity. In 2005, S.C. Chan and M.A. Barteau [66] prepared Ag and Au on TiO_2 by photodeposition. They found that this technique distinguishes individual Au or Ag nanoparticles with highly uniform metal nanoparticles in the 1-2 nm size range and provides a new route to generate supported metal catalysts with highly uniform sites on the nanoscale, which is not possible with other techniques as shown in Figure 2.4.

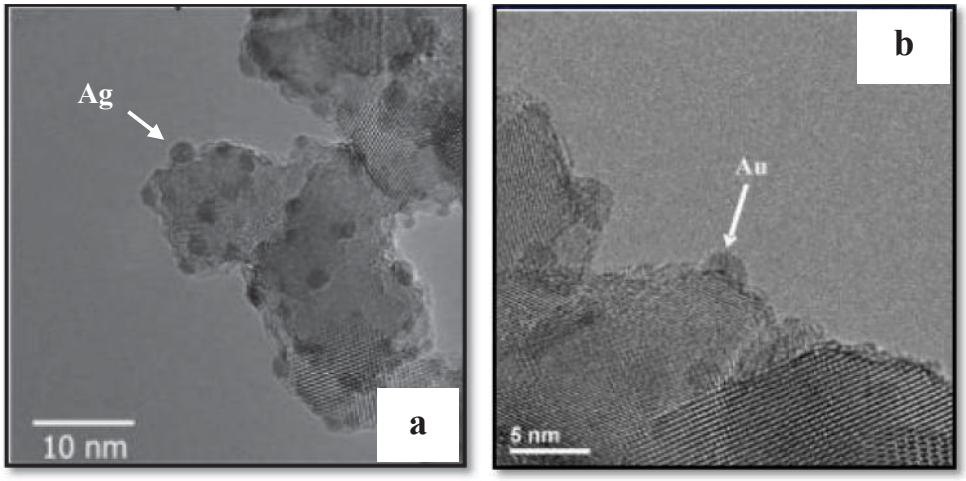

Figure 2.4 TEM image of Ag particles (a) and Au particles (b) on TiO_2 by photodeposition method [66]

M.A. Behnajady et al. [67] compared Ag loading by photodeposition and liquid impregnation methods for photodegradation of C.I. Acid Red 88. They found that the photocatalytic activity of Ag-photodeopsited TiO_2 was much higher than of silver loaded TiO_2 prepared by liquid impregnation method. The difference in the photoactivity of silver doped TiO_2 prepared with different methods can be discussed in terms of the oxidation state of silver on TiO_2 surface. During the preparation process by photodeposition method, Ag^+ ions in the suspension were reduced to Ag, but in the liquid impregnation method silver deposited at TiO_2 surface as Ag^+ ions. In the silver doped TiO_2 with liquid impregnation method (Ag^+-TiO_2), the reduction of silver ions to metallic silver consumes electrons, resulting photoactivity decreased than photodeposition. Moreover, an optimum value metal content in photodeposition method less than liquid impregnation method. So that, photodeposition method is a promissing for loading expensive metal, especially noble metal. However, photocatalyticactivity of metal cocatalyst loading on based photocatlyst by photodeposition method depend on conditions during photodeposition in preparation. M.C. Hidalgo et al. [68] reported that conditions in photodeposited reparation of Au over TiO_2 such as pH, light intensity and deposition time showed to have a high influence on the photodegradation of phenol. Conditions during the photodeposition

process, especially light intensity and deposition time, were provento have a high influence on the final properties of gold deposits. Photodeposition using illumination at high light intensity appeared as an ineffective method for obtaining Au-TiO_2 photocatalysts for photocatalytic applications as this condition lead to very large and heterogeneously distributed gold deposits. On the contrary, when the photodeposition was performed with low light intensity the resulted gold deposits were much smaller obtaining materials with improved photocatalytic activity for phenol degradation. By illumination at low light intensity, amount of gold effectively deposited, aggregation and oxidation state can be controlledby changing the deposition time, enabling a feasible method of tailoring Au-TiO_2 with the appropriate properties for a high photocatalytic activity.

2.5 Metal cocatalyst doping

Modification of cocatalyst by doping method are high efficiency in photocatalytic activity because good dispersion of doped cocatalyst in the final product is attianed and there appears to be more interaction between based photocatalyst, resulting in excellent photocatalytic performance over conventional methods [63,69]. Moreover, this method is more straightforward method for loading a metal cocatalyst than incipient wetness impregnation. T. Sreethawong et al. [69] prepared Cu, Pd and Au loaded mesoporous TiO_2 photocatalyst by this method for photocatalytic H_2 production. Their XRD and EDS results confirm that the cocatalysts were well dispersed through the mesopous TiO_2 support via the single-step sol-gel preparation. In 2010, this method was used by T. puangpetch et al. [63] in metal cocatalyst loaded mesoporous $SrTiO_3$ nanophotocatalyst for photocatalytic H_2 production. From XRD patterns, found that all the loaded metals at low loadings in the range of 0.1-1.5 wt.% do not significantly affect the crystallinity and purity of the synthesized $SrTiO_3$ photocatalysts. Besides, no crystalline phases of the metals loaded via the single-step sol-gel method were observed in the XRD patterns, probably due to their high dispersion through the mesoporous-assembled structures. XRF results confirm that this method used for loading metals is reliably effective in controlling any desired cocatalyst loading. Morover, metal loaded based photocatalyst by this method showed small nanoparticle size of metal cocatalysts, resulting in enhancing of

photocatalytic activity. For example, Au cocatalyst loaded mesoporous $SrTiO_3$ by single-step sol-gel gave small Au particle size in the rang of 10-15 nm [79] as show in Figure 2.5.

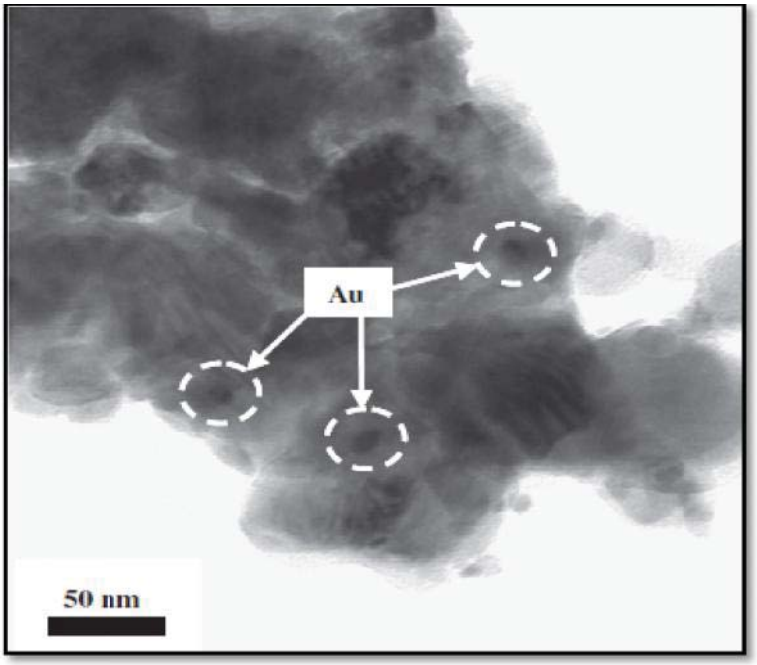

Figure 2.5 TEM image of the 1 wt.% Au-loaded mesoporous $SrTiO_3$ photocatalyst [79]

CHAPTER 3

THEORY

3.1 Basic principles of photocatalytic H_2 production

The photocatalytic decomposition of water has been extensively studied on various systems, however, sustained and overall water decomposition into H_2 and O_2 has been accomplished in only a limited number of cases. At the present stage, the quantum efficiency (QE) for overall water splitting is still very low (QE < 2%) under visible light over such a semiconductor particle photocatalyst due to water decomposition is a very difficult and complex reaction because it involves a four-photon process for O_2 evolution and a two-photon process for H_2 evolution. The various intermediate chemical steps represent a kinetic limitation that decreases the efficiency of the reaction and a rapid reverse-reaction between the produced H_2 and O_2 and/ or reaction intermediates on the surface of the small semiconductor particles. Thus, a critical problem to be resolved for an efficient up-hill reaction is to prevent such a thermodynamically-favored reverse-reaction. One possible way to overcome this problem is the use of sacrificial electron donors or hole scavengers (alcohol, organic acid, sulfide ions and others) with a high QE (>10%) because this reaction is down-hill reaction, the photo-energy absorbed by a photocatalyst induces thermodynamically favored reactions, accompanied by a large negative change in the Gibbs free energy ($\Delta G < 0$). Specially, photocatalysis of organic compounds and water into CO_2 and H_2, if organic compound is organic wastes, not only produce economic H_2 but also solution of enviromental problems. The basic principle of photocatalytic reaction for hydrogen generation using sacrificial electron donor reagents is depicted schematically in Figure 3.1

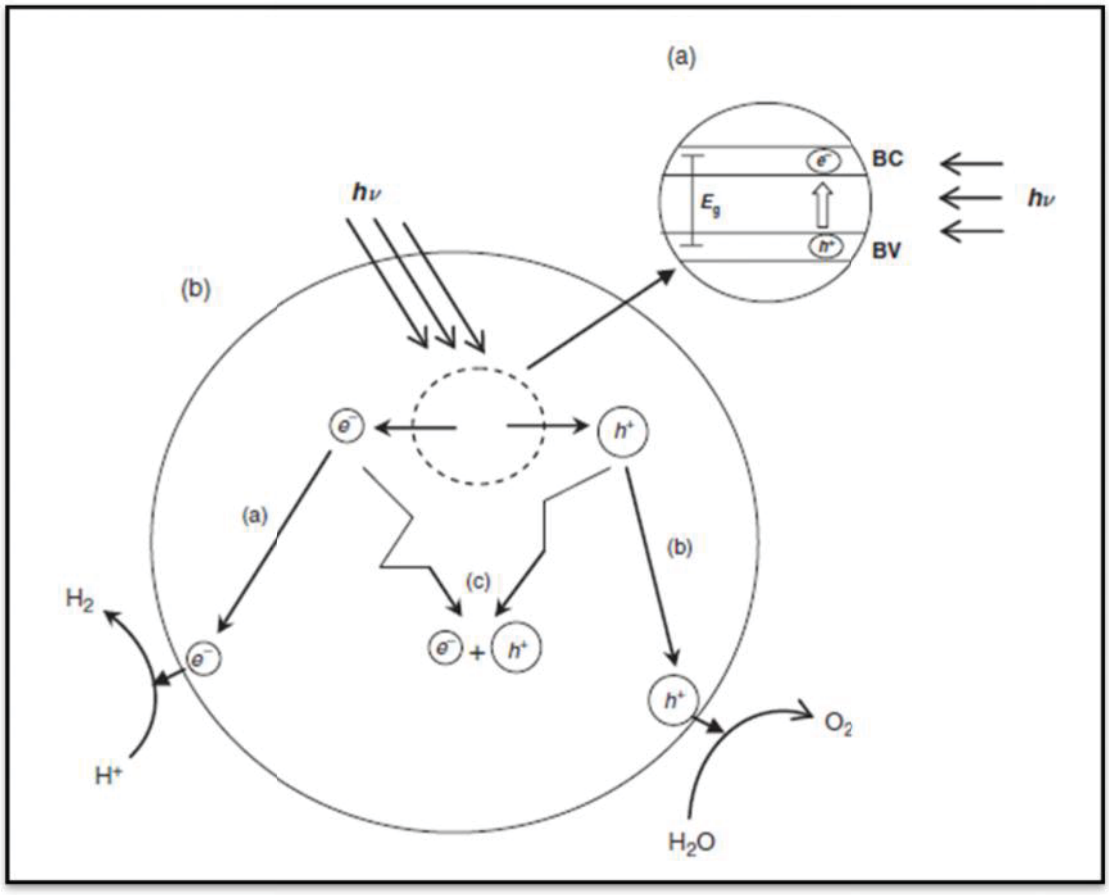

Figure 3.1 The principle of photocatalytic H_2 production in the presence of electron donor reagent: (A) photoelectronic excitation in the phototcatalyst generating electron-hole pairs and (B) processes occurring on photocatalyst particle following photoelectronic excitation [4]

When a photosemiconductor absorbs light photons with energies greater than its band gap energy (Eg). This absorption creates excited photoelectrons in the conduction band (CB) and holes in the valence band (VB) of the semiconductor, as schematically depicted in Figure 3.1(A). As indicated in Figure 3.1(B), once the photogenerated electron-hole pairs have been created in the semiconductor bulk, they must separate and migrate to the surface (paths a and b in Figure 3.1(B)) competing effectively with the

electron-hole recombination process (path c in Figure 3.1(B)) that consumes the photocharges generating heat. At the surface of the semiconductor, the photoinduced electrons and holes reduce adsorbed water to produce gaseous hydrogen and oxidize adsorbed organic as reducing reagent to produce carbondioxide by the following reactions:

$$\text{Organic compound} + H_2O \xrightarrow{h\nu,\ \text{Photocatalyst}} H_2 + CO_2 \qquad 3.1$$

Because the photogenerated holes irreversibly oxidize the reducing electron donors instead of H_2O, it enriches electrons in a photocatalyst and if the bottom of the conduction band of the photocatalyst is located at a more negative potential than the water reduction potential, this then facilitates water reduction by the photogenerated electrons in the conduction band as illustrated in Figure 3.2.

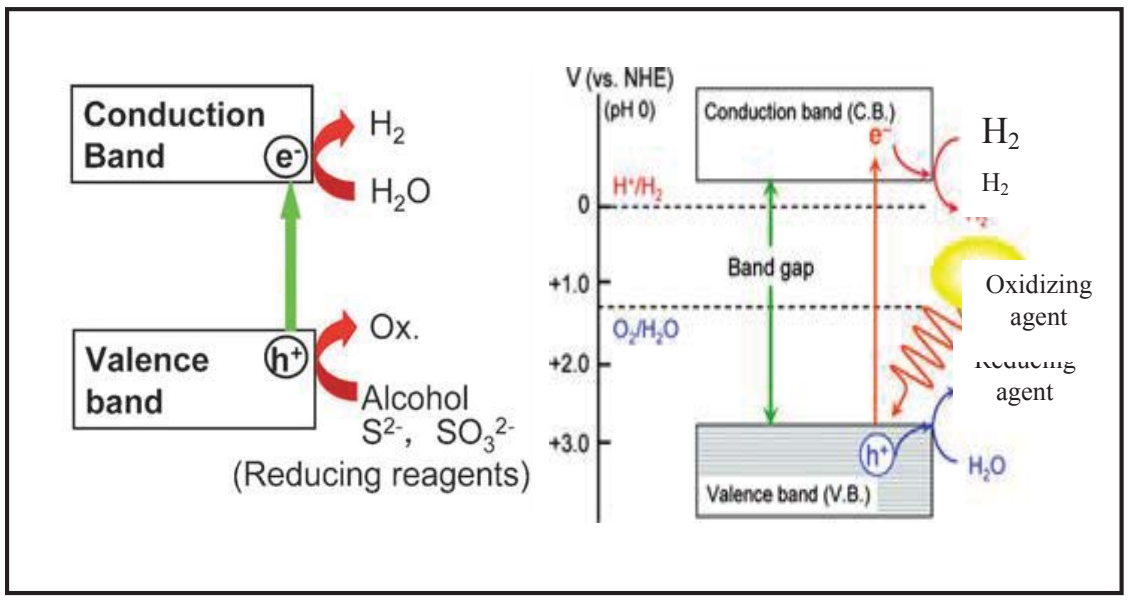

Figure 3.2 Schematic diagram of photocatalytic H_2 production in the presence of reducing reagent [5]

3.2 Evaluation of photocatalytic H_2 production

There are two apparent indicators that should be paid attention in evaluating the hydrogen generation through photocatalysis. One is photocatalytic activity and the other one is photocatalytic stability.

3.2.1 Photocatalytic activity

The efficiency of photocatalytic hydrogen generation from photocatalysis can be measured directly on the amount of hydrogen gas evolution or indirectly on the electrons transferred from semiconductor to water within a certain time period under light irradiation. Different photocatalytic setup configurations, such as inner irradiation type and top irradiation type, and light sources, such as Xe lamp and Hg lamp, are commonly used by different research groups and scientists, which may give different rates of gas evolution when exactly the same photocatalyst is used. This makes it difficult to make direct comparison across the results from different research groups and photocatalytic hydrogen generation systems. Nevertheless, it seems helpful to get approximate correlations between various results if normalize the rates of gas evolution to the amount of photocatalyst employed within a unit of time. Here, using the rate of H_2 gas evolution with units such as $\mu mol.h^{-1}$ and $\mu mol.h^{-1}.g^{-1}_{cat}$ to make the measurable comparison between different photocatalysts under similar experimental conditions. The apparent quantum yield, as an extension from the overall quantum yield in a homogeneous photochemical system, becomes important and acceptable to evaluate the photocatalytic activity for water splitting. The overall quantum yield and apparent quantum yield are defined by the following eqs 3.2, 3.3 and 3.4, respectively:

$$\text{Overall quantum yield } (\%) = \frac{\text{Number of reacted electrons}}{\text{Number of absorbed photons}} \times 100 \qquad 3.2$$

$$\text{Apparent quantum yield (QY, \%)} = \frac{\text{Number of reacted electrons}}{\text{Number of incident photons}} \times 100 \quad 3.3$$

$$\text{Or for } H_2 \text{ evolution} = \frac{2 \times \text{Number of evolved } H_2 \text{ molecules}}{\text{Number of incident photons}} \times 100 \quad 3.4$$

The apparent quantum yield is estimated to be smaller than the total quantum yield because the number of absorbed photons is usually smaller than that of incident light. In addition to the quantum yield, the solar energy conversion efficiency that is usually used for evaluation of solar cells is also sometimes reported in the literature. It is defined as following eq 3.5:

$$\text{Solar energy coversion (\%)} = \frac{\text{Output energy of } H_2 \text{ evolved}}{\text{Energy of incident solar light}} \times 100 \quad 3.5$$

3.2.2. Photocatalytic stability

As a good photocatalyst, it should have a good stability for H_2 and/or O_2 production, besides a high photocatalytic activity or quantum yield. To test the photocatalytic stability, a long-time experiment or a repeated experiment is always necessary. Photocorrosion is considered to be the main reason causing the poor stability of photocatalysts, especially the metal sulfide photocatalysts. CdS has frequently been reported to be unstable for photocatalytic H_2 evolution. S^{2-} in CdS rather than water is self-oxidized by photoinduced holes in the valence band of CdS. The photocorrosion reaction occurs as following eq 3.6:

$$CdS + 2h^+ \rightarrow Cd^{2+} + S \quad 3.6$$

Moreover, ZnO is also photocorroded under band gap excitation even if it is an oxide photocatalyst, which the reaction occurs as following eq 3.7:

$$ZnO + 2h^+ \rightarrow Zn^{2+} + 1/2O_2 \quad 3.7$$

3.2 Techniques to enhance photocatalytic H_2 production

3.3.1 Surface modification by deposition of cocatalysts

The deposition of noble metals (such as Pt, Rh, and Au) or metal oxides (such as NiO and RuO_2) onto photocatalyst surfaces is an effective way of enhancing photocatalyst activity. The cocatalyst improves the efficiency of photocatalysts, as shown in Figure 3.3, as a result of (i) the capture of CB electrons or VB holes from the photocatalysts, thereby reducing the possibility of electron-hole recombination and (ii) the transference of electrons and holes to surface water molecules, thereby reducing the activation energy for the reduction/oxidation of water. The activity of the cocatalysts is found to be strongly dependent on electrochemial preperties, cocatalyst preparation method and the quantity of cocatalysts deposited on the photocatalyst surface. When the amount exceeds a critical limit, the cocatalysts act as electron-hole recombination centers, reducing the efficiency of the host photocatalyst.

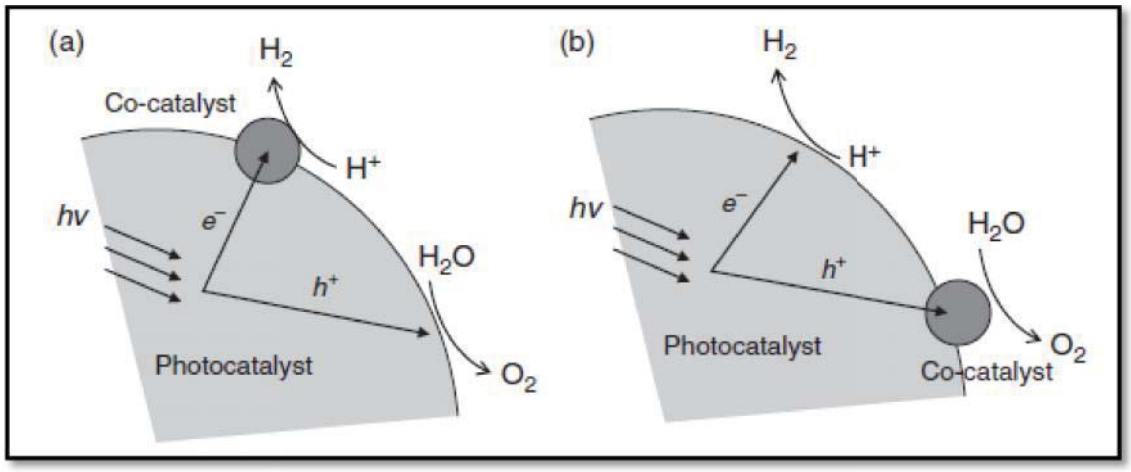

Figure 3.3 Schematic diagram of photocatalyst surface modification by the addition of cocatalyst to facilitate the hydrogen (a) or oxygen (b) evolution in water splitting [4]

3.3.2 Particle size and Surface area

General based on heterogeneous catalysis is that the efficiency of a catalytic reaction increases with increase in surface area of the catalyst. Moreover a low surface photocatalyst recombination rate is an essential condition for carriers reaching interface to react with suitable adsorbed species, whereas a large surface areas, diffusion length of charge carriers was large compared to size of the particles. For very small particles, no internal electric field is necessary to separate photogenerated electron-hole pairs. Therefore, possibility for the charge carriers to reach the interface increased as the size of particles decreased. Nanoparticle was most interested which very small particles and large surface area in order to enhance hydrogen production.

3.3.3 Organic sacrificial electron donor reagents for photocatalytic H_2 production

Organic compounds, such as alcohols (methanol, ethanol, isopropanol, etc.), organic acids (formic acid,acetic acid, etc.), and aldehydes (formaldehyde, acetaldehyde, etc.) have all been used as electron donors for photocatalytic hydrogen generation. Among them, methanol was most widely used, and the hydrogen generation process is described as eqs 3.8-3.12:

$$h^+ + H_2O \rightarrow \cdot OH + H^+ \quad 3.8$$

$$\cdot OH + CH_3OH \rightarrow \cdot CH_2OH + H_2O \quad 3.9$$

$$\cdot CH_2OH \rightarrow HCHO + H^+ + e^- \quad 3.10$$

$$2e^- + 2H_2O \rightarrow 2OH^- + H_2 \quad 3.11$$

$$\therefore \text{ Overall reaction: } CH_3OH \xrightarrow{h\nu,photocatalyst} HCHO + H_2 \qquad 3.12$$

The product, formaldehyde (HCHO), could be further oxidized to methanoic acid HCOOH and subsequently to CO_2 to gether with hydrogen generation via eqs 3.13 and 3.14:

$$HCHO + H_2O \xrightarrow{h\nu,photocatalyst} HCOOH + H_2 \qquad 3.13$$

$$HCOOH \xrightarrow{h\nu,photocatalyst} CO_2 + H_2 \qquad 3.14$$

In these photocatalytic systems, organic compounds are oxidized and decomposed by the photogenerated holes. Meanwhile, the remaining photogenerated electrons reduce water to hydrogen. Thus, it can be envisaged that a bifunctional photocatalytic system could be constructed, in which organic pollutants will be used to act as electron donors that achieve photocatalytic production of hydrogen from polluted water and simultaneous degradation of organicpollutants.

3.4 Crystal structure and properties of TiO_2 [9-11,14]

Titanium dioxide, also known as titanium (IV) oxide, with molecular weight of 79.87 $g.mol^{-1}$ is the naturally occurring oxide of titanium with the chemical formula TiO_2. Titanium dioxide is extracted from a variety of naturally occurring ores that contain ilmenite, rutile, anatase and leucoxene, which are mined from deposits throughout the world. Titanium dioxide has a wide range of applications. It is used mostly as a pigment in paints, sunscreens, ointments, and toothpaste since its commercial production in the early twentieth century. Titanium dioxide pigments are inorganic chemical products used for imparting whiteness, brightness and opacity to adiverse range of applications and end-use markets, including coatings, plastics, paper and other industrial and consumer products. TiO_2 is considered a "quality-of-life" product with demand affected by gross domestic product in various regions of the world. TiO_2 as a pigment derives value from its whitening properties and opacifying ability (commonly referred to as hiding power). As a result of TiO_2's high refractive

index rating, it can provide more hiding power than any other commercially available white pigment.

Crystals of titanium dioxide can exist in one of the three crystalline forms: rutile, anatase or brookite and they have different properties as shown in Table 3.1. In their structures, the basic building block consists of a titanium atom surrounded by six oxygen atoms in a more or less distorted octahedral configuration. In all the three TiO_2 structures, the stacking of the octahedra results in three fold coordinated oxygen atoms. The fundamental structural unit in these three TiO_2 crystals forms from TiO_6 octahedron units and has different modes of arrangement and links as presented in Figure 3.4. In the rutile form, TiO_6 octahedra link by sharing an edge along the c-axis to formchains. These chains are then interlinked by sharing corner oxygen atoms to form a three-dimensional framework. Conversely in anatase, the three-dimensional framework is formed only by edge-shared bonding among TiO_6 octahedrons. It means that octahedral in anatase share four edges and are arranged in zigzag chains along. In brookite, the octahedra share both edges and corners, formingan orthorhombic structure. In coming up with these crystal structures and to estimate thecrystal grain size of anatase, rutile and brookite the X-ray diffraction (XRD) experimental method is used. Anatase peaks in X-raydiffraction are occurred at $\theta = 12.65^o$, 18.9^o, and 24.054^o, the rutile peaks are found at $\theta = 13.75^o$, 18.1^o, and 27.2^o while brookite peaks are encountered at $\theta = 12.65^o$, 12.85^o, 15.4^o, and 18.1^o. θ represents the X-ray diffraction angle.

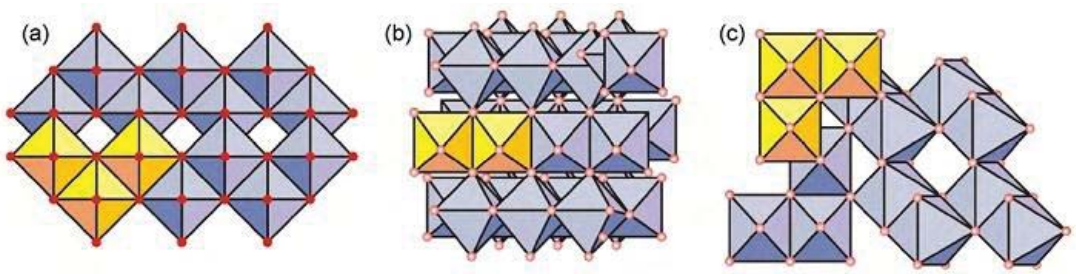

Figure 3.4 Crystalline structure of: (A) anatase, (B) brookite and (C) rutile [14]

Crystal structure	System	Space group	Lattice constants (nm)			
			a	*b*	*c*	*c*/*a*
Rutile	Tetragonal	D_{4h}^{14}-$P4_2/mmm$	0.4584	–	0.2953	0.644
Anatase	Tetragonal	D_{4h}^{19}-$I4_1/amd$	0.3733	–	0.937	2.51
Brookite	Rhombohedral	D_{2h}^{15}-Pbca	0.5436	0.9166	–	0.944
Density (kg/m^3)						
Rutile	4240					
Anatase	3830					
Brookite	4170					
Dielectric properties	Frequency (Hz)	Temperature (K)	Dielectric constant			
Rutile, perpendicular to optical *c*-axis	10^8	290–295	86			
Rutile, parallel to optical *c*-axis	–	290–295	170			
Rutile, perpendicular to optical *c*-axis	10^4	298	160			
Rutile, along *c*-axis	10^7	303	100			
Anatase, average	10^4	298	55			
Band gap (eV)						
Rutile	3.05					
Anatase	3.26					
Refractive index	n_g	n_p				
Rutile	2.9467	2.6506				
Anatase	2.5688	2.6584				
Brookite	2.809	2.677				

Table 3.1 Some bulk properties of the three main polymorphs of TiO_2 (anatase, rutile, and brookite) [9]

Thermodynamic calculations based on calorimetric data predict that rutile is the stablest phase at all temperatures and pressures up to 60 kbar. The small differences inthe Gibbs free energy (4–20 kJ/mole) between the three phases suggest that themetastable polymorphs are almost as stable as rutile at normal pressures and temperatures. Particle size experiments affirm that the relative phase stability may reverse when particle sizes decrease to sufficiently low values due to surface-energy

effects (surface free energy and surface stress, which depend on particle size). If the particle sizes of the three crystalline phases are equal, anatase is most thermodynamically stable at sizes less than 11 nm, brookite is most stable between 11and 35 nm, and rutile is most stable at sizes greater than 35 nm. The enthalpy of the anatase → rutile phase transformation is low. A survey ofthe literature reveals widespread disagreement, with values ranging from -1.3 to -6.0 ± 0.8 kJ/mol. Kinetically, anatase is stable, i.e., its transformationinto rutile at room temperature is so slow that the transformation practically does not occur. At macroscopic scale, the transformation reaches a measurable speedfor bulk TiO_2 at T > 600 ^oC. During the transformation, anatasepseu-do closed-packed planes of oxygen are retained as rutile closed-packed planes and a co-operative rearrangement of titanium and oxygen ions occurs within this configuration. The proposed mechanism implies at least spatial disturbance ofthe oxygen ion framework and a minimum breaking of Ti-O bonds as aresult of surface nucleation and growth. The nucleation process is very much affected by the interfacial contact in nanocrystalline solids, and once initiated, it quickly spreads out and grain growth occurs. The monotropic anatase→rutile conversion has been studied for both mechanistic and application-driven reasons, because the TiO_2 phase (i.e.,anatase or rutile) is one of the most critical parameters determining the use as aphotocatalyst, catalyst, or as ceramic membrane material. This transformation, achieved by increased temperature or pressure.

One of the important properties of the inorganic solid TiO_2 nanomaterials is its photocatalytic activity, which are largely used as a photocatalyst owing to its beneficial characteristics which include high photocatalytic efficiency, physical and chemical stability, low cost and low toxicity. Moreover, TiO_2 has suitable redox potential for photocatalytic H_2 production or organic decomposition as shown in Figure 3.5, the redoxpotential for photogenerated holes is +2.53V versus the standard hydrogen electrode (SHE) in pH 7 aqueous solution. After reaction with water, these holes can produce hydroxyl radicals, whose redox potentialis only slightly decreased and is in fact still more positive than that for ozone. The redox potential for conduction

band electronsis −0.52 V, which is negative enough to reduce dioxygen to superoxide or water to hydrogen. In addition to the wide energy band gap, TiO_2 exhibits many other interesting properties, such as transparency to visible light, high refractive index and a low absorption coefficient. Anatase and rutile, the two principal polymorphs of TiO_2, are associated with energy band gap energies of 3.2 and 3.1 eV, respectively. It has been pointed out that the photodegradation reaction rate is much more rapid over anatase than in the case of rutile. This reactionrate is mainly affected by the crystalline state and textural properties such as surface area and particle size of TiO_2 powder. However,these factors often vary in opposite ways, since a high degree of crystallinity is generally achieved through a high temperature thermal treatment leading to a reduction in the surface area. Thus, optimal conditions for the synthesis TiO_2 nanomaterials have been sought to obtain materials of high photoactivity. Since photocatalytic reactions are generally studied in aqueous suspensions, problems arise from the formation of hard agglomerates throughthe diffusion of reactants and products as well as light absorption. The crystal structure of TiO_2 greatly affects its photocatalytic activity. Amorphous TiO_2 seldom displays photocatalytic activity due to the presence of nonbridging oxygen atoms in the bulk TiO_2, whose Ti-O atomic arrangement defects could act as the recombination centers of the photogenerated electron–hole pairs. The photocatalytic performance of TiO_2 depends not only onits bulk energy band structure but also, to a large extent, on its surface properties. The larger the surface area per mass, the higher the photocatalytic activity. So that, development of preparation method to obtain high both specific surface area and crystallinity is necessary for high photocatalytic activity.

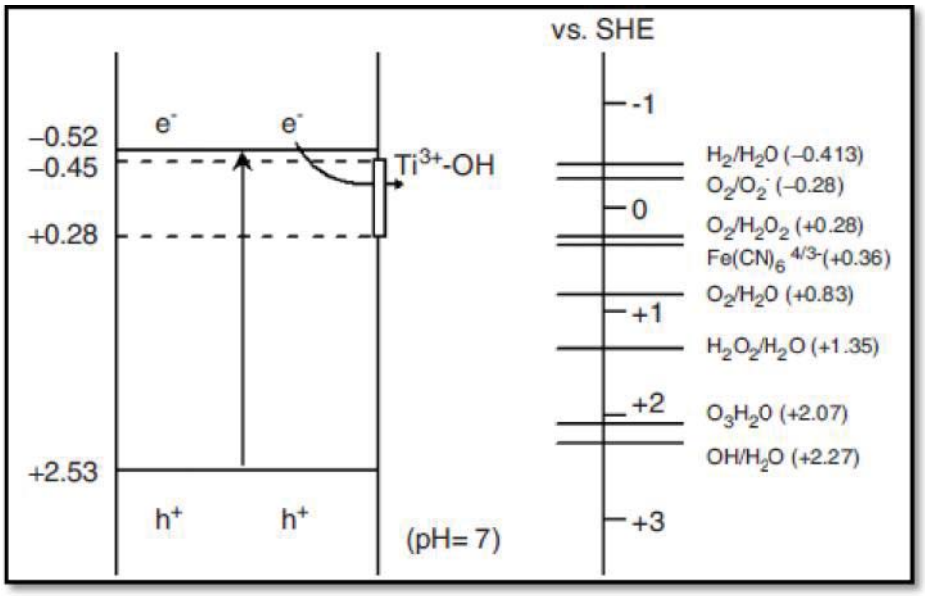

Figure 3.5 Schematic diagram showing the potentials for various redox processes occurring on the TiO_2 surface at pH 7 [10]

3.5 Flame spray pyrolysis [31,32,36,70]

Flame aerosol synthesis of catalytically active nanoparticles can give access to novel structures and materials with closely controlled characteristics such as particle size, Crystal stucture, morphology, shape and phase composition, that are not available through conventional techniques. Today, mostly wet-phase techniques are used for the industrial manufacturing of catalysts: incipient wetness impregnation, sol-gel, precipitation, grafting and solid-state reactions, just to name a few, are batch processes requiring several after-treatment steps, such as filtration, drying and calcination. Figure 3.6 shows a schematic of wet and flame processes for the synthesis of Pt/Al_2O_3 catalysts. Morover, flame technology is a scalable, continuous and well-established method for the production of nanoparticles in large quantities. For decades it has been used for the large-scale manufacture of simple commodities, such as carbon black, pigmentary titania, wave guide preforms, fumed silica and alumina. In presently, depending on the precursor state (aqueous-based, solventbased,vapour) and combustion conditions, flame aerosol syntheses fall into three general categories: (a)

vapour-fedaerosol flame synthesis (VAFS) where a metal precursor is supplied in the form of vapour, (b) flame-assisted spray pyrolysis (FASP) where precursor is supplied in the state of low combustion enthalpy solution (<50% of total combustion energy) usually in aqueous solvent, and because of this, its combustion needs to be assisted by an external hydrogen or hydrocarbon flame and (c) flame spray pyrolysis (FSP) where the precursor is also in liquid form, but with significantly higher combustion enthalpy (>50% of total energy of combustion), usually in an organic solvent. FSP is the youngest of the three processes, has important technological elements such as self sustaining flame, usage of liquid feeds and less volatile precursors, proven scalability, high temperature flames and large temperature gradients. It is also themost heavily explored in recent years for the production of complex and functional nanomaterials. Some of the most notable applications are in the areas of catalysis, optics and photonics, sensors, health care, magnetic materials, electroceramicsfor fuel cells and composite materials. A key feature in the use of FSP as a convenient tool in synthesising these nanomaterials is the ability to up scale its production, while closely preserving its tailored properties.

In the FSP process, the metal precursor is a combustible liquid that is sprayed and ignited, resulting in produce nanoparticles. The organic precursor solution is dispersed by gas (O_2 or air) convection through a nozzle forming a fine spray which is ignited as show in Figure 3.7.

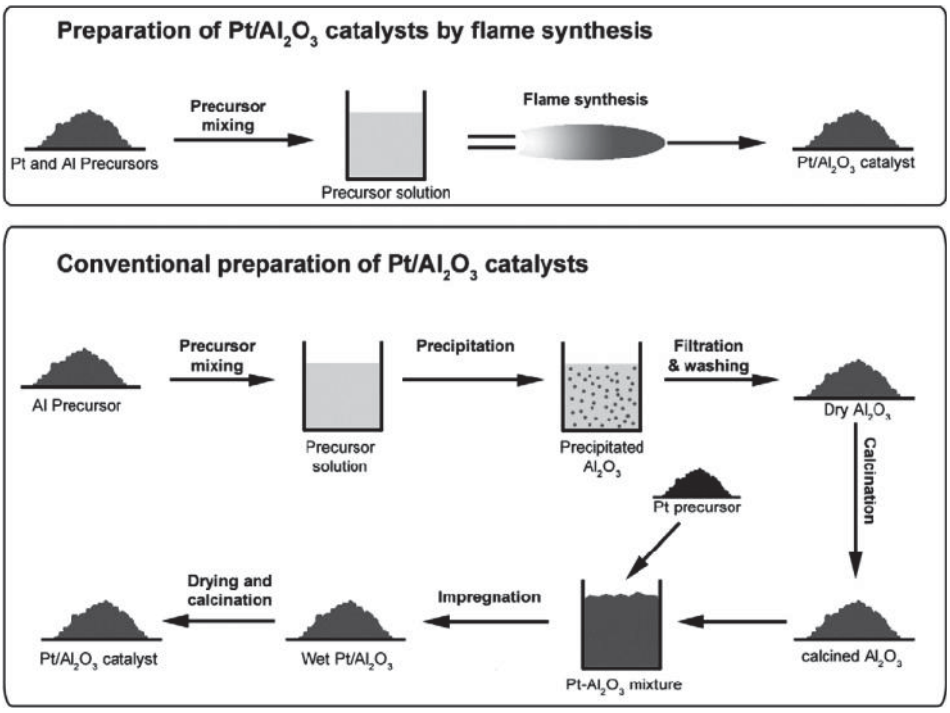

Figure 3.6 Comparison of conventional wet-phase and flame methods for the synthesis of Pt/Al_2O_3 catalyst [31]

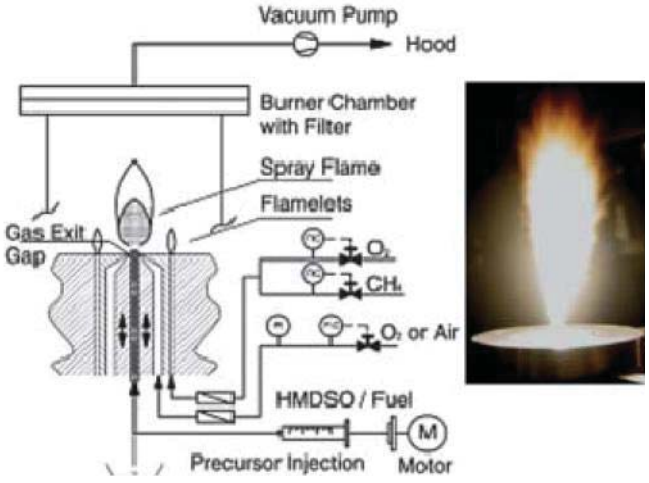

Figure 3.7 Schematic of configurations used for the synthesis of catalysts by FSP [36]

The metal precursors evaporate in this spray flame and are combusted. Particles are then formed by nucleation from the gas phase. The process featuresshort residence times (a few milliseconds) and high maximum process temperatures (up to 3000 K). Afterwards, mention the different categories of particle configurations that may form in the gas-to-particle route in FSP. These particles form in sequential stages of: (1) precursor spray evaporation/decomposition forming metal vapor; (2) nucleation as a result of super saturation; (3) growth by coalescence and sintering; and (4) particles aggregation (forming hard agglomerates by chemicalbonds) and agglomeration (forming soft agglomerates by mainlyphysical bonds) as shown in Figure 3.8. Futhermore, Figure 3.9 shows the different synthesis parameters influencing the particle formation and thus the final characteristics of the material.

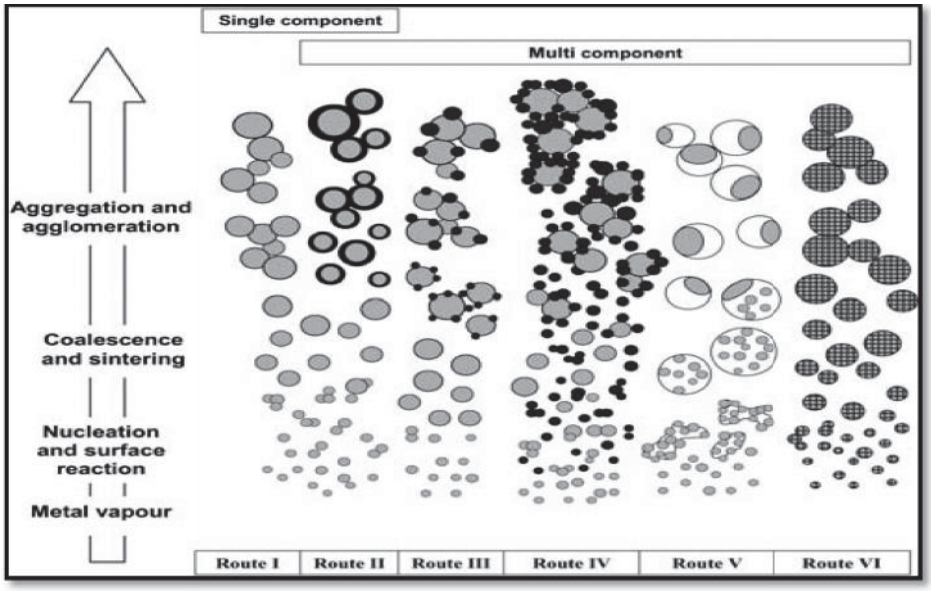

Figure 3.8 The formation of different particle configurations via the gas-to-particlemechanism for single and multi-component systems in FSP process [36]

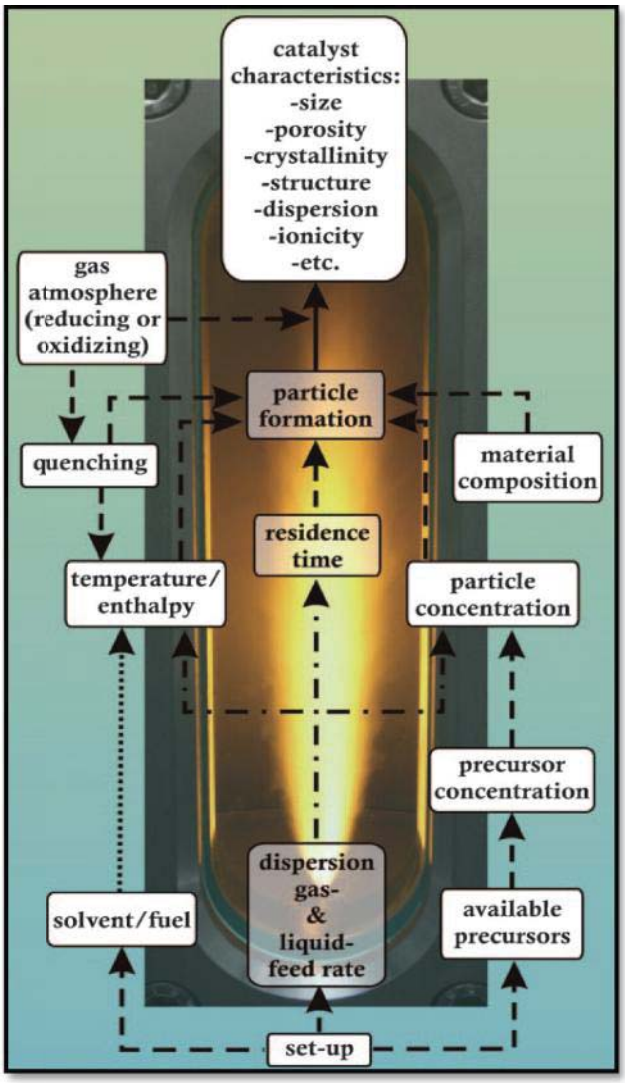

Figure 3.9 Schematic of the main parameters influencing properties of flame synthesized materials [70]

3.6 Solvothermal method [18,24,71]

A solvothermal process can be defined as ‘‘a chemical reaction in a closed system in the presence of a organic solvent at a temperature higher than that of the boiling point of such a solvent’’. Consequently a solvothermal process involves high pressures. The selected temperature (sub-or supercritical domains) depends on the required reactions for obtaining the target-material through the involved process. The

solvothermal treatment could be used to control grain size, particle morphology, crystalline phase and surface chemistry by regulating sol composition, reaction temperature, pressure, nature of solvent, additives, and aging time. In particular, the particles prepared by this method have larger surface area, smaller particle size, and more stable than those obtained by other methods such as the sol–gel one. Main two types of parameters are involved in solvothermalreactions as show in Figure 3.10.

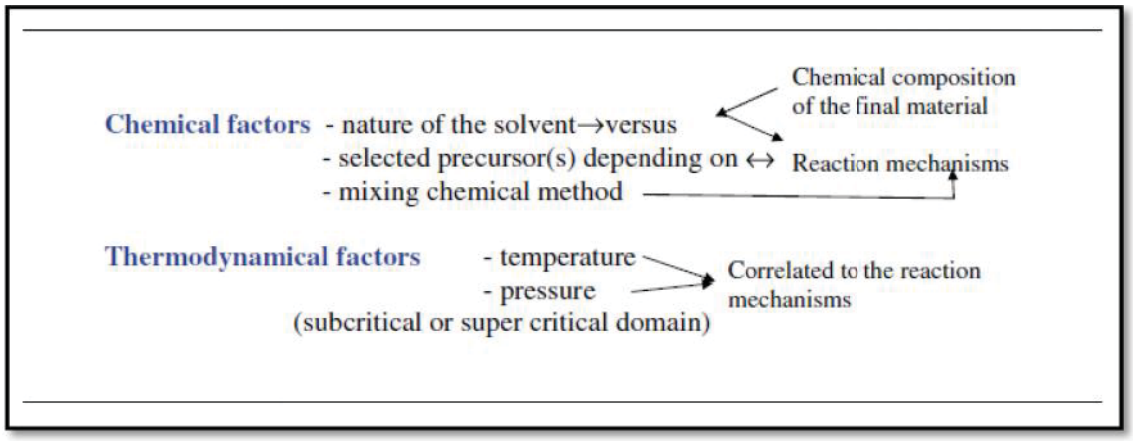

Figure 3.10 Main factors governing solvothermal processes [24]

Chemical parameters:

Two different parameters can be taken into account (i) the nature of the reagents and (ii) the nature of the solvent. The chemical composition of the precursors must be appropriated to that of the target-materials. In addition, the concentration of the precursors seems to play a role on the control of the shape of nanocrystallites resulting of a solvothermal process. The interactions between reagents and solvent play an important role in the solvothermal reactions. Consequently the nature of the solvent can act on the reactivity and the morphology of the resulting crystallites. The physicochemical properties of the selected solvent can also play an important role for orienting the structural form of the final material.

The thermodynamical parameters:

These parameters are: temperature, pressure and the reaction time. The solvothermal reactions are mainly developed in mild temperature conditions: ($T<400^{o}C$). Temperature and pressure improving in the major cases the solubility, the increase of such parameters induces an enhancement of the precursors concentration into the solvent and then favours the growing process (in particular in the preparation of micro- or nanocrystallites). The brief analysis of the main factors governing solvothermal reactions underlines that the nature of the selected solvent plays a key role, in particular for controlling the chemical mechanisms involved in the solvothermal reactions.

This technique was introduced into the field of ceramic materials synthesis, such as ZrO_2, Ce_2O_3 and Al_2O_3. This method could be employed as an alternative to calcinations for the promotion of crystallization under mild temperature. The detailed solvothermal method is illustrated in Figure 3.11, and allows for the crystallization of the metal oxide nucleus during thermal treatment at high temperature and pressure (c). The crystallized metal oxide nucleus then develops into the primary particle via homocoagulation (d, e), at which point, the excess solvents partially suppress further crystal growth. As a result, the particle size produced via the solvothermal method is finer than that of the sol–gel method. Finally, the crystallized metaloxide particles are attained without the calcination step (f). To prepare the required structure, the excess thermal treatment stephas to be consistent (g). Unlike the solvothermal method, the sol-gel method moved directly from b) to f) via a heterogeneous coagulation step. This mehod can control the grain size, particle morphology, crystalline phase and surface chemistry under various sol compositions, reaction temperatures, pressures, solvent species, additives and agingtime. In particular, the particles prepared using the solvothermal method have been reported to be more stable, have a larger surface area and smaller particle size compared to those obtained using other methods, such as the sol-gel method.

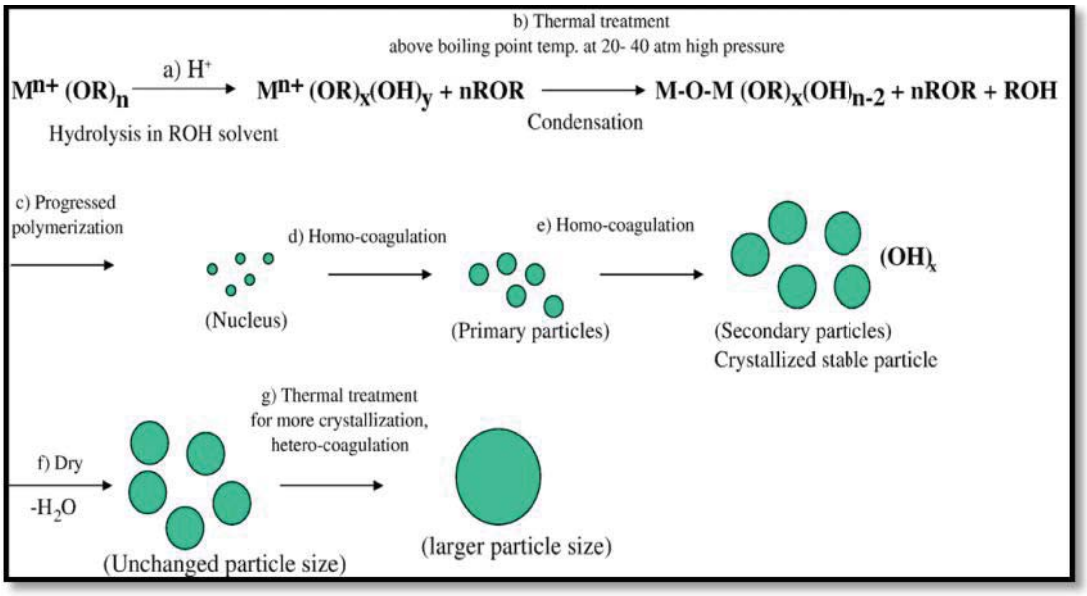

Figure 3.11 Expected mechanism for the synthesis of particles using the solvothermal method [71]

CHAPTER 4

EXPERIMENTS

4.1 Chemicals

The chemicals were used in the Au modified TiO_2 photocatalyst preparation are all analytical grades as listed in Table 4.1. It is noted that specification of these chemicals about physical properties is exhibited later in Appendix A.

Table 4.1 The details of chemicals used in the photocatalyst preparation

Chemicals	Formula	Grade	Manufacture
Tetraisoproply orthotitanate (TIPT)	$(C_3H_7O)_4Ti$	≥ 98%	Merck Schuchardt OHG, Germany
Hydrogen tretachloroauratetrihydrate	$HAuCl_4.3H_2O$	99.99%	Sigma-Aldrich Chemie GmbH, Germany
Formic acid	HCOOH	90%	Ajax Finechem Pty Ltd
Methanol	CH_3OH	99.9%	J.T. Baker
Ethanol	CH_3CH_2OH	99.9%	J.T. Baker
Acetylacetone	$C_5H_8O_2$	99%	Merck Schuchardt OHG, Germany
1-Butanol (BN)	$CH_3(CH_2)_3OH$	99.8%	Sigma-Aldrich Chemie GmbH, Germany
Ethylene Glycol (EG)	$HOCH_2CH_2OH$	99%	J.T. Baker
1,4-Butanediol (BD)	$HO(CH_2)_4OH$	99%	Sigma-Aldrich Chemie GmbH, Germany
n-Pentane (PT)	C_5H_{12}	≥ 99%	Sigma-Aldrich Chemie GmbH, Germany
Xylene (XL)	C_8H_{10}	99.0%	Panreac Guimica S.A.U.

Chemicals	Formula	Grade	Manufacture
n-Cyclohexane (CHX)	C_6H_{12}	99.5%	Sigma-Aldrich Chemie GmbH, Germany
n-Heptane (HT)	C_7H_{16}	99%	Sigma-Aldrich Chemie GmbH, Germany
Toulene (TE)	$C_6H_5CH_3$	≥ 99.9%	Merck Schuchardt OHG, Germany
Octane (OT)	C_8H_{18}	≥ 99.5%	Sigma-Aldrich Chemie GmbH, Germany

4.2 TiO_2 based photocatalyst preparation

4.2.1 TiO_2 preparation by sol-gel method

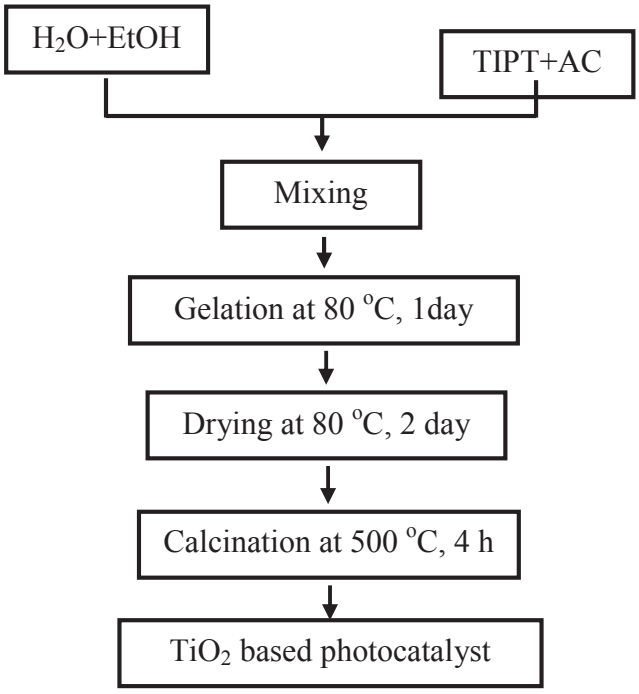

Figure 4.1 Schematic of the TiO_2 based photocatalyst synthesis procedure by sol-gel method

Acetylacetone (ACA) is first added into tetraisoproply orthotitanate (TIPT) at an equimolar, and the mixed solution is then allowed to cool to room. Afterwards, it is added to solution of water and ethanol with continuously stirring at room temperature to obtain a clear solution. Then, the both solution is mixed to obtain a clear yellow solution while stirring continuously at room temperature. The resulting mixture is kept at 80°C for 1 day to obtain complete gel formation and the resulting gel is dried at 80°C for 2 day. Finally, the obtained zero gel (dried residue) is calcined at 500 ^{o} for 4 h with heating rates of 10 °C/min to remove the impurity to yield the TiO_2 nanocrystal photocatalyst. The schematic diagram of the synthesis procedure is shown in Figure 4.1.

4.2.2 TiO_2 preparation by solvothermal method

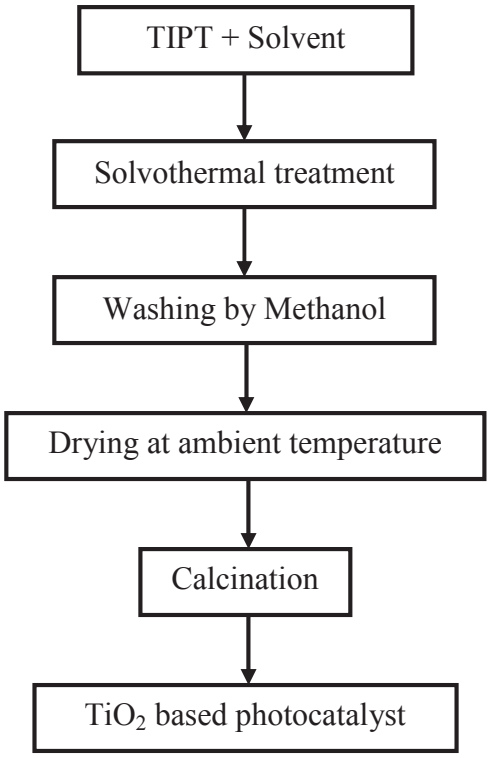

Figure 4.2 Schematic of the TiO_2 based photocatalyst synthesis procedure by solvothermal method

The preparation of the TiO_2 photocatalysts by solvothermal method is shown in Figure 4.2. TIPT is dissolved in organic solvent in a test tube, which was then placed in a 300 cm^3 autoclave as shown in Figure 4.3. The gap between the test tube and the autoclave wall is filled with 30 cm^3 of the same solvent use in the test tube. The autoclave is purged completely by nitrogen before heating up to the desired temperature at a rate of 2.5 ^oC/min and the vessel is rotated at 300 rpm during the solvothermal reaction. Autogeneous pressure during the reaction gradually increase as the temperature is raised. After the prescribed temperature is reached, the temperature is held constant for desired period of time, and then cool down to room temperature. The resultant product is obtained by centrifugation, washed three times with methanol and dried in air at room temperature. For thermal treatment, the synthesized product is calcined in air with flow rate 30 cm^3/min and a heating rate of 10 ^oC/min for 4 h to yield the TiO_2 based photocatalyst. Table 4.2 showed condition in studied parameter for preparation of TiO_2 by this method such as solvent type, temperature of preparation, concentration of TIPT and temperature of calcination.

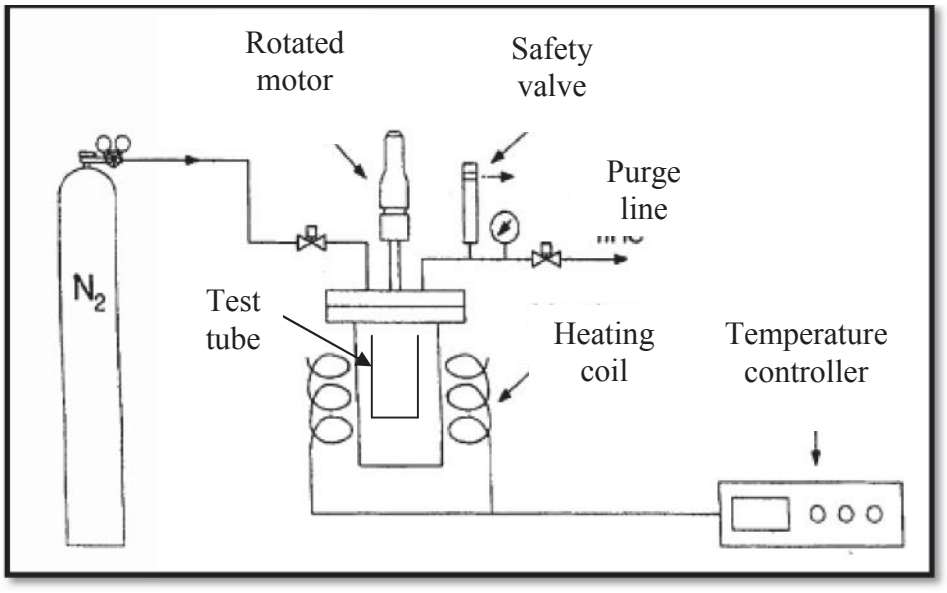

Figure 4.3 Autoclave used to synthesis TiO_2.

Table 4.2 Condition of studied paramerter in TiO_2 prepared by solvothermal

Studied parameter	Condition			
	Solvent type	**Solvothermal temperature (^oC)**	**TIPT (TIPT ml:100 ml solvent)**	**Calcined Temperature (^oC)**
Solvent type	BN, EG, BD, PT, CHX, HT, TE, OT, XL	300	10	500
Temperature of preparation	CHX HT TE	250 300	10	500
Concentration of Ti	HT	300	5 10 15 20	500
Temperature of calcination	HT	300	10	300 400 500 600

4.2.3 TiO_2 preparation by flame spray pyrolysis method

TIPT is used as the feed precursor. It is dissolved in organic solvent to obtain a clear solution. In a typical run, the liquid precursor is fed in the center of a methane/oxygen flame by syringe pump and dispersed by oxygen (Thai Industrial Gas Co., Ltd.) forming a fine spray. The precursor feed rate is 5 ml/min. The pressure drop at the capillary tip is kept constant at 1.5 atm by adjusting the orifice gap area at the nozzle. The photocatalyst powder is collected on a glass microfiber filter (Whatman) with the aid of a vacumm pump.

4.3 Au cocatalyst modification

4.3.1 Au cocatalyst modification by impregnation

The Incipient impregenation procedure are as follows:

1. Dissolve appropriate amount of $HAuCl_4$ in distillated water.
2. TiO_2 powder is impregnated with the Au solution.
3. The impregnated sample is kept at room temperature for 6 h.
4. The sample is dried in oven at 110 °C overnight.
5. The dried sample is reduced with H_2 at 200 °C for 4 h.

Finally, the Au modified TiO_2 photocatalyst is obtained.

4.3.2 Au cocatalyst modification by photodeposition

In the photodeposition method, Au metal loaded on TiO_2 is prepared by photoreducing Au^{3+} ions to Au metal on the TiO_2 surface according to the following steps shown in Figure 4.4. First, TiO_2 powder is suspended in aqueous solution of 0.5 vol.% methanol and the required amount of $HAuCl_4.3H_2O$. The mixture is then

irradiated with UV light (Hg lamp, TUV 11 W PL-S, Phillip), washed with distillated water and then dried at 110 ^{o}C for 12 h.

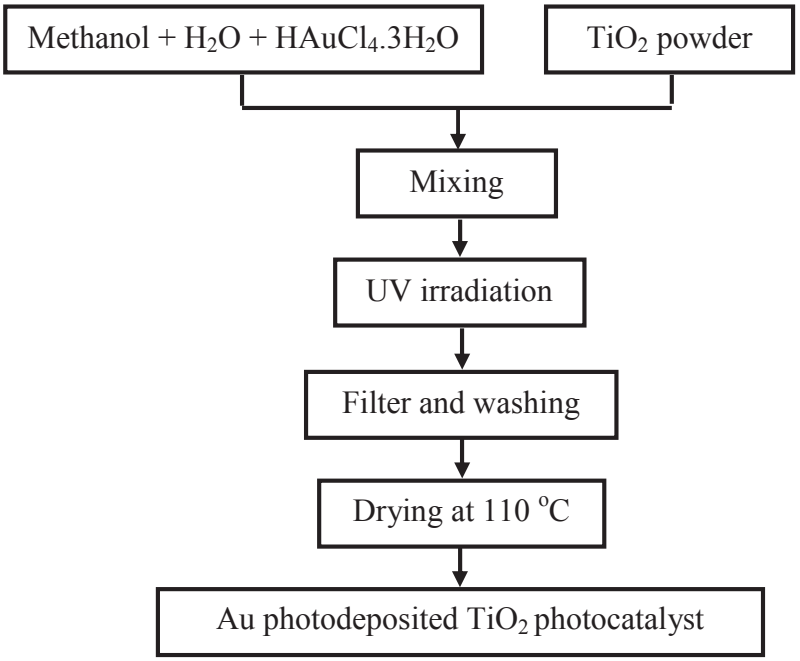

Figure 4.4 Schematic of synthesis procedure of Au photodeposition over TiO_2

4.3.3 Au cocatalyst modification by doping

In the case of the Au doped TiO_2 based photocatalyst is synthesized by add $HAuCl_4$ precursor simultaneously TiO_2 based photocatalyst preparation.

4.4 Photocatalyst characterization

4.4.1 X-Ray diffraction (XRD)

The crystalline size, the structure and purity of a photocatalyst can be analyzed using X-ray diffraction analysis. The refraction or diffraction of the X-rays is monitored at various angles with respect to the primary beam X-ray diffraction analysis using an X-ray refractometer, with Ni-filtered Cu Kα radiation in the 2θ range of 20 to 80° using the continuous scanning mode at a rate of 2^{o}C min^{-1} and operating conditions of 30 kV and 15 mA. The crystallite size is calculated from Scherrer's equationas described by eq 4.1.

$$D = \frac{K\lambda}{\beta Cos\theta} \tag{4.1}$$

where*K* is the Sherrer constant (0.89), λ is the wavelength of the X-ray radiation (0.15418 nm for CuK_{α}), β is the full width at half maximum (FWHM) of the diffraction peak measures at 2θ , and θ is the diffraction angle. Fraction of rutile in the product is calculated according to the following eq 4.2 [22]:

$$\%Rutile = \frac{1}{((A/R) \times 0.884) + 1} \times 100 \tag{4.2}$$

where A and B are the peak area for the major anatase and rutile phase, respectively.

4.4.2 N_2 physisorption

The surface area, average pore size diameter and pore size distribution are determined by N_2 physisorption using the BET BELSORP Π (surface area and porosity analyzer). The catalyst is firstly pretreated in inert helium gas flow of 50 ml/min at 150 °C for 3 h to removes water bound to the particle surface from air moisture. After cools down to the ambient temperature, the weight of dried sample is collected. Sample cell is installed to the adsorption part which has liquid nitrogen in dewar. The requisite data are input to the software before the measurement. During the measurement the sample

cell connectes to vacuum port is dipped in liquid nitrogen. The volume of N_2 is measured at different partial pressure at of N_2 -196 ^oC.

4.4.3 Transmission electron microscopy (TEM)

The crystalline image is determined using transmission electron spectroscopy operates at 80 kV. The sample is dispersed in ethanol to obtain the uniform dispersion of sample. A drop of liquid is deposited onto a copper mesh sample grid that supports a holey carbon support film. The grid is resting on a filter paper and is allowed to dry for several minutes before being moved. The scans are done many times in different areas as much as possible until the good representative image for all areas is obtained.

4.4.4 Inductively coupled plasma (ICP)

The actual amount of Au in synthesis of photocatalyst are determined by inductively coupled plasma (ICP).

4.4.5 UV-vis diffuse reflectance spectra (UV-vis DRS)

Diffuse reflectance spectra of the samples are measured at room temperature with a UV-visible spectrophotometer in the range 200-800 nm. Afterwards, the diffuse reflectance spectra are analyzed to estimate the band gap wavelength (E_g, nm) by using theKabelkae-Munk function (F(R)), as expressed by the following eq 4.3:

$$F(R) = \frac{(1-R)^2}{2R} \qquad 4.3$$

where*R* is the ratio of the reflected light intensity to the reflected light intensity of the reference and the band gap energy (Eg) wasthen determined by using the following eq 4.4:

$$E_g = \frac{1240}{\lambda_g} \qquad 4.4$$

4.4.6 H_2 Chemisorption

H_2 chemisorption was used to determine a number of gold metal atoms on the photocatalyst surface and overall gold dispersion. The total hydrogen consumption was calculated from the number of injection of a known volume. N_2 and H_2 were used as a carrier gas and a adsorbent gas, respectively. 0.05 g of a photocatalyst sample was placed in a quartz tubular reactor. Under N_2 atmosphere at a flow rate of 30 ml/min, the photocatalyst sample was heated up to 150 °C at a heating rate of 10 °C/min and held for 2 h at this temperature in order to remove adsorbed water on surface. Afterwards, the system was cooled down to room temperature by N_2 at a flow rate of 30 ml/min. At this temperature, the photocatalyst sample was ready to be measure the metal active sites. 20 μl of the purity H_2 gas was injected into the injection port to adsorb on the metal surface of the catalyst sample. Injection of H_2 was continuously repeated until saturation. This situation was occurred when an obtained chromatogram area of any injection, after adsorption of the H_2 pulse in the first injection had proceeded, was kept nearly constant compared with that of the former injection.

4.4.6 Photoluminescence spectroscopy (PL)

The photoluminescence spectroscopy was used to studied recombination rate of photogenerated e^-/h^+ pairs. The photoluminescence emission spectra were measured at room temperature in range 350-750 nm with exited at 325 nm.

4.5 Photocatalytic H_2 production testing

The photocatalytic reactions are carried out in a gas circulation system and are performed in an outer-irradiation and air-tight Pyrex glass reactor with a total volume of 750 cm^3. The reaction temperature is controlled by using a water-cooling system. A set of 176 W fluorescent lamps (16 lamps, 11 W PL-S 2P, Phillip) are employed as simulated sunlight source with total irradiance of about 90 $W.m^{-2}$. Spectrum of the lamp consisted of fluorescent emission predominantly in the visible region along with a UV contribution of about 3% [27]. In a typical experiment, each photocatalyst sample is suspended in 0.1 M formic acid aqueous solution (250 ml) with 0.1 g/l. Prior to the reaction testing, the suspension is left in the dark while simultaneously being thoroughly deaerates by Ar gas (UHP, Thai Industrial Gas Ltd) bubbling for 20 min, and then adjusts flow Ar with 30 cm^3/min before the suspension is irradiated by turning on the lamps and the reaction temperature is controlled at 30^oC. After every 30 min, hydrogen gas is analyzed by an online gas chromatograph equipped with a thermal conductivity detector (TCD), as show in Figure 4.5. The operating conditions for TCD gas chromatograph instrument is shown in the Table 4.3.

Table 4.3 The operating conditions of TCD gas chromatograph for the photocatalytic H_2 production testing

Gas chromatograph	**Shimadzu GC-14B**
Detector	TCD
Column	Unibead C
Carrier gas	Ar (UHP)
Carrier gas flow	30 ml/min
Injector temperature	150 °C
Detector temperature	150 °C
Column temperature	40 °C
Analysis gas	H_2, CO, CO_2

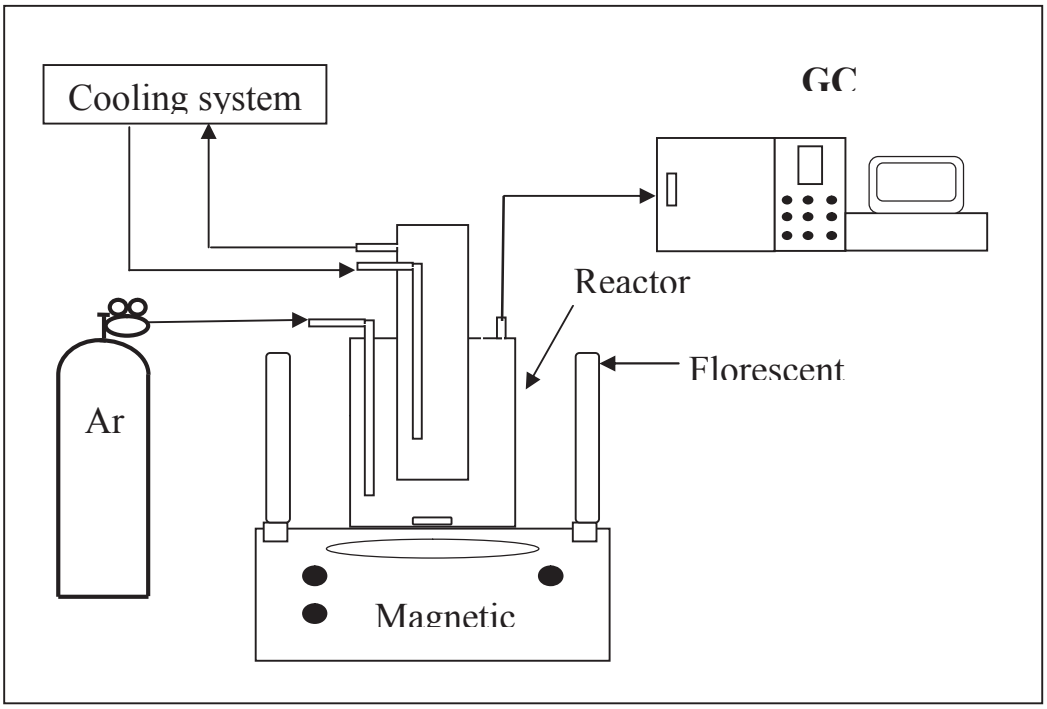

Figure 4.5 The photocatalytic hydrogen production system used in this study

CHAPTER 5

RESULTS AND DISCUSSION

5.1 Photocatalyst characterization

5.1.1 Effect of TiO_2 preparation method

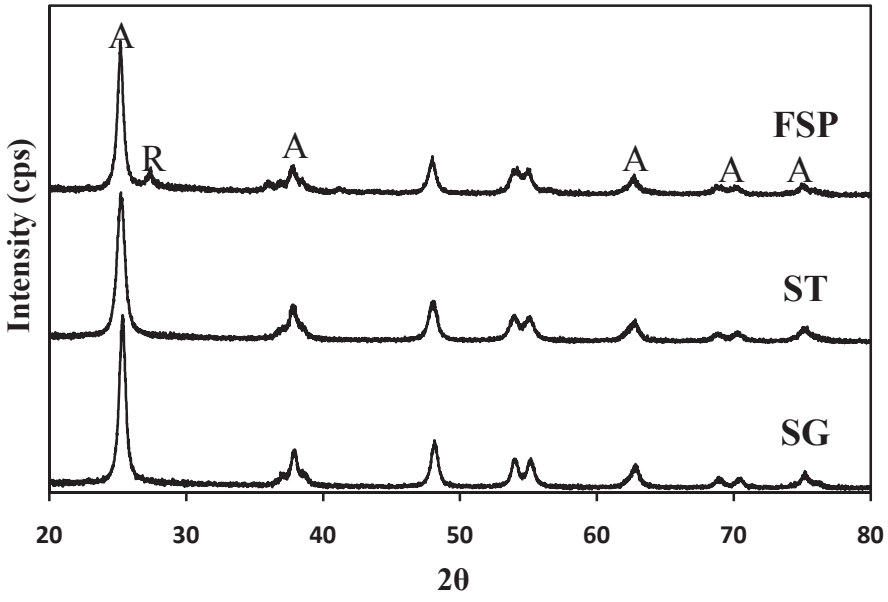

Figure 5.1 XRD pattern of TiO_2 based photocatalysts prepared by flame spray pyrolysis (FSP), sol-gel (SG) and solvothermal (ST) (A: anatae, R: rutile)

Nanosized TiO_2 particles was successfully prepared by using sol-gel, solvothermal (using 1,4-Butanediol as solvent) and flam spray pyrolysis methods. The

XRD patterns of them, as shown in Figure 5.1. TiO_2 prepared by SG and ST show the dominant peaks at 2θ of about 25.2, 37.9, 48.3, 53.8, 62.7, 68.9 and 75.3, which correspond to the indices of (101), (103), (200), (105), (213), (116) and (107) planes [50], respectively, reveal the crystalline structure of the pure anatase phase. However, TiO_2 prepared by FSP shows two additional very low intense peaks corresponding to rutile phase at 2θ of about 27.5, which correspond to the indices of (110) plane [50] with approximately 5% rutile content, besides that of the major anatase phase.

Table 5.1 Physical properties of TiO_2 prepared by SG, ST and FSP

Preparation method	Phase[a] content (wt.%)	d_{XRD}[b] (nm)	d_{TEM}[c] (nm)	Relative[d] crystallinity	S_{BET}[e] (m^2/g)	S_{XRD}[f] (m^2/g)	S_{BET}/S_{XRD}	Pore[e] diameter (nm)	Pore[e] volume (cm^3/g)
SG	A (100)	14.4	14.8	1.32	21.8	109.1	0.20	3.8	0.0591
ST	A (100)	11.8	12.1	1.00*	89.3	94.3	0.95	21.7	0.3716
FSP	A (86.8) R (13.2)	16.4 17.0	17.1	1.00	116.9	132.8	0.88	11.8	0.3856
P25	-	-	-	-	61.8	-	-	28.0	0.3626

a) Calculated according to equation proposed by W. Payakgul et al. [22]

b) Base on XRD line broadening

c) Average particle size from TEM

d) Comparison of height main peak of anatase by using ST as reference

e) N_2 physisorption analysis

f) Calculated surface area assuming that the particles are nonporous spheres ($S=6/\rho d_{XRD}$)

The physical properties of TiO_2 prepared by SG, ST and FSP methods were showed in Table 5.1. It can be seen that the crystallite sizes of TiO_2 particles calculated from the Scherrer equation decreases in the order FSP >SG >ST. However, the

crystallinity of TiO_2 preparation by SG exhibited higher crystallinity than TiO_2 preparation by ST and FSP, while both ST and FSP provided same crystallinity. TEM was performed to evaluate the morphology and particle size of TiO_2 particles. TEM image of TiO_2 particles prepared by SG, ST and FSP are shown in Figure 5.4-5.6, respectively, they exhibited spherical particles. TiO_2 prepared by SG and ST exhibit nawrrow particle size distribution. On the other hand, TiO_2 prepared by FSP shows wide particle size distribution. Moreover, they can be seen that average particle size from TEM image, which agree with the crystallite sizes of TiO_2 particles calculated from the Scherrer equation as shown in Table 5.1. Hence, each primary particle observed by TEM is a nanosized single crystal TiO_2 [22].

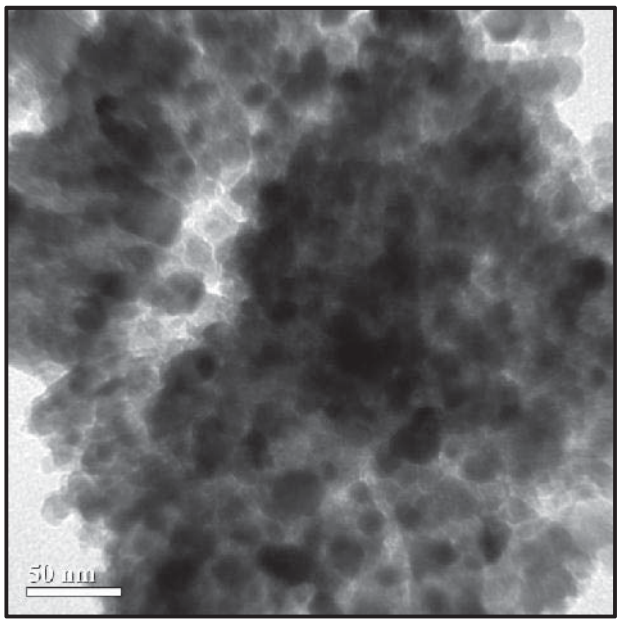

Figure 5.2 TEM image of TiO_2 preparation by SG

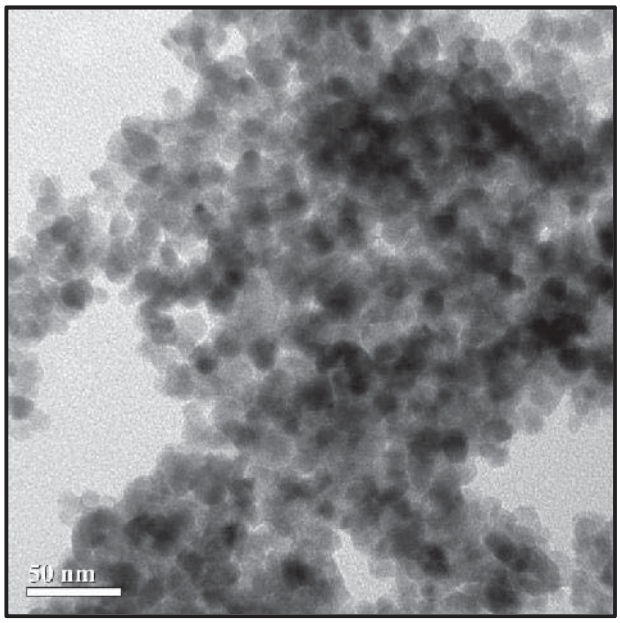

Figure 5.3 TEM image of TiO_2 preparation by ST

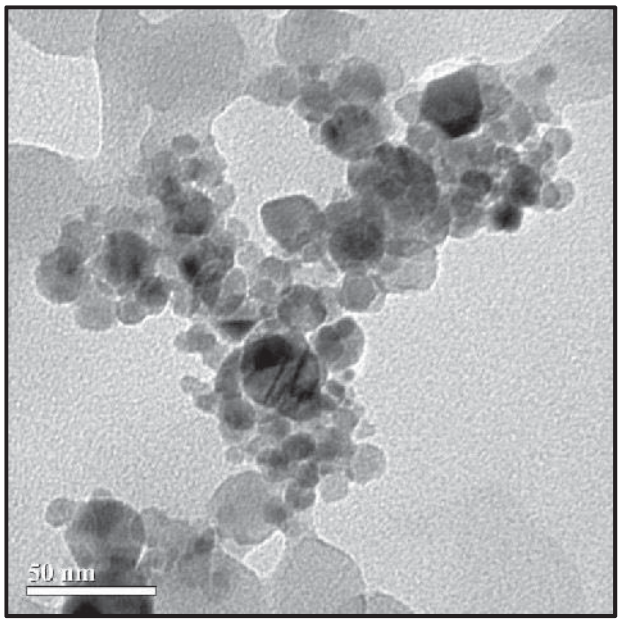

Figure 5.4 TEM image of TiO_2 preparation by FSP

The BET surface area of all products decreases in the order ST >FSP >SG. Moreover, Table 5.1 also compares BET surface area (S_{BET}) measured by N_2 physisorption and the surface area calculated from a crystallite size (S_{XRD}), assume that the crystals are non-porous spheres. It is noticed that S_{BET} is smaller than S_{XRD} for all the preparation methods, W. Payakgul et al. [22] proposed that this behavior was the result from the agglomeration of TiO_2 crystals. So that, the agglomeration of crystals increases in the order FSP >ST >SG, which agree with the TEM observation. N_2 adsorption-desorption isotherm was used to verify the mesoposity of the studied photocatalysts sine the isotherm shape reveals the characteristics of powder structure, which consist of an assembly of numerous particles with large open packing [50]. Figure 5.2 shows N_2 adsorption-desorption isotherm of TiO_2 prepared by SG, ST and FSP, provided information related to the porous texure. The isotherm of TiO_2 prepared by SG and ST reveal the typical IUPAC type IV pattern with the H2 hysteresis loop, characteristic of mesoporous materials (2-50 nm) [42]. A sharp increase in the adsorption volume of N_2 was clearly observed and located in the relative partial pressure rang of 0.5-0.9. This sharp increase can be attributed to the capillary condensation of N_2 inside the mesopores [50], it can be clearly seen from TiO_2 prepared by SG method. However, hysteresis loop TiO_2 prepared by ST method shift at relative high partial pressure than SG because of larger pore size, which according to pore size as shown in Figure 5.3. The isotherm of TiO_2 prepared by FSP gave rise to hysteresis at relative high partial pressure and correspond to the IUPAC type II pattern [42], as shown in Figure 5.3. However, the N_2 adsorption-desorption isotherm for TiO_2 particles prepared by FSP correspond to the IUPAC type II pattern [42], as shown in Figure 5.2. It can be seen that they possess the non-mesoporous characteristic, due to the absence of both a distinct hysteresis loop and an adsorption plateau at very high relative pressure, indicating that there is no capillary condensation of N_2 into the pores. The pore size distributions, as shown in Figure 5.3 are quite broad. This result show that the average pores of TiO_2 obtained by FSP are quite spacious because their pore size distributions are not only present in the mesoporous region (mesopore size between 2 and 50 nm) but also mostly exist in the macroporous region (pore diameter >50 nm), which it is quite typical for nanoparticles

obtained by FSP method that contained only large pore [77]. Furthermore, total pore volume of the TiO_2 products in Table 5.1 increases in the order SG >ST >FSP. This result is attributed to the agglomeration effect and crystallite size [27]. From these characterization results, it is evident that the TiO_2 products prapared by different method have diffent physical properties.

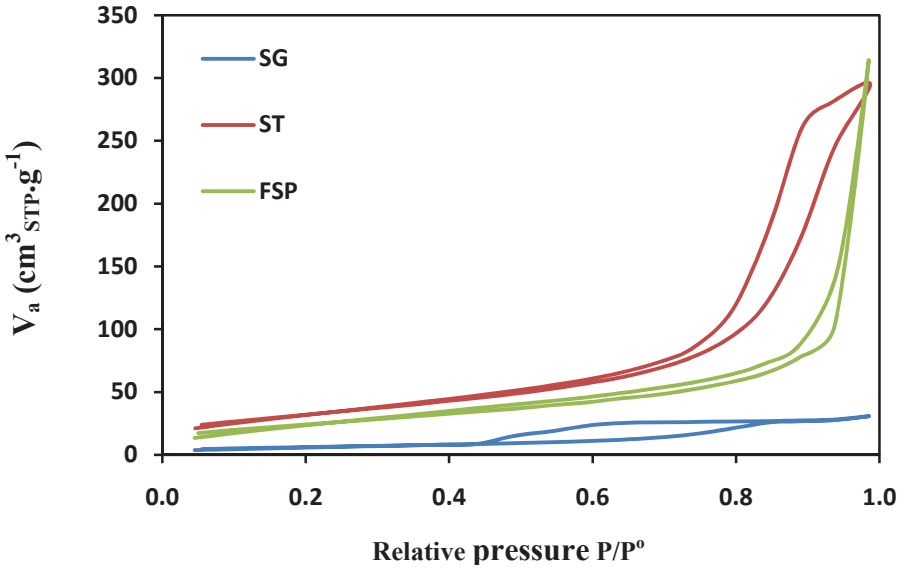

Figure 5.5 N_2 adsorption/desorption isotherms of TiO_2 preparation by SG, ST and FSP

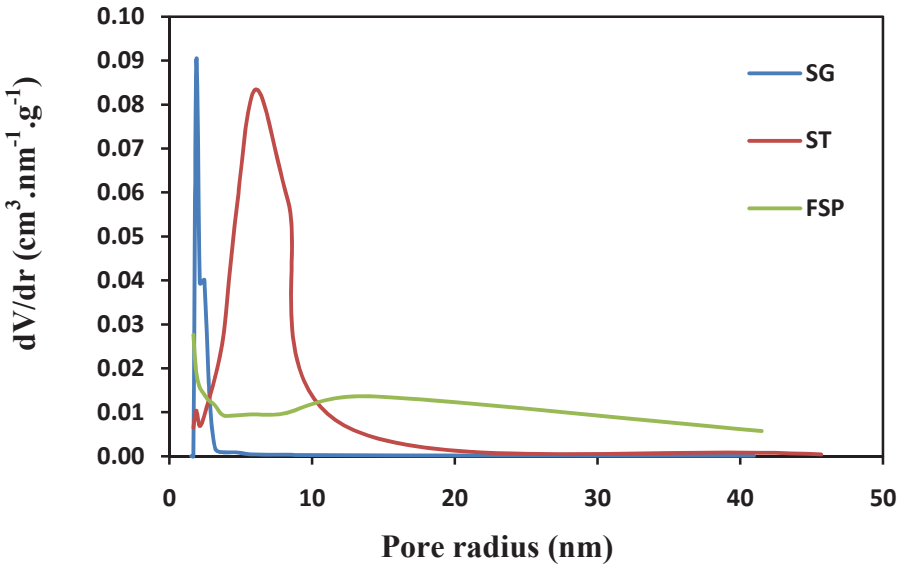

Figure 5.6 Pore size distributions of TiO_2 preparation by SG, ST and FSP

5.1.2 Effect of solvent type in TiO_2 preparation by solvothermal

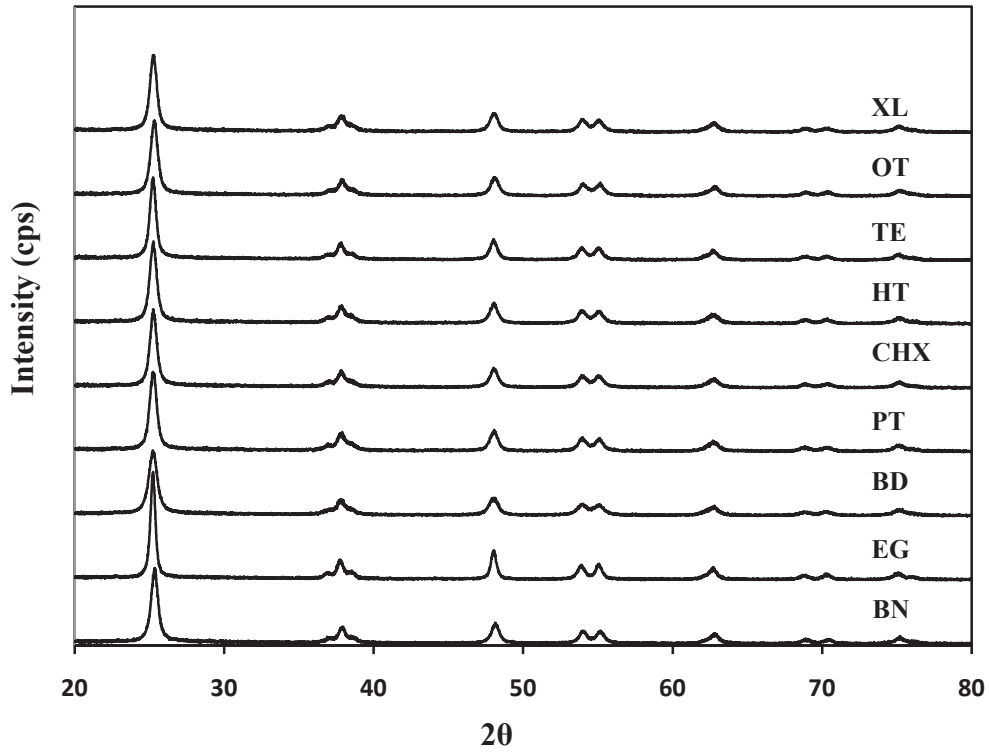

Figure 5.7 XRD pattern of TiO_2 based photocatalysts prepared by ST with using different solvent

The solvents in this research can be divided two main groups, (1) –OH compound solvents, e.g. butanol (BN), ethylene glycol (EG) and 1,4-butanediol (BD) and (2) without –OH compound solvents, e.g. pentane (PT), cyclohexane (CHX), heptane (HT), toluene (TE), octane (OT) and xylene (XL). Generally, type of solvent used in solvothermal for catalyst preparation affect the phase composition extremely during the solvothermal preparation [25]. However, in the this research, all the TiO_2 products prepared by solvothermal method with studied solvents were indentified as anatase phase, as shown in Figure 5.7. Moreover, the effect of solvent type on physical properties of TiO_2 products such as crystallinity, crystallite size, specific surface area, pore size

diameter were shown in Table 5.2. In the polar solvents, the crystallinity increases in the order EG >BN >BD, which agree with polarity of solvent, because nanocrystalline anatase TiO_2 prepared in polar solvent crystallized directly from the solution [22]. Hence, polarity of solvent effect to crystallinity of TiO_2 product, high polarity solvent provided higher crystallinity than lower polarity solvent. On the other hand, the nonpolar solvents provided same crystallinity of TiO_2 products, which agree with polarity of solvent, because nanocrystalline anatase TiO_2 prepared in polar solvent crystallized directly from the solution [22]. Hence, polarity of solvent effect to crystallinity of TiO_2 product, high polarity solvent provided higher crystallinity than lower polarity solvent. On the other hand, crystallinity of TiO_2 prepared in nonpolar solvents were similar crystallinity because of similar polarity. In addition, when nonpolar solvent was used as reaction medium for solvothermal preparation of TiO_2, amorphous product was initially formed in the solution and later transformed to anatase crystal via solid state reaction, which it opposite reaction in polar solvent.

Figure 5.8 show N_2 adsorption-desorption isotherm of TiO_2 prepared with using BN, EG and BD, provided information related to the porous texure. The isotherm of TiO_2 in using BN, EG and BD reveal characteristic of mesoporous materials with different shap of the hysteresis loop, it mean that this solvent provided shap of pore structure. Morover, they gave different pore size distribution, BN gave narrow pore size distribution, while EG and BD gave wide pore size distribution as shown in Figure 5.10, because the number of –OH in the moleculer structure might be the factor that affect the TiO_2 formation. The isotherm of TiO_2 prepared using PT, CHX, HT, TE, OT and XL as solvents reveal similar the typical IUPAC type IV pattern as shown in Figure 5.9, since these solvents have no effect of –OH to direct crystalline formation, TiO_2 praticles were prepared by using these solvents may provided same pore size and similar pore size distribution as shown in Figure 5.11. So that, these characterization results, it is evident that the TiO_2 products prapared in different solvent type with solvotermal method have diffent physical properties of TiO_2 product.

Table 5.2 Physical properties of TiO_2 prepared by ST with different solvent

Sovent type	Phase content[a] (wt.%)	d_{XRD}[b] (nm)	Relative[c] crystallinity	S_{BET}[d] (m^2/g)	S_{XRD}[e] (m^2/g)	S_{BET}/S_{XRD}	Pore[d] diameter (nm)	Pore[d] volume (cm^3/g)
BN	A (100)	14.5	1.08	53.2	108.0	0.49	6.4	0.1178
EG	A (100)	20.1	1.66	59.2	77.8	0.76	11.5	0.2085
BD	A (100)	11.8	1.00*	116.9	132.8	0.88	11.8	0.3856
PT	A (100)	14.0	1.24	80.7	112.2	0.72	9.3	0.2483
CHX	A (100)	14.0	1.24	93.2	111.7	0.83	9.2	0.3020
HT	A (100)	14.3	1.27	100.1	109.8	0.90	9.3	0.4027
TE	A (100)	14.6	1.22	104.6	107.2	0.98	9.4	0.3384
OT	A (100)	13.9	1.20	81.6	112.3	0.73	9.4	0.2583
TE	A (100)	14.2	1.22	79.6	100.2	0.72	9.3	0.3408

a) Calculated according to equation proposed by W. Payakgul et al. [22]

b) Base on XRD line broadening

c) Comparison of height main peak of anatase by using ST as reference

d) N_2 physisorption analysis

e) Calculated surface area assuming that the particles are nonporous spheres ($S=6/\rho d_{XRD}$)

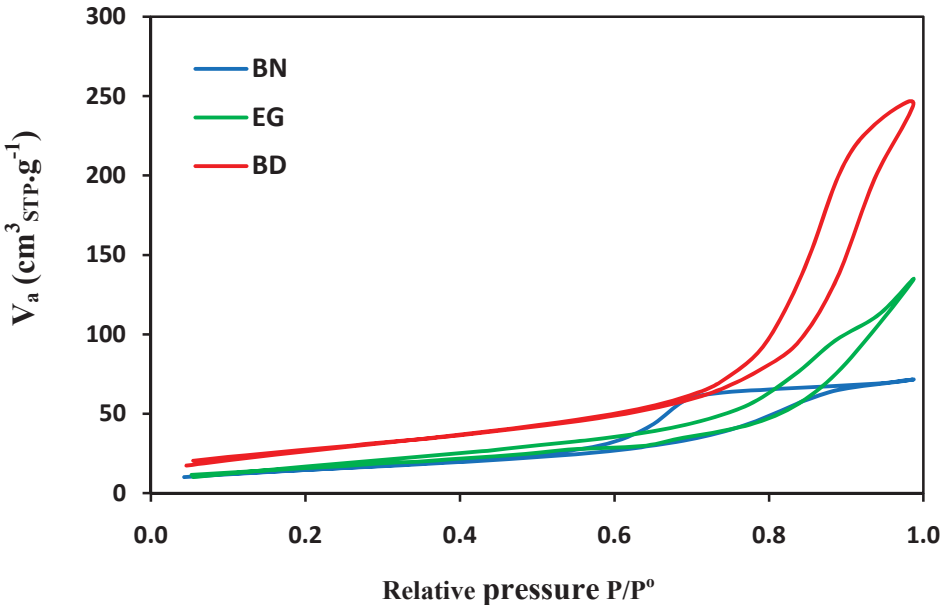

Figure 5.8 N_2 adsorption/desorption isotherms of TiO_2 preparation by ST with using –OH compound solvent

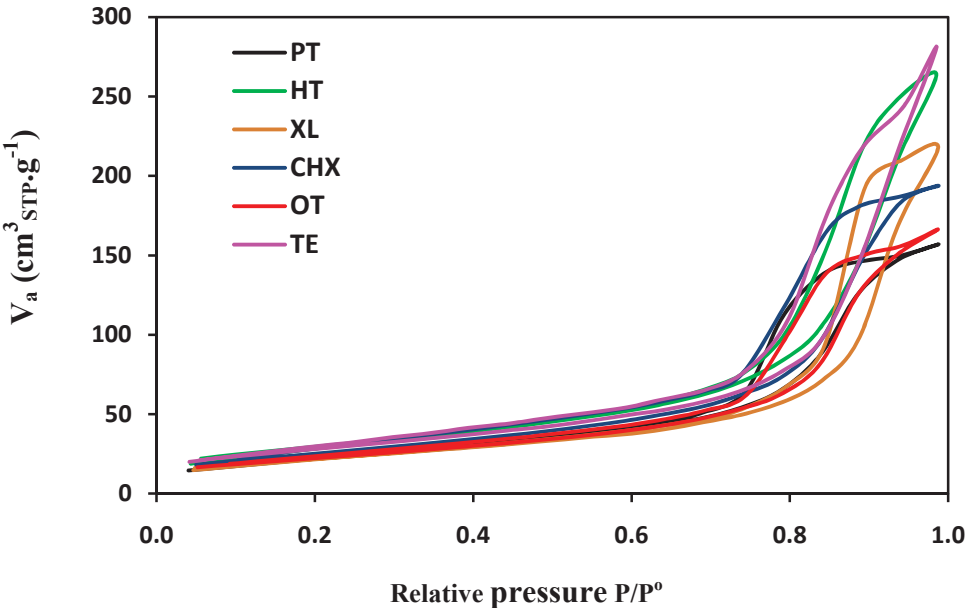

Figure 5.9 N_2 adsorption/desorption isotherms of TiO_2 preparation by ST with without –OH compound solvent

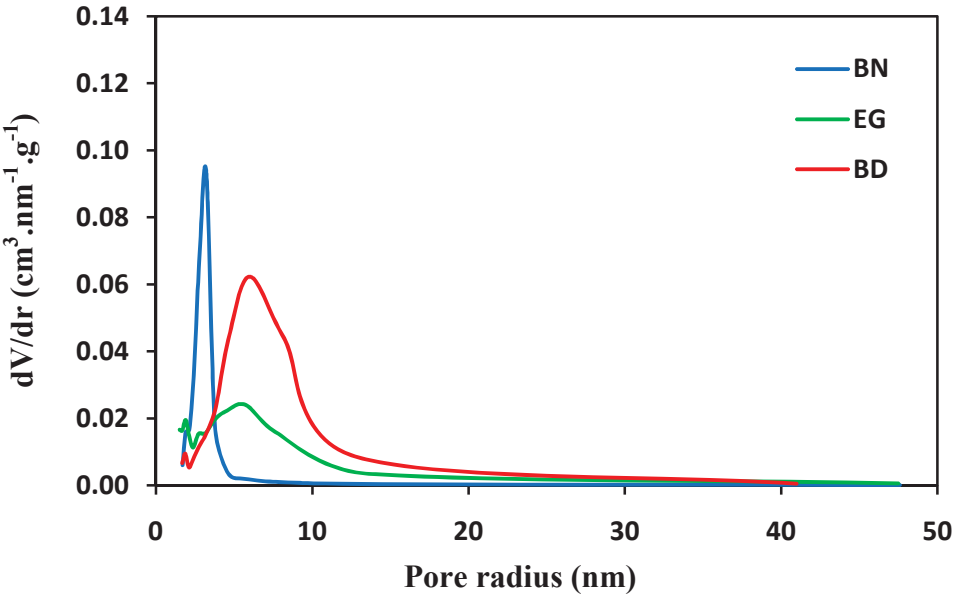

Figure 5.10 Pore size distribution of TiO_2 preparation by ST with using –OH compound solvent

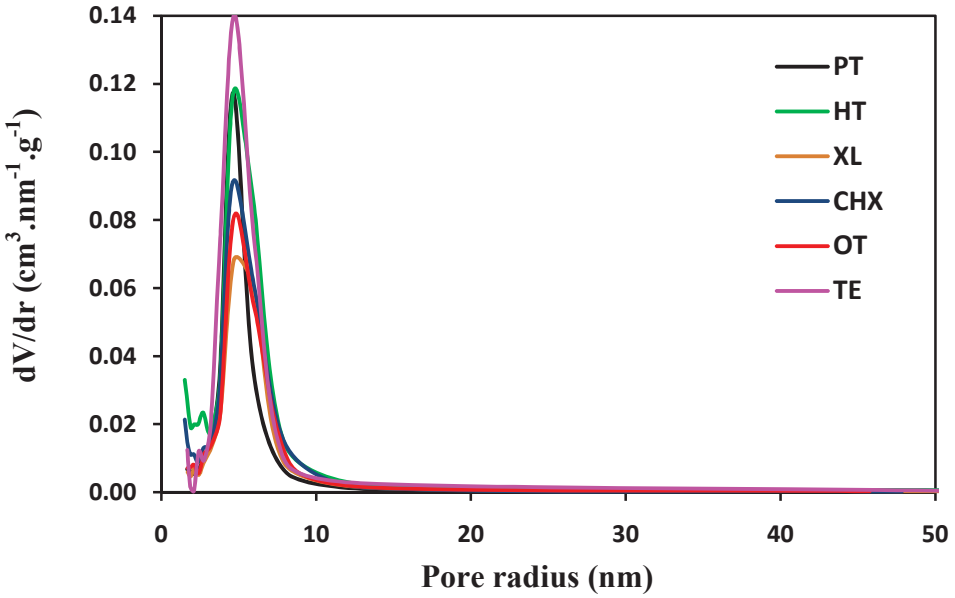

Figure 5.11 Pore size distribution of TiO_2 preparation by ST with using without –OH compound solvent

5.1.3 Effect of temperature in TiO_2 preparation by solvothermal

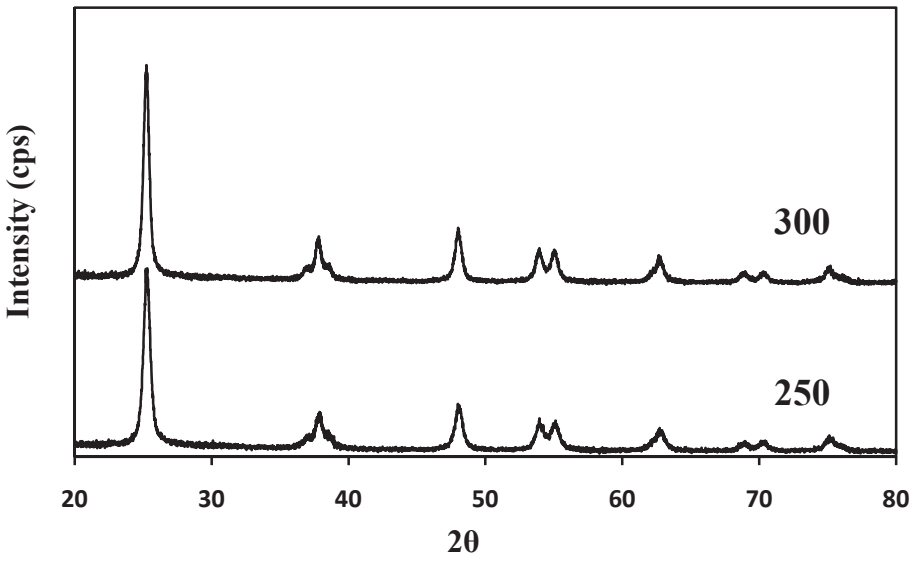

(a)

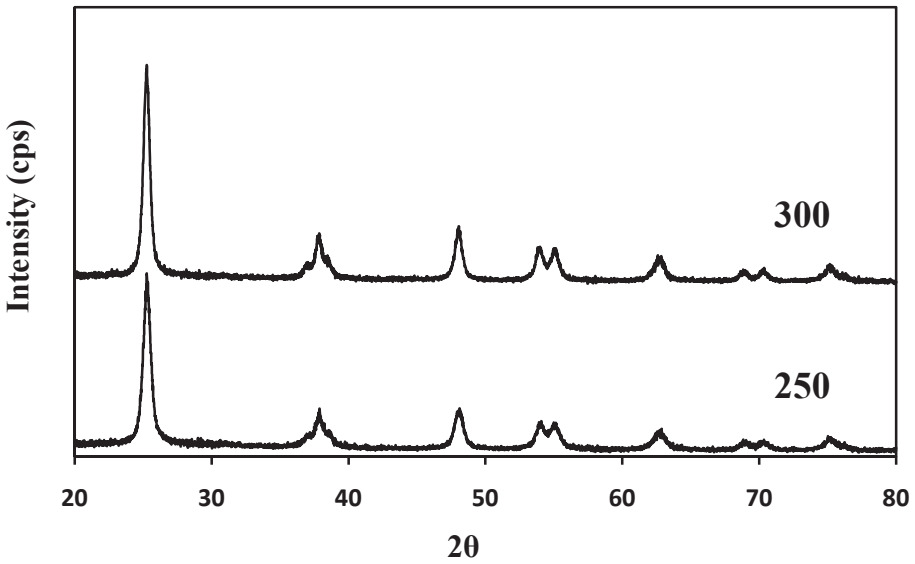

(b)

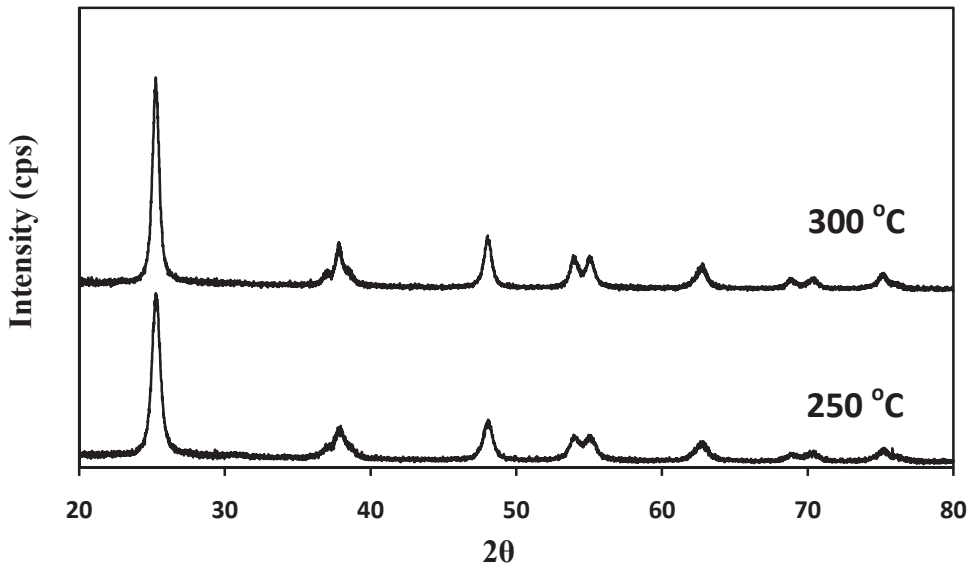

(c)

Figure 5.12 XRD patterns of TiO_2 based photocatalysts prepared by ST at 250 °C and 300 °C in CHX (a), HT (b) and TE (c) solvent

Further investigation of the solvothermal reaction was conducted by varying the solvothermal temperature at 200, 250 and 300 °C, respectivly. It is found that the solvothermal reaction temperature of 200 °C is too low to from any TiO_2 particles for these all studied solvents, such as cyclohexane (CHX), heptane (HT) and toluene (TE). The solvothermal reaction in these solvent is suggested that amorphous product initial precipitates from the solution, then the solid state transformation from the amorphous product to anatase TiO_2 occuring during subsequent heating period [22]. Figure 5.12 depicts the XRD patterns of the TiO_2 powders derived from solvothermal method at 250 and 300 °C in CHX, HT and TE, respectively. As can be seen, the diffraction peacks of anatase phase for all products become stronger and sharper upon enhancing the solvothermal temperature, indicating the improved crystallinity of TiO_2 products, it can be seen crystallinity in Table 5.3.

Table 5.3 Physical properties of TiO_2 prepared by ST with different solvothermal temperature

Temperature (^oC)	Solvent type	d_{XRD}[b] (nm)	Relative[c] crystallinity	S_{BET}[d] (m^2/g)	S_{XRD}[e] (m^2/g)	S_{BET}/S_{XRD}	Pore[d] diameter (nm)	Pore[d] volume (cm^3/g)
200	CHX				No product			
	HT				No product			
	TE				No product			
250	CHX	11.8	1.00	140.5	132.9	1.06	7.1	0.2765
	HT	12.2	1.09	138.3	128.0	1.02	7.9	0.2835
	TE	11.7	0.97	145.7	133.5	1.10	7.0	0.2931
300	CHX	14.1	1.25	93.2	111.7	0.83	9.2	0.3020
	HT	14.0	1.28	100.1	112.2	0.89	9.3	0.4027
	TE	14.6	1.23	103.6	107.2	0.97	9.4	0.3384

a) Base on XRD line broadening

b) Comparison of height main peak of anatase by using temperature at 250 ^oC in CHX as reference

c) N_2 physisorption analysis

d) Calculated surface area assuming that the particles are nonporous spheres ($S=6/\rho d_{XRD}$)

Moreover**,** it was found that TiO_2 particles preparation at 300 ^oC provided larger crystallite size and pore size than preparation at 250 ^oC as shown in Table 5.3, indicating that high temperature enhanced crystallite size, indicating the TiO_2 particles grow slightly with an increase temperature, resulting increase pore size. Table 5.3 also exhibited that S_{BET} determined from N_2 physisorption was higher than S_{XRD} calculated based on the crystallite size for all the TiO_2 particle prepared at 250 ^oC, it was proposed that this behavior was the result of an amorphous-like phase contaminated in the particles of TiO_2[22]. While ,TiO_2 prepared at 300 ^oC, it was found that S_{BET} was smaller than S_{XRD} for all products, indicating that this temperature provide TiO_2 crystalline and agglomerate of TiO_2 crystals [22], resulting increase pore volume of product. Moreover,

solvothermal temperature effect to porosity, it can be seen in Figure 5.13-5.15. Pore size distribution is narrow at high temperature.

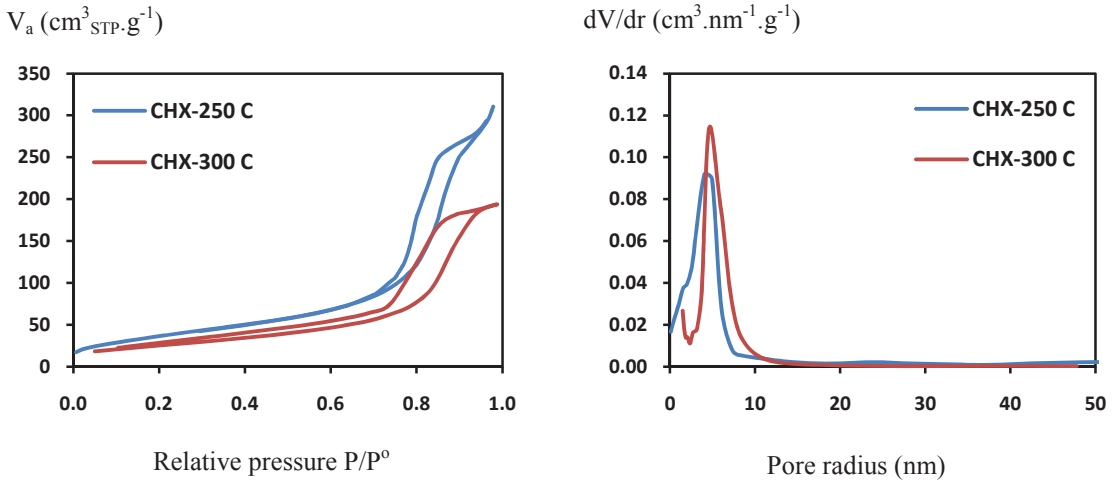

(a) (b)

Figure 5.13 N_2 adsorption/desorption isotherms (a) and pore size distribution (b) of TiO_2 prepared by ST in CHX at 250 and 300 ^oC

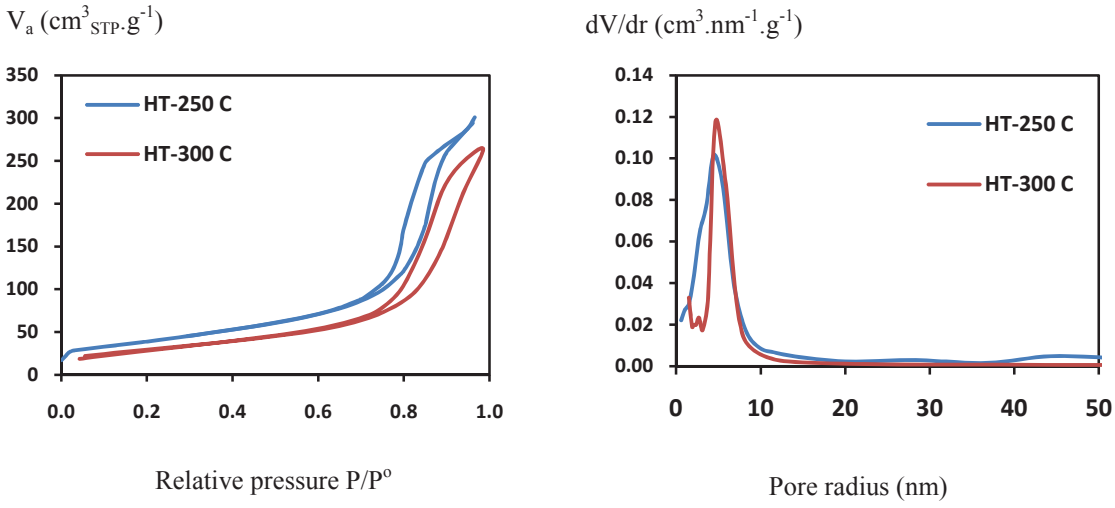

(a) (b)

Figure 5.14 N_2 adsorption/desorption isotherms (a) and pore size distribution (b) of TiO_2 prepared by ST in HT at 250 and 300 °C

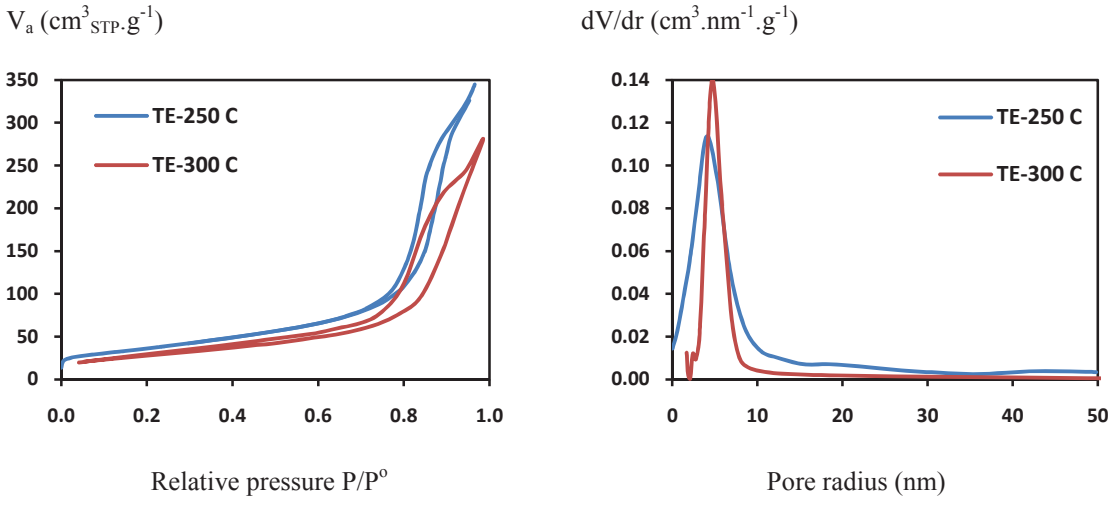

(a) (b)

Figure 5.15 N_2 adsorption/desorption isotherms (a) and pore size distribution (b) of TiO_2 prepared by ST in TE at 250 and 300 °C

5.1.4 Effect of Ti concentration in TiO_2 preparation by solvothermal

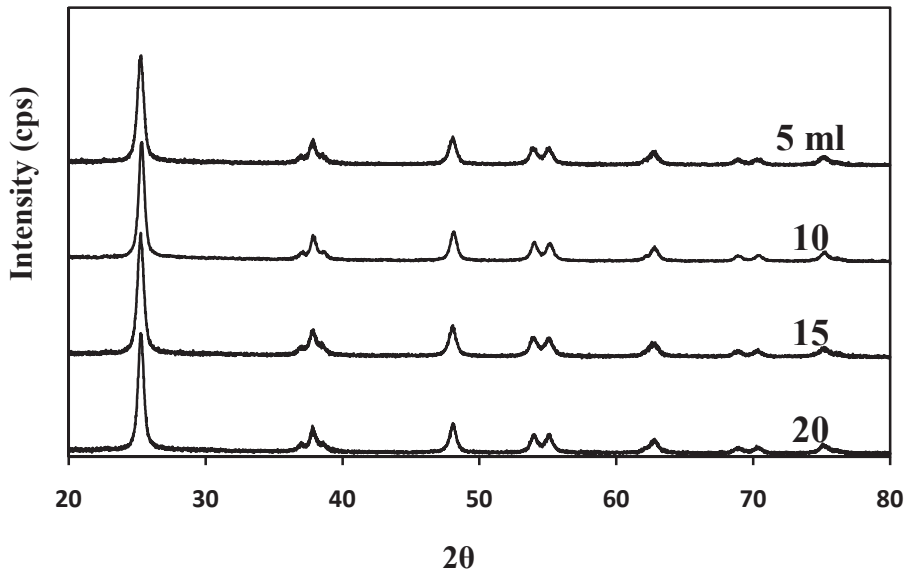

Figure 5.16 XRD patterns of TiO_2 based photocatalysts prepared by ST with differrent TIPT concentration

The effect of amount of Ti was studied by varied TIPT as Ti precursor with 5, 10, 15 and 20 ml in 100 ml of heptane solvent. The XRD patterns of this effect are shown in Figure 5.16. It can be obviously seen that the phase structure of the particles is crystalline and exclusively of anatase phase with similar intensity of peak, indicating that all studied Ti concentration have similar crystallinity. The average crystallite size was calculated according to the Debye-Scherrer equation, as shown in Table 5.4. The average crystallite size of all the samples is about 14 nm. Therefore, it can be concluded that Ti concentration does not change the crystalline phase, crystallite size and crystallinity of products in this studied condition. BET surface areas of all the samples are given in Table 5.4. It can be seen that increasing Ti concentration resulted in decrease in the surface area of TiO_2 product. This result is supported from agglomeration of TiO_2

particle, indicating that high Ti concentration promote agglomeration of TiO_2 particle, resulting in decrease the surface area. However,concentration of Ti does not effect to porosity of product, which was obtained from N_2 physisorption analysis as shown in Figure 5.17 and 5.18. The products with different Ti concentration are similar of N_2 adsorption-desorption isotherm and pore size distribution.

Table 5.4 Physical properties of TiO_2 prepared by ST with different Ti concentration

TIPT (ml)	d_{XRD}[a] (nm)	Relative[b] crystallinity	S_{BET}[c] (m^2/g)	S_{XRD}[d] (m^2/g)	S_{BET}/S_{XRD}	Pore[c] diameter (nm)	Pore[c] volume (cm^3/g)
5	13.8	1.00	112.3	113.4	0.99	9.3	0.2659
10	14.0	1.02	100.1	112.2	0.89	9.4	0.4027
15	14.6	1.05	78.0	107.2	0.73	9.4	0.3348
20	14.3	1.03	64.5	109.8	0.59	9.3	0.2836

a) Base on XRD line broadening

b) Comparison of height main peak of anatase by using 5 ml of TIPT as reference

c) N_2 physisorption analysis

d) Calculated surface area assuming that the particles are nonporous spheres ($S=6/\rho d_{XRD}$)

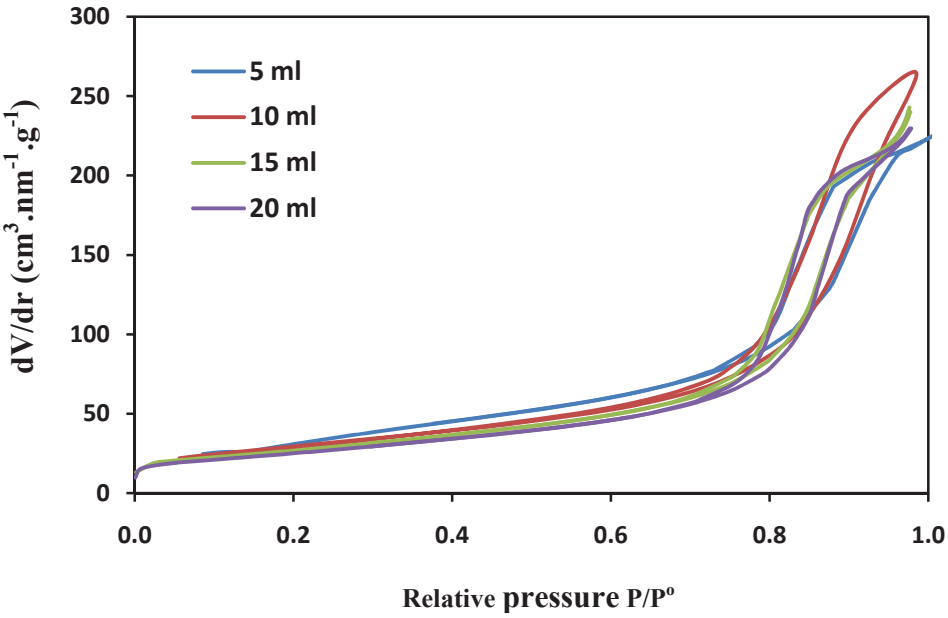

Figure 5.17 N_2 adsorption/desorption isotherms of TiO_2 prepared by ST in HT with different amount of TIPT

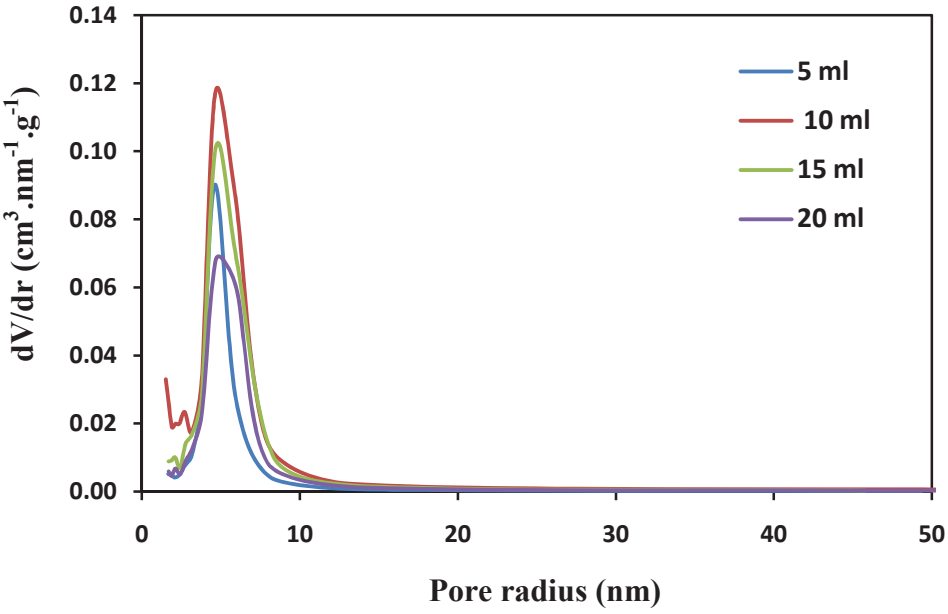

Figure 5.18 Pore size distribution of TiO_2 prepared by ST in HT with different amount of TIPT

5.1.5 Effect of calcined temperature

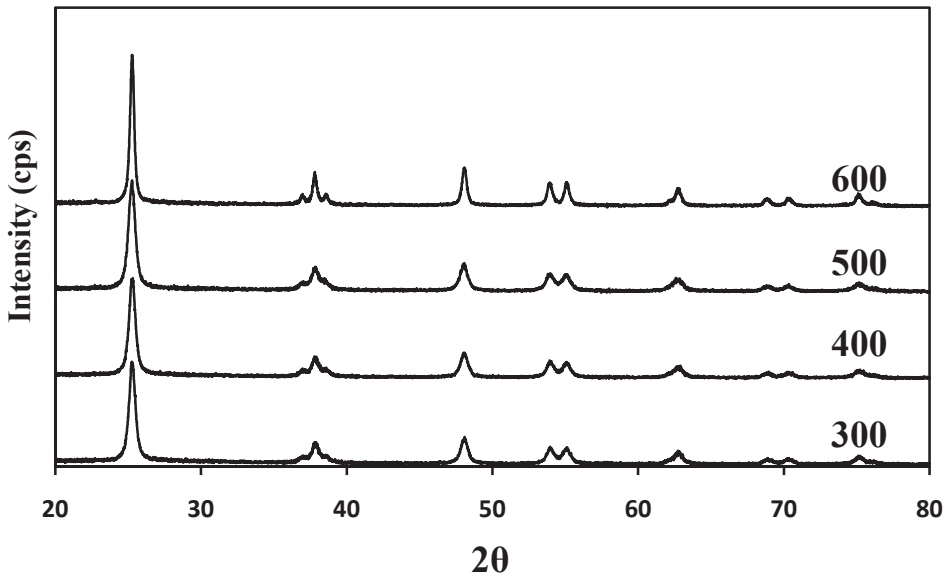

Figure 5.19 XRD patterns of TiO_2 based photocatalysts prepared by ST with diferrent calcined temperature

Generally, calcination of synthezied TiO_2 particles in order to remove impurity, enhancing crystallinity and phase transfromation of TiO_2. Temperature calcination of this research was varied at 300, 400, 500 and 600 ^oC, respectively. However, the result of calcination in this work is found that at 300-600 ^oC does not change phase structure, all samples are anatase phase as shown in Figure 5.19. TiO_2 prepared by sol-gel method consisted small rutile phase at calcination temperature of 600 ^oC [50]. So that, TiO_2 prepared by solvothermal method provide stability of anatase phase, which according to W. Payakgul et al. [22], they prepared TiO_2 particles by solvothermal method in toluene. Moreover, in the range of 300-500 ^oC was also found that crystalinity and crytallite size are unchanged, indicating that increasing temperature do not effect in increasing crytallinity and crystallite size, it is explaned that crytallinity

and crytallite size are carried out in preparation of TiO_2 by solvothermal step. On the other hand, at 600 ^oC clearly enhance crytallinity and crystallite size. This result indicates that the temperature effect on enhancing of crystallinity and crystallite size of TiO_2 crystals because temperature of calcination rearrang in TiO_2 crystals and promote sintering of TiO_2 crystal, resulting in improving of crystallinity and crystallite size, repectively as shown in Table 5.5. The BET surface area and porosity of TiO_2 products with calcination at 300-600 ^oC are given in Table 5.5. It can be seen that surface area and pore size increases in the order at 300 ^oC until 500 ^oC because of impurity removing. Calcinnation at 600 ^oC carried out sintering of TiO_2 crystals, resulting of surface area decreasing. However, N_2 adsorption-desorption isotherm in Figure 5.20 and pore size distribution in figure 5.21 of all samples show similar feature, indicating that the pore structure is similar in different temperature of calcination.

Table 5.5 Physical properties of TiO_2 prepared by ST with different calcined temperature

Temperature (^oC)	**d_{XRD}[a] (nm)**	**Relative[b] crystallinity**	**S_{BET}[c] (m^2/g)**	**Pore[c] diameter (nm)**	**Pore[c] volume (cm^3/g)**
300	14.1	1.00	79.8	6.7	0.3255
400	14.2	0.99	87.6	7.8	0.3632
500	14.0	1.05	100.1	9.4	0.4027
600	24.2	1.52	62.2	16.0	0.2877

a) Base on XRD line broadening

b) Comparison of height main peak of anatase by using 300 ^oC of calcined temperature as reference

c) N_2 physisorption analysis

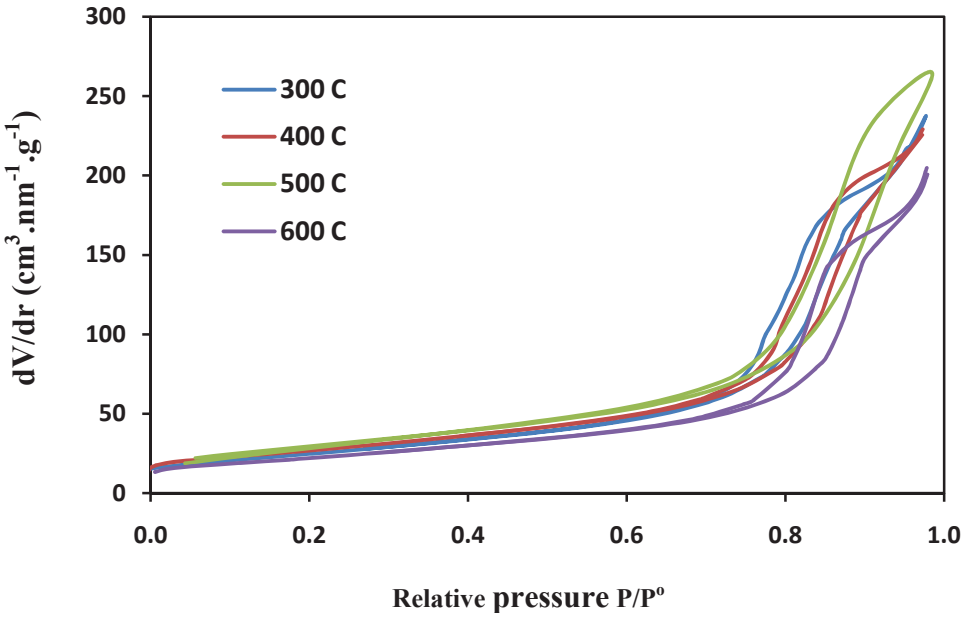

Figure 5.20 N_2 adsorption/desorption isotherms of TiO_2 prepared by ST in HT with different calcined temperatures

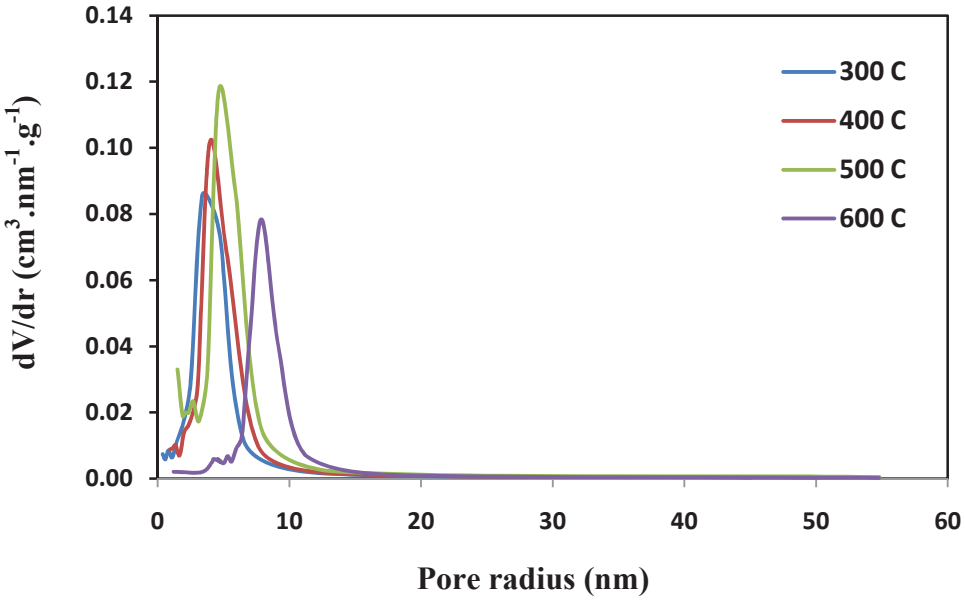

Figure 5.21 Pore size distribution of TiO_2 prepared by ST in HT with different calcined temperatures

5.1.6 Effect of Au modified TiO_2 method

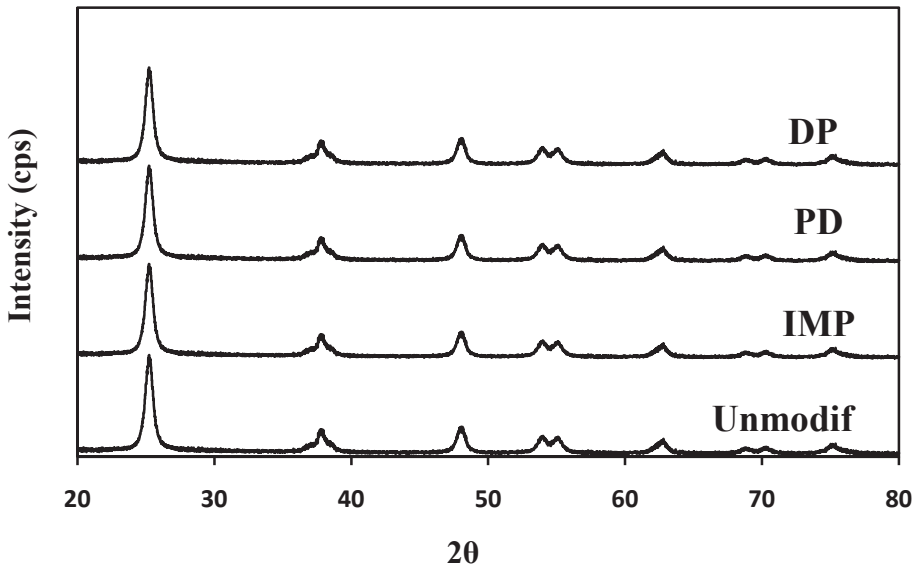

Figure 5.22 XRD patterns of Au modified TiO_2 by PD, DP and IMP

From XRD patterns of Au modified TiO_2 based photocatalyst by photodeposition (PD), impregnation (IMP), and doping (DP), when TiO_2 based photocatalyst prepared by ST in BD at 300 ^oC show in Figure 5.22, the diffactrograms mainly exhibit the crytalline structure of the anatase phse, which is similar to that of the unmodified TiO_2. From the XRD results, the indistinguishable presence of the diffraction peak of Au at 44.0 [68] indicates that the loaed Au particles are in vary high dispersion. As the minimum detection limit of the XRD technique for any crystalline materials is around 5 nm, it is inferred that the crystallite sizes of the Au particles may be approximately equal to or below this value. In addition, the loaded Au content was relatively low [49]. Moreover, all the methods do not change physical properties from unmodified TiO_2 such as crystallite size, BET surface area and porosity as shown in Table 5.6 and Figure 5.23 and 5.24. The actual metal loadings of the Au modifed TiO_2

photocatalysts obtained from ICP were not significantly different from the nominal Au loadings for DP and IMP method, while PD differently provide between actual and nominal Au loading as shown in Table 5.6. This implies that the IMP and DP methods used for Au modified TiO_2 is reliably effective in controlling any desired cocatalyst loading than PD method. From resulte of H_2 chemisorption in Table 5.6 is found that active site of Au particle modified TiO_2 by PD and DP are clearly higher than IMP because of high dispersion of Au particles.

Table 5.6 Physical properties of Au modified TiO_2 by IMP, PD and DP

Au modified method	Actual Au loading[a] (wt.%)	d_{XRD}[b] (nm)	S_{BET}[c] (m^2/g)	Pore[c] diameter (nm)	E_g[d] (eV)	H_2 Chemisorption[e] (µmol/g)	Au Dispersion[e] (%)
Unmodified	-	11.8	116.9	11.8	3.26	n.d.	-
PD	0.26	11.7	101.2	11.3	3.18	12.1	36.67
IMP	0.25	11.7	112.5	12.2	3.10	7.9	23.94
DP	0.26	12.1	115.2	12.1	3.10	10.8	32.73

n.d. = not detected

a) ICP analysis (Nominal Au loading : 1.00, 0.26 and 0.26 wt.% of PD, DP and IMP, respectively)

b) XRD analysis

c) N_2 physisorption analysis

d) UV-visible spectroscopy analysis

e) H_2 chemisorption analysis

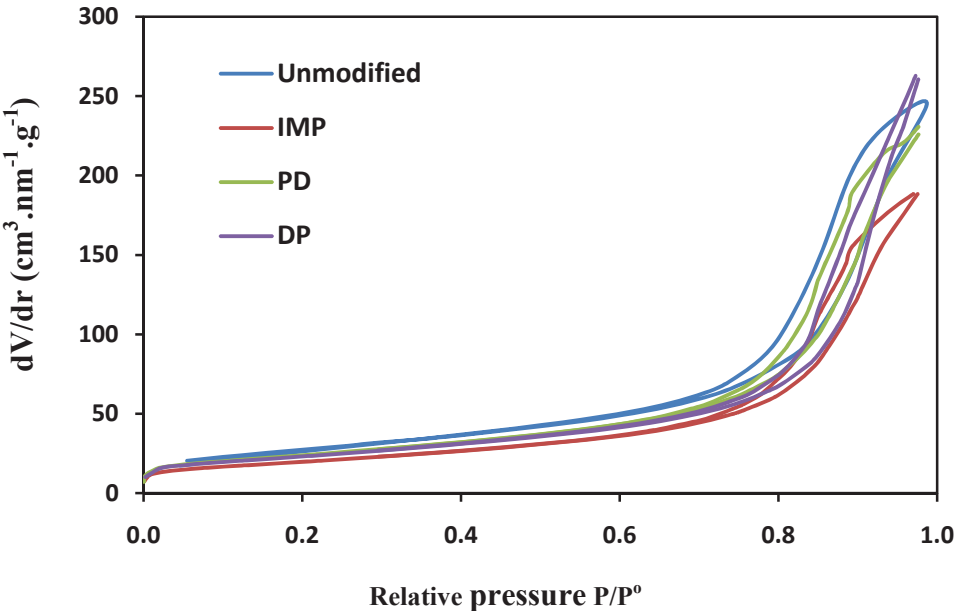

Figure 5.23 N_2 adsorption/desorption isotherms of Au modified TiO_2 by IMP, PD and DP

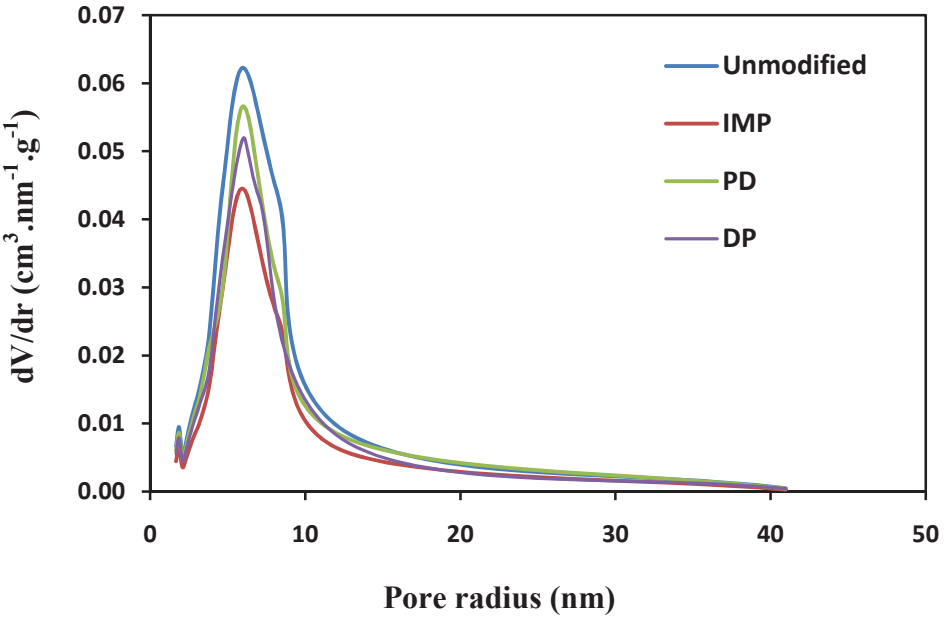

Figure 5.24 Pore size distribution of Au modified TiO_2 by IMP, PD and DP

The light-harvesting ability of all the Au modified methods were determined from their UV-vis DRS in the range from 200 to 800 nm. The UV part of the spectra was very similar for all the samples, presenting the characteristic absorption threshold around 400 nm, i.e. very close to that of pure anatase. Band gap energys were found that Au modified TiO_2 with these methods hardly change main band gap energy when comparing to unmodified TiO_2 (see Table 5.6). However, all the Au modified methods also show that the presence of Au greatly contributes to the increase in the light-harvesting ability within the visible region (λ >400 nm), which it significantly enhanced the visible light-harvesting ability up to a wavelength of 800 nm, as shown in Figure 5.25. In the visible part of the spectra the surface plasmon band of metallic gold could be observed for the Au modified TiO_2 by PD, DP and IMP around 540, 550 and 600 nm, respectively. For gold nanoparticles a strong dependence between particle size and plasmon bandwidth and position has been reported [68]. The bandwidth of the surface plasmon absorption (SPA) grows upon increasing the mean particle size for gold deposits larger than 25 nm [68]. Thus, the difference of bandwidths in the samples prepared with PD,IMP and DP would confirm the larger size of the gold deposits obtained IMP. The position of the absorption maximum of the SPA also depends on the particle size, with red-shifts when increasing the particle diameters for gold particles larger than 25 nm and both red- and blue-shifts for smaller metal particles [68]. For this reason, considering that in our case the difference in the position of the SPA between the PD and DP is just about 10 nm, the position of the SPA does not ensure any valid indication about the size of the deposits. The PL emission spectra can be used to disclose the efficiency of charge carrier trapping, immigration, transfer and to understand the fate of photo-induced electrons and holes in semiconductor [80]. It is known that the PL spectrum is the result of the recombination of excited electrons and holes, the lower PL intensity may indicate the lower recombination rate of electrons-holes under light irradiation [80]. Figure 5.26 shows the PL spectra of Au modified TiO_2 photocatalyst. The PL intensities vary in the following order: DP > PD > IMP > Unmodified TiO_2. This result can be concluded that an Au can reduce the recombination rate of photoinduced electrons and holes in Au modified TiO_2 and the recombination rate also depends Au modified method. Au

modified TiO_2 by is least recombination rate of charges, it may contribute decreasing recombination in both bulk and surface photocatalyst. In addition, this also shows that the PL curve does not shifted to the right (the longer wavelength) in Au modified TiO_2 compared to unmodified TiO_2. This result means that the band gap of TiO_2 anatase was not changed to low energy [21], which according to the result from UV-vis DRS.

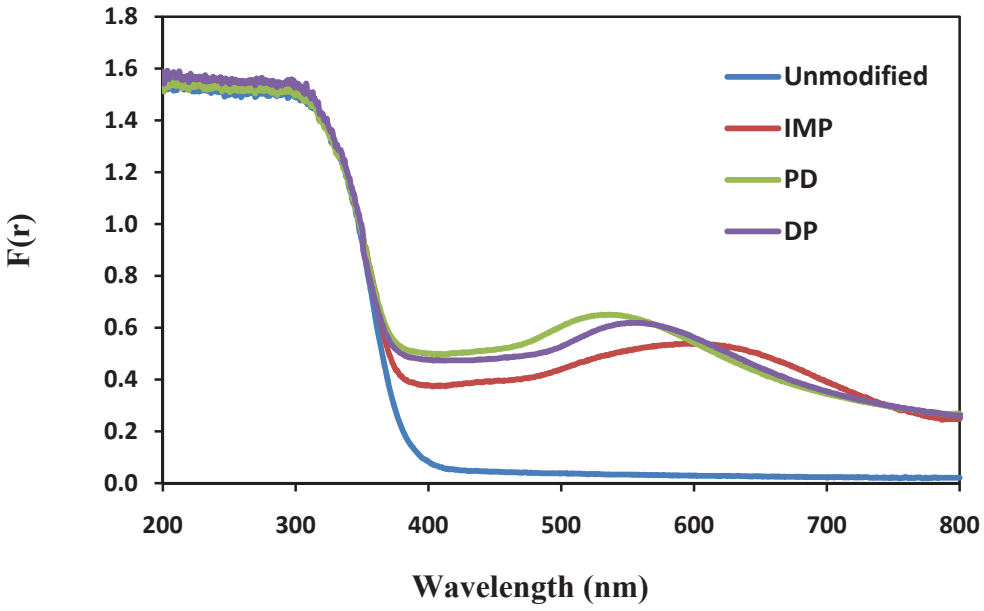

Figure 5.25 UV-vis DRS of Au modified TiO_2 by IMP, PD and DP

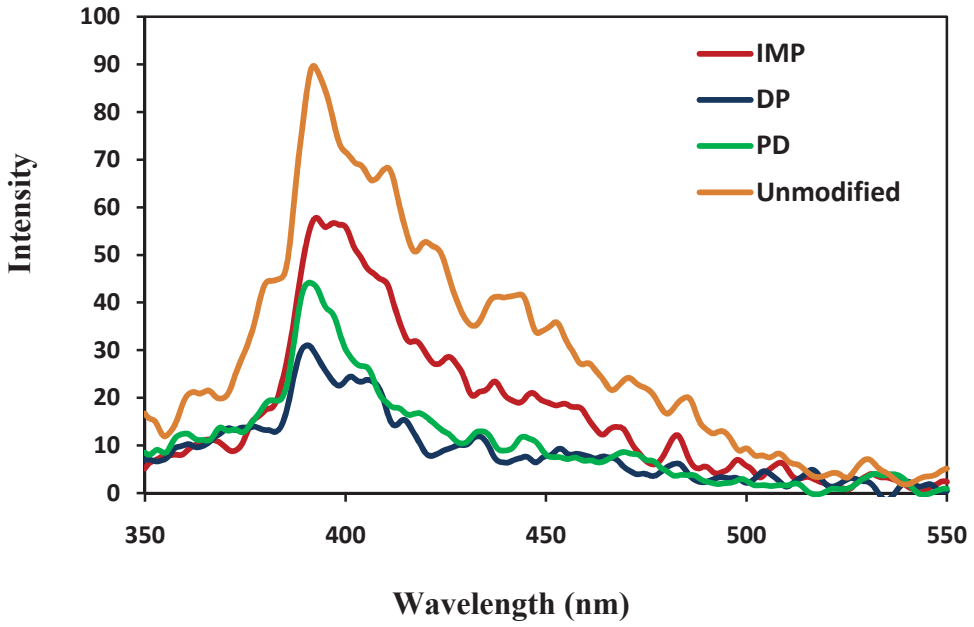

Figure 5.26 The PL emission spectra of Au modified TiO_2 by IMP, PD and DP

5.2 Photocatalytic H_2 production

5.2.1 Effect of TiO_2 preparation method

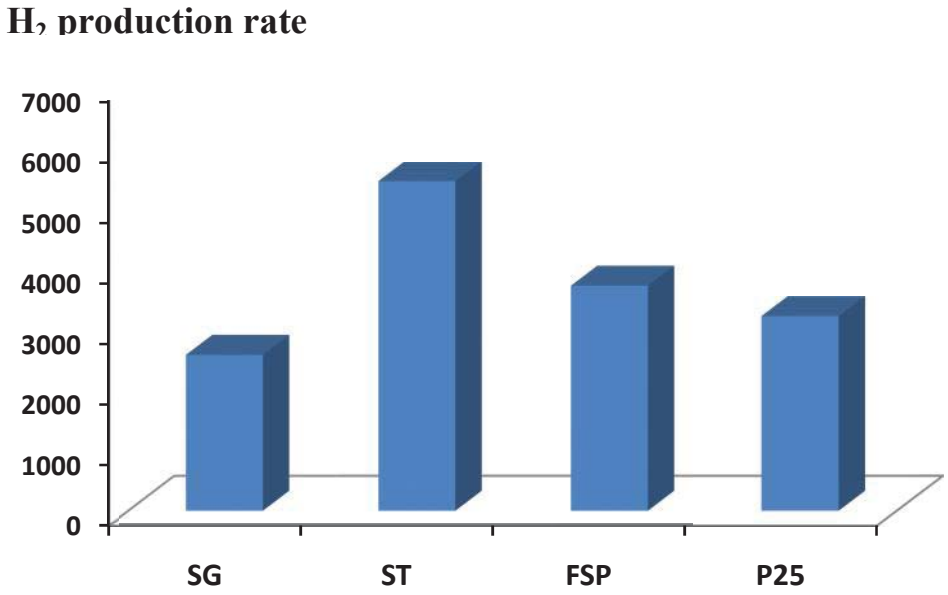

Figure 5.27 Effect of preparation method of TiO_2 particles on photocatalytic H_2 production rate

The photocatalytic activity of TiO_2 particles prepared by SG, ST and FSP with comparing to P25 as commercial TiO_2 were examined by measurement of the photocatalytic H_2 production rate from aqueous formic acid solution with 0.26wt.% of Au loading by photodeposition under simulated solar light. As shown in Figure 5.12, the photocatalytic H_2 production rate of TiO_2 prepared by ST is highest in among of the studied methods because this method provided highest specific surfacarea and smallest nanocrystallite size of TiO_2. It well known that high surface area and small crystallite

size promote active site and fast transference of e^-/h^+ onto the surface of TiO_2. In addition, this method provided suitable pore size in mesoporous rang. The mesopore have been proved increasing of photocatalytic activity of photocatalysts. From the result of photocatalytic H_2 production with different preparation method, it can said that the preparation method of TiO_2 photocatalyst highly affected physical properties of TiO_2 particles and their photocatalytic activity. So that, ST method was selected in preparation of TiO_2 particles for photocatalytic H_2 production and it was determined suitable condition for praparation of TiO_2 with high photocatalytic activity.

5.2.2 Effect of solvent type in TiO_2 preparation by solvothermal

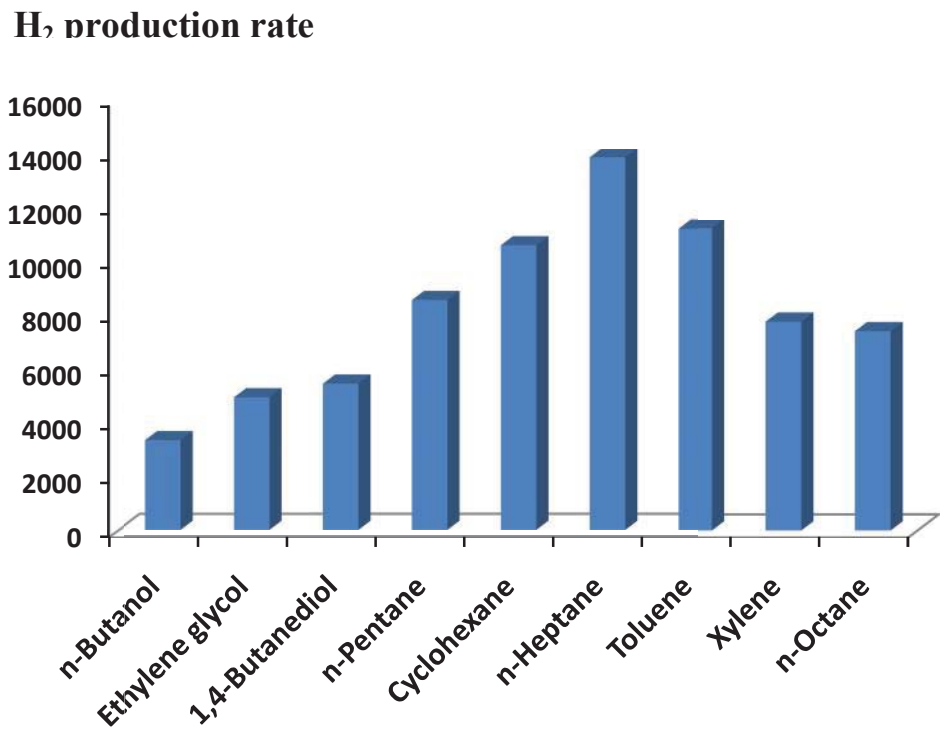

Figure 5.28 Effect of solvent type of TiO_2 preparation by ST on photocatalytic H_2 production rate

Generally, solvent extremely affect physical and chemical properties of photocatalyst and their photocatalytic activity for photocatalyst preparation by solvothermal method [24], so that, the type of solvent were firstly varied in the TiO_2 prepared by this method. Figure 5.13 show the photocatalytic H_2 production rate of TiO_2 preparation by solvothermal method with using different solvents. Usually, photocatalytic H_2 production rate related specsific surface area, high surface area provided high active size, hence, high photocatalytic activity. Although TiO_2 prapared in 1,4 butanediol provided highest surface area but provided low crystallinity, which crystallinity affect charge transference, hence, the photocatalytic H_2 production rate of them were lower than other studied solvent with lower specific surface area. On the other hand, TiO_2 prepared in heptane and toluene provied similar surface are, but heptane was higher H_2 production rate than toluene, because it was higher agglomeration of crytallite TiO_2 than in toluene. The agglomeration of TiO_2 crystals decrease recombination rate of e^-/h^+ pair, increasing photocatalytic activity.

5.2.3 Effect of temperature in TiO_2 preparation by solvothermal

Figure 5.29 shows effect of solvothermal temperrature in preparation of TiO_2 powders on photocatalytic H_2 production in aqueous formic acid solution with 0.26 wt.% of Au loading by photodeposition under simulated solar light. It can be seen that preparation at 300 ^oC is higher than 250 ^oC for all studied solvents because solvothermal temperature at 300 ^oC of TiO_2 preparation provide high crystallinity and consists of anatase crystals without contamination of amorphous phase in the TiO_2 particles even if smaller surface area and crystallite size. Although high surface area and small nanocrytallite size provide high active sive and fast transference of charges to surface of photocatalyst, respectively. This indicates that cystallinity has effect to photocatalytic activity, it is well known that high crystallinity contributes easy mobility of charges in

the bulk photocatalyst while amorphous TiO_2 does not active in photocatalytic reaction [5,14].

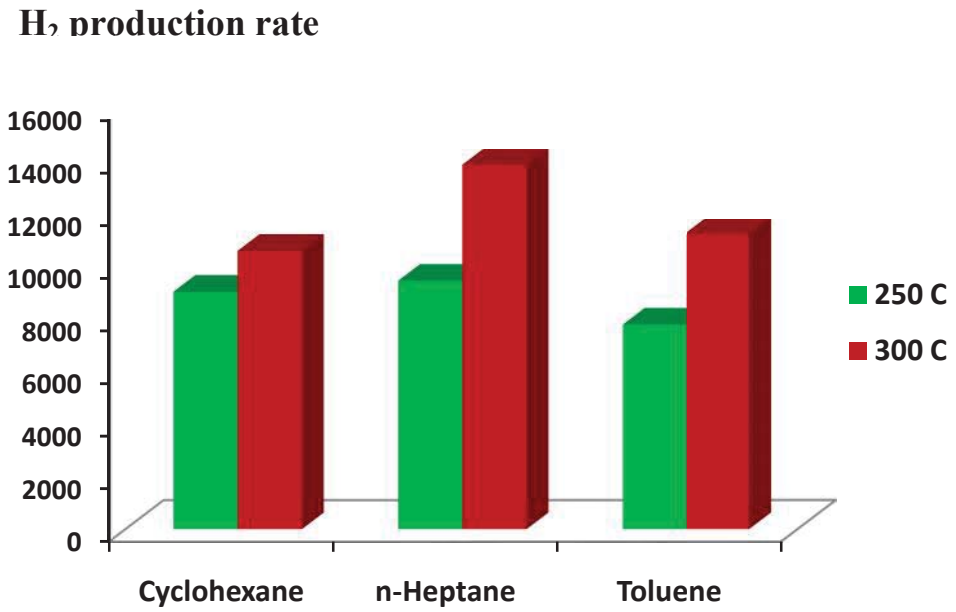

Figure 5.29 Effect of temperature in TiO_2 preparation by ST on photocatalytic H_2 production rate

5.2.4 Effect of Ti concentration in TiO_2 preparation by solvothermal

The photocatalytic H_2 production was examined to studied the effect of Ti concentration in TiO_2 preparation by solvothermal method. This result is shown in Figure 5.30. It was found that TIPT-to-solvent volume ration is 10/100 gave optimum concentration for providing TiO_2 with highest H_2 production rate. The H_2 production rate increased with increasing TIPT until 10 ml of TIPT, after that the H_2 production rate decreased with increasing TIPT. This result was explained that TiO_2 particles preparation with 5 ml of TIPT hardly agglomerated althrough highest surface area. Generally, agglomeration of TiO_2 particles contribute decreasing of charge recombination rate, resulting in increase photocatalytic activity. While the higher TIPT than 10 ml, TiO_2

particles significantly agglomerated, resulting in decreased surface area. Therefore, photocatalytic H_2 production rate decreased when increasing TIPT.

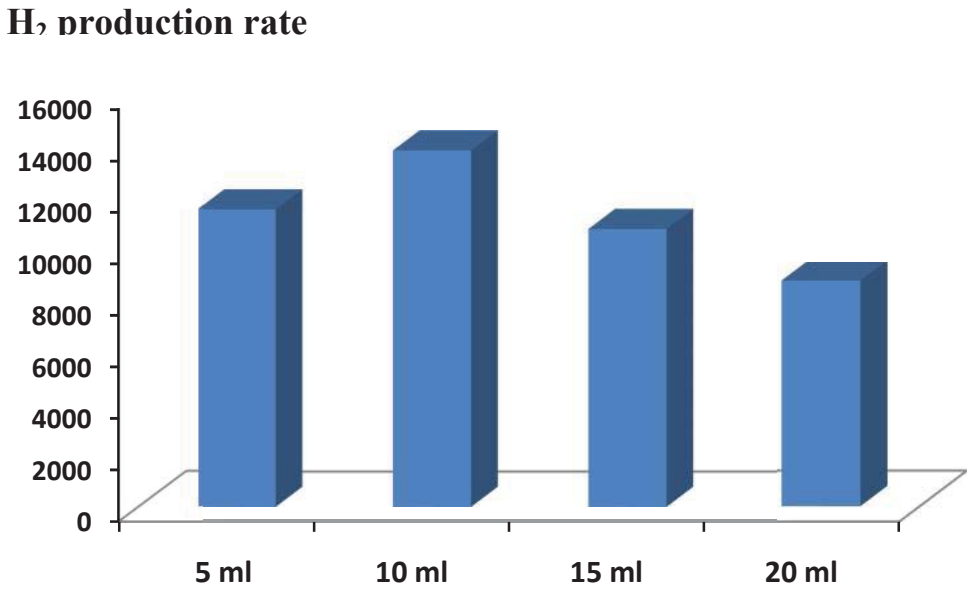

Figure 5.30 Effect of TIPT concentration in TiO_2 preparation by ST on photocatalytic H_2 production rate

5.2.5 Effect of calcined temperature

The effect of calcine temperature of synthesized TiO_2 by solvothermal is shown in Figure 5.31. It was found that photocatalytic H_2 production rate increased with increasing temperature of calcination, after that the H_2 production rate decreased at 600 ^oC of calcined temperature. This result was explained that at lower calcined temperature at 500 ^oC provided low surface area because the TiO_2 particle contaminated impurity, while the higher temperature of calcination at 500 ^oC carried out significant sintering of TiO_2 particle to large particle size, resulting in decreased surface area of suface reaction even if high crystallinity. Therefore, photocatalytic H_2 production rate is highest at 500 ^oC of temperature of calcination.

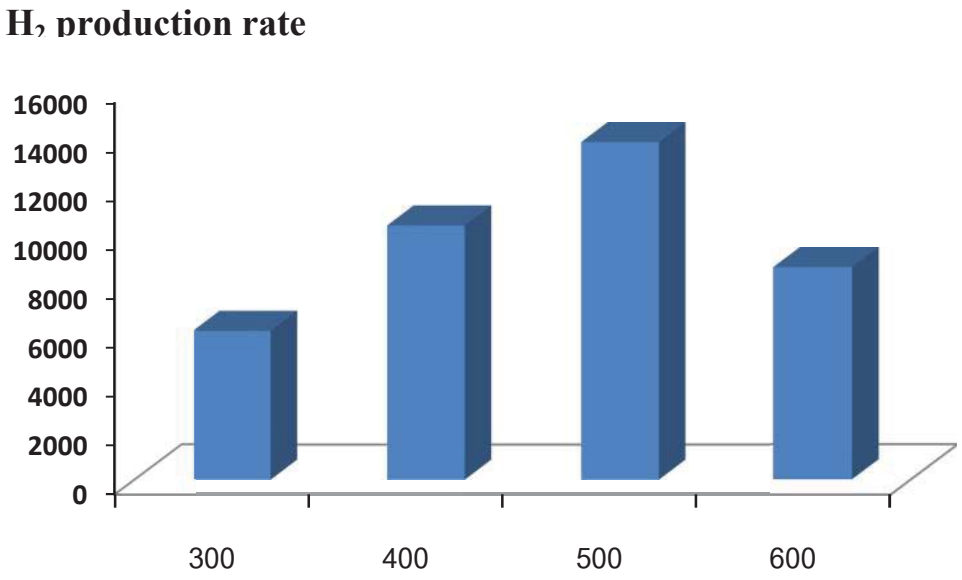

Figure 5.31 Effect of calcined temperature on photocatalytic H_2 production rate

5.2.6 Effect of Au cocatalyst modified method

The photocatalytic H_2 production rate in Figure 5.32 is exhibited the effect of Au modified TiO_2 with photodeposition (PD), impregnation (IMP) and doping (DP) compared to unmodified TiO_2. It was found that TiO_2 was modified by Au greatly enhanced photocatalytic activity. This result was explained the roles of Au seem to involve the attraction and trapping of photogenerated electrons, the reduction of protons and the formation and desorption of H_2 [65]. The H_2 production rate of DP and PD method exhibited higher than IMP because these method provided high absorption of visible light, small nanoparticle size of Au, high active sites of Au and low charges recombination rate, resulting photocatalytic activity of them are higher than IMP method [63,64]. However, DP and PD method show the same photocatalytic H_2 rate. Althrough the Au active sites of DP are smaller than PD, but charges recombination rate in DP is smaller than in PD. So that, the both method showed same high efficiency of cocatalyst modification for photocatalysis.

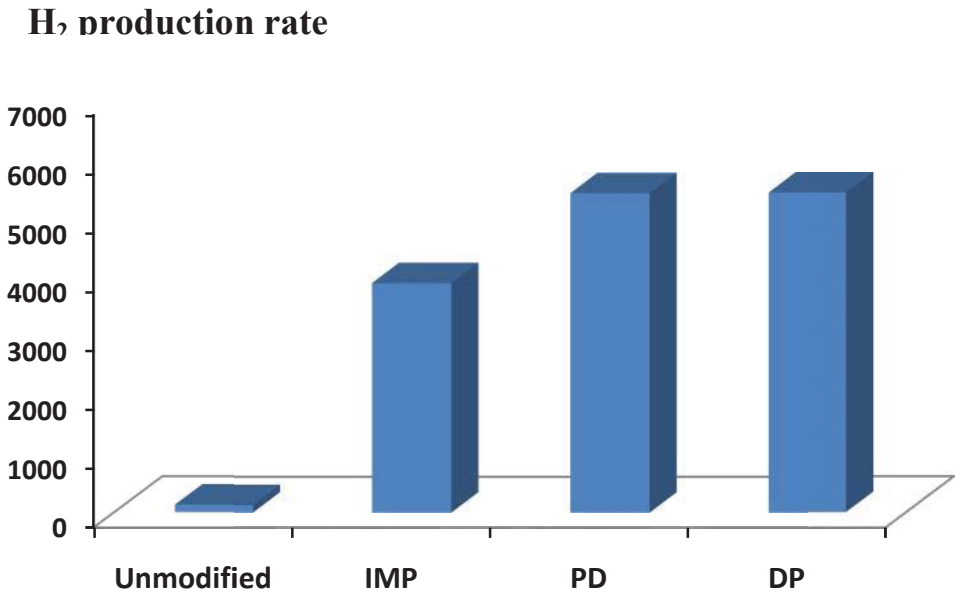

Figure 5.32 Effect of Au modified method on photocatalytic H_2 production rate

CHAPTER 6

CONCLUSIONS AND RECOMMENDATION

The physical properties such as surface area, crytallinity and porosity of TiO_2 particles can be modified by using different preparation method or different condition. The balance of surface area, crystallinity, porosity and pore structure were found to be responsible for the activity of the photocatalytic H_2 production, these properties were obtained from selecting suitable preparation method and suitable condition. The suitable method is the solvothermal method with preparation condition of heptane as solvent, synthesized temperature of 300 ^oC, TIPT-to-heptane volume ratio of 10:100 and calcination temperature of 500 ^oC.

Due to the H_2 production results, the loaded Au particles can significantly increased the photocatalytic activity of TiO_2 under simulated solar light. Photodeposition and doping methods were found to be the suitable method for the TiO_2 modification with Au. The best Au modified TiO_2 exhibited the H_2 production rate of 13,786 $\mu mol.h^{-1}.g_{cat}^{-1}$.

The recommendations for further study were suggested as follows:

1. The Au modified TiO_2 should be developed to decreased band gap energy by using cation or anion doping and to enhanced oxidation reaction on photocatalyst surface by loading oxidation site such as RuO_2 or IrO_2.

2. The optimal amount of Au loading should be investigated to enhanced the photocatalytic H_2 production activity of the TiO_2 based photocatalyst.

BIBLIOGRAPHY

[1] T. Sakata. “Photocatalysis of irradiated semiconductor surfaces:its application to water splitting and some organic reaction.” J. Photochem. 29 (1985) : 205-215.

[2] A. Patsoura, D.I. Kondarides, and X.E. Verykios. “Photocatalytic degradation of organic pollutants with simultaneous production of hydrogen.” Catal. Today 124 (2007) : 94-102.

[3] M. Matsuoka, M. Kitano, M. Takeuchi, K. Tsujimaru, M. Anpo, and J.M. Thomas. “Photocatalysis for new energy production recent advances in photocatalytic water splitting reactions for hydrogen production.” Catal. Today 122 (2007) : 51-61.

[4] R.M. Navarro, F. del Valle, J.A. Villoria de la Mano, M.C. Alvarez-Galvan, and J.L.G. Fierro. “Photocatalytic water splitting under visible light: concept and catalysts development.” Adv. Chem. Eng. 36 (2009) : 111-143.

[5] A. Kudo and Y. Miseki. “Heterogeneous photocatalyst materials for water splitting.” Chem. Soc. Rev. 38 (2009) : 253-278.

[6] X. Chen, S. Shen, L. Guo, and S.S. Mao. “Semiconductor-based photocatalytic hydrogen generation.” Chem. Rev. 110 (2010) : 6503-6570.

[7] H. Bahruji, M. Bowker, P.R. Davies, L.S. Al-Mazroai, A. Dickinson, J. Greaves, D. James, L. Millard, and F. Pedrono, “Sustainable H_2 gas production by photocatalysis.” J. Photochem. Photobiol. 216 (2010) : 115-118.

[8] F.E. Osterloh and B.A. Parkinson. “Recent developments in solar water-splitting photocatalysis.” Mater. Res. Soc. 36 (2011) : 17-22.

[9] O. Carp, C.L. Huisman,and A. Reller. “Photoinduced reativity of titanium dioxide.” Prog. Solid State Chem. 32 (2004) : 33-177.

[10] A. Fujishima and X. Zhang. “Titanium dioxide photocatalysis: present situation and future approaches.” C.R. Chimie 9 (2006) : 750-760.

[11] G. Liu, L. Wang, H.G. Yang, H.M. Cheng, and G.Q. Lu. “Titania-based photocatalysts---crystal growth, doping and heterostructuring.” J. Mater. Chem. 20 (2010) : 831-843.

[12] M. Ni, M.K.H. Leung, D.Y.C. Leung, and K. Sumathy. “A review and recent developments in photocatalytic water-splitting using TiO_2 for hydrogen production.” Renew. Sustain. Energy Rev. 11 (2007) : 401-425.

[13] A. Fujishima, X. Zhang, and D.A. Tryk. “TiO_2 photocatalysis and related surface phenomena.” Surf. Sci. Rep. 63 (2008) : 515-582.

[14] A.R. Khtaee and M.B. Kasiri. “Photocatalytic degradation of organic dyes in the presence of nanostructured titanium dioxide: Influence of the chemical structure of dyes.” J. Mol. Catal. 328 (2010) : 8-26.

[15] F.E. Osterloh. “Inorganic materials as catalysts for photochemical splitting of water.” Chem. Mater. 20 (2008) : 35-54.

[16] J. Zhu and M. Zach. “Nanostructured materials for photocatalytic hydrogen production.” Curr. Opin. Colloid Interface Sci. 14 (2009) : 260-269.

[17] M. Kang, S.Y. Lee, C.H. Chung, S.M. Cho, G.Y. Han, B.W. Kim, and K.J. Yoon. “Characterization of a TiO_2 photocatalyst synthesized by the solthermal method and its catalytic performance for $CHCl_3$ decomposition.” J. Photochem. Photobiol. 144 (2001) : 185-191.

[18] M. Kang. “Synthesis of Fe/TiO_2 photocatalyst with nanometer size by solvothermal method and the effect of H_2O addition on structural stability and photodecomposition of methanol.” J. Mol. Catal. 197 (2003) : 173-183.

[19] W.S. Nam and G.Y. Han. “Characterization and photocatalytic performance of nanosize TiO_2 powders prepared by the solvothermal method” Korean J. Chem. Eng. 20 (2003) : 1149-1153.

[20] D.Wanga, R. Yu, Y. Chen, N.Kumada, N.Kinomura, and M. Takano. “Photocatalysis property of needle-like TiO_2 prepared from a novel titanium glycolate precursor.” Solid State Ionics 172 (2004) : 101-104.

[21] M. Kang, Y.R.Ko, M.K.Jeon, S.C. Lee, S.J.Choung, J.Y. Park, S. Kim,and S.H. Choi. “Characterization of Bi/TiO_2 nanometer size particle synthesized by solvothermal method and CH_3CHO decomposition in a plasma-photocatalytic system.” J. Photochem. Photobiol. 173 (2005) : 128-136.

[22] W. Payakgul, O. Mekasuwandumrong, V. Pavarajarn, and P. Praserthdam. "Effects of reaction medium on the synthesis of TiO_2 nanocrystals by thermal decomposition of titanium (IV) n-butoxide." Caram. Int. 31 (2005) : 391-397.

[23] W. Kongsuebchart, P. Prasertdam, J. Panpranot, A. Sirisuk, P. Supphasrirongjaroen, and C. Satayaprasert. "Effect of crystallite sie on the surface defect of nano-TiO_2 prepared via solvothermal synthesis." J. Crystal Growth 297 (2006) : 234-238.

[24] G. Demazeau. "Solvothermal reactions: an original rote for th synthesis of novel materials." J. Mater. Sci. 43 (2008) : 2104-2114.

[25] S. Yin, S. Akita, M. Shinozaki, R. Li, and T. Sato. "Synthesis and morphological control of rare earth oxide nanoparticles by solvothermal reaction." J. Mater. Sci. 43 (2008) : 2234-2239.

[26] A. Sirisuk, E. Klansorn, and P. Prasertdam."Effects of reaction medium and crystallite size on Ti^{3+} surface defects in titanium dioxide nanoparticles prepared by solvothermal method." Catal. Commun. 9 (2008) : 1810-1814.

[27] R. Sasikala, V. Sudarsan, C. Sudakar, R. Naik, L. Panicker, and S.R. Bharadwaj. "Modification of the photocatalytic properties of self doped TiO_2 nanoparticles for hydrogen generation using sunlight type radiation." Int. J. Hydrogen Energy 34 (2009) : 6105-6113.

[28] Y. Lee, J. Chae, and M. Kang. "Comparison of the photovoltaic efficiency on DSSC for nanometer sized TiO_2 using a conventional sol-gel and solvothermal methods." J. Ind. Eng. Chem. 16 (2010) : 609-614.

[29] R. Mueller, L. Madler, and S.E. Pratsinis. "Nanoparticle synthesis at high production rates by flame spray pyrolysis." Chem. Eng. Sci. 58 (2003) : 1969-1976.

[30] W.Y. Teoh, L. Madler, D. Beydoun, S.E. Pratsinis, and R. Amal. "Direct(one-step)synthesis of TiO_2 and Pt/TiO_2 nanoparticles for photocatalytic mineralization of sucrose." Chem. Eng. Sci. 60 (2005) : 5852-5861.

[31] R. Strobel, A. Baiker, and S.E. Pratsinis. "Flame aerosol synthesis of smart catalysts." Adv. Powd. Techno. 17 (2006) : 457-480.

[32] R. Strobel and S.E. Pratsinis, “Flame aerosol synthesis of smart nanostructured materials.” J. Mater. Chem. 17 (2007) : 4743-4756.

[33] G.L. Chiarello, E. Selli, and L. Forni. “Photocatalytic hydrogen production over flame spray pyrolysis-synthesised TiO_2 and Au/TiO_2 .” Appl. Catal. 84 (2008) : 332-339.

[34] G.L. Chiarello, M.H. Aguirre, and E. Selli. “Hydrogen production by photocatalytic steam reforming of methanol on noble metal-modified TiO_2 .” J. Catal. 273 (2010) : 182-190.

[35] P. Pawinrat, O. Mekasuwandumrong, and J. Panpranot. “Synthesis of Au-ZnO and Pt-ZnO nanocomposites by one-step flame spray pyrolysis and its application for photocatalytic degradation of dyes.” Catal. Commun. 10 (2009) : 1380-1385.

[36] W.Y. Teoh, R. Amal, and L. Madler. “Flame spray pyrolysis: An enabling technology for nanoparticles design and fabrication.” Nanoscale 2 (2010) : 1324-1347.

[37] M. Ashokkumar. “An overwivew on semiconductor particulate systems forphotoproduction of hydrogen.” Int. Hydrgen Energy 23 (1998) : 427-438.

[38] R. Abe, K. Hara, K. Sayama, K. Domen, and H. Arakawa. “Steady hydrogen evolution from water on Eosin Y-fixed TiO_2 photocatalyst using a silane-coupling reagenr under visible light irradiation.” J. Photochem. Photobiol. 137 (2000) : 63-69.

[39] R. Abe, K. Sayama, and H. Arakawa. “Efficient hydrogen evolution from aqueous mixture of I^- and acetonitrile using a merocyanine dye-sensitized Pt/TiO_2 photocatalyst under visible light irradiation.” Chem. Phys. Lett. 362 (2002) : 441-444.

[40] J.S. Jang, S.M. Ji, S.W. Bae, H.C. Son, and J.S. Lee. “Optimization of CdS/TiO_2 nano-bulk composite phocatalysts for hydrogen production from Na_2S/Na_2SO_3 aquesous electrolyte solution under visible light ($\lambda \geq 420$ nm).” J. Photochem. and Photobiol. 188 (2007) : 112-119.

[41] Z. Zhang, P.A. and Maggard, "Investigation of photocatalytically-active hydrated forms of amorphous titania, $TiO_2.nH_2O$." J. Photochem. Photobiol. 186 (2007) : 8-13.

[42] T. Sreethawong, S. Laehsalee and S. Chavadej. "Comparative investigation of mesoporous- and non-mesoporous-assembled TiO_2 nanocrystals for photocatalytic H_2 production over N-doped TiO_2 under visible light irradiation." Int. J. Hydrogen Energy 33 (2008) : 5947-5957.

[43] T. Peng, K. Dai, H. Yi, D. Ke, P. Cai, and L. Zan. "Photosensitization of different ruthenium(II) complex dyes on TiO_2 for photocatalytic H_2 evolution under visible-light." Chem. Phys. Lett. 460 (2008) : 216-219.

[44] J.S. Jang, H.G. Kim, U.A. Joshi, J.W. Jang, and J.S. Lee. "Fabrication of CdS nanowires decorated with TiO_2 nanoparticles for photocatalytic hydrogen production under visible light irradiation." Int. J. Hydrogen Energy 33 (2008) : 5975-5980.

[45] M.A. Khan, S.I. Woo, and O.B. Yang,Int. "Hydrothemally stabilized Fe(III) doped titania active under visible light for water splitting reaction." J. Hydrogen Energy 33 (2008) : 5345-5351.

[46] T.Peng, D.Ke, P.Cai, K.Daia, L. Ma, and L.Zan. "Influence of different ruthenium(II) bipyridyl complex on the photocatalytic H_2 evolution over TiO_2 nanoparticles with mesostructures."J. Power Sources 180 (2008) : 498-505.

[47] Y.J. Zhang, W. Yan, Y.P. Wu, and Z.H. Wang. "Synthesis of TiO_2 nanotubes coupled with CdS nanoparticles and production of hydrogen by photocatalytic water decompodition." Mater. Lett. 62 (2008) : 3846-3848.

[48] A.A. Nada, H.A. Hamed, M.H. Barakat, N.R. Mohamed, and T.N. Veziroglu. "Enhancement of photocatalytic hydrogen production rate using photosensitized TiO_2/RuO_2-MV^{2+}." Int. J. Hydrogen Energy 33 (2008) : 3264-3269.

[49] T. Sreethawong, S. Laehsalee, S. Chavadej. "Use of Pt/N-doped mesoporous-assembled nanocrystalline TiO_2 for photocatalytic H_2 production under visible light irradiation." Catal.Commun. 10 (2009) : 538-543.

[50] T.Sreethawong, C.Junbua, and S.Chavadej. “Photocatalytic H_2 production from water splitting under visible light light irradiation using Eosin Y-sensitized mesoporous-assembled Pt/TiO_2 nanocrystal photocatalyst.” J. Power Sources 190 (2009) : 513-524.

[51] J.S. Jang, S.J. Hong, J.Y. Kim, and J.S. Lee. “Heterojunction photocatalyst TiO_2/$AgGaS_2$ for hydrogen production from water under visible light.” Chem. Phys. Lett. 475 (2009) : 78-81.

[52] G. Kim, and W. Choi. “Charge-transfer surface complex of EDTA-TiO_2 and its effect on photocatalysis under visible light.” Appl. Catal. 100 (2010) : 77-83.

[53] C. Li, J. Yuan, B. Han, L. Jiang, and W. Shangguan. “TiO_2 nanotubes incorporated with Cds for photocatalytic hydrogen production from splitting water under visible light irradiation.” Int. J. Hydrogen Energy 35 (2010) : 7073-7079.

[54] D.Chatterjee. “Effect of excited state redox properties of dye sensitizers on hydrogen production through photo-splitting of water over TiO_2 photocatalyst.” Catal. Commun. 11 (2010) : 336-339.

[55] H. Yan, and H. Yang,J. “TiO_2-g-C_3N_4 composite materials for photocatalytic H_2 evolution under visible light irradiation.” Alloys Compd. 509 (2011) : 26-29.

[56] P. Zeng, X. Zhang, X. Zhang, B. Chai, and T.Peng. “Efficient photocatalytic hydrogen production over Ni@C/TiO_2 nanocomposite under visible light irradiation.” Chem. Phys. Lett. 503 (2011) : 262-265.

[57] B.S. Huang, and M.Y. Wey. “Properties and H_2 production ability of Pt photodeposited on the anatase phase transition of nitrogen-doped titanium dioxide.” Int. J. Hydrogen Energy 36 (2011) : 9479-9486.

[58] L. Xiong, F. Yang, L. Yan, N. Yan, X. Yang, M. Qiu, and Y. Yu. “Bifunctional photocatalysis of TiO_2/Cu_2O composite under visible light: Ti^{3+} in organic pollutant degradation and water splitting.” J. Phys. Chem. Solids 72 (2011) : 1104-1109.

[59] O. Rosseler, M.V. Shankar, M.K. Le Du, L. Schmidlin, N. Keller, and V. Keller. “Solar light photocatalytic hydrogen production from water over Pt and

Au/TiO_2(anatase/rutile) photocatalysts: Influence of noble metal and porogen promotion." J. Catal. 269 (2010) : 179-190.

[60] K. Yu, K.L. Kelly, N. Sakai, and T. Tatsuma. "Morphologies and surface plasmon resonance properties of monodisperse bumpy gold nanoparticles." Langmuir 24 (2008) : 5849-5854.

[61] T.A. El-Brolossy, T. Abdallah, M.B. Mohamed, S. Abdallah, K. Easawi, S. Negm, and H. Talaat. "Shape and size dependence of the surface Plasmon resonance of gold nanoparticles studied by photoacoustic technique." Eur. Phys J. Special Topics 153 (2008) : 361-364.

[62] A. Iwase, H. Kato, and A. Kudo. "Nanosized Au particles as an efficient cocatalyst for photocatalytic overall water splitting." Catal. Lett. 108 (2006) : 7-10.

[63] T. Puangpetch, T. Sreethawong, and S. Chavadej. "Hydrogen production over metal-loaded mesoporous-assembled $SrTiO_3$ nanocrystal photocatalysis: Effects of metal type and loading." Int. J. Hydrogen Energy 35 (2010) : 6531-6540.

[64] C.G. Silva, R. Juarez, T. Marino, R. Molinari, and H. Garcia. "Influence of excitation wavelength (UV or visible light) on the photocatalytic activity of titania containing gold nanoparticles for the generation of hydrogen or oxygen from water." J. Am. Chem. Soc. xxx (xxxx).

[65] G.R. Bamwenda, S. Tsubota, T. Nakamura, and M. Haruta. "Photoassisted hydrogen production from a water-ethanol solution: a comparison of activities of $Au\text{-}TiO_2$ and $Pt\text{-}TiO_2$." J. Photochem. Photobiol. 89 (1995) : 177-189.

[66] S.C. Chan and M.A. Barteau. "Preparation of highly uniform Ag/TiO_2 and Au/TiO_2 supported nanoparticle catalysis by photodeposition." Langmuir 21 (2005) : 5588-5595.

[67] M.A. Behnajady, N. Modirshahla, M. Shokri, and B. Rad. "Enhancement of photocatalytic activity of TiO_2 nanoparticles by silver doping: photodeposition versus liquid impregnation methods." Global NEST J. 10 (2008) : 1-7.

[68] M.C. Hidalgo, J.J. Murcia, J.A. Navio, and G. Colon. “Photodeposition of gold on titanium dioxide for photocatalytic phenol oxidation.” Appl. Catal. 397 (2011) : 112-120.

[69] T. Sreethawong, and S. Yoshikawa. “Comparative investigation on photocatalytic hydrogen evolution over Cu-, Pd-, and Au-loaded mesoporous TiO_2 photocatalysts.” Catal. Commun. 6 (2005) : 661-668.

[70] B.Schimmoeller, S.E. Pratsinis, and A.Baiker. “Flame aerosol synthesis of metal oxide catalysts with unprecedented structural and catalytic properties.” Chem. Catal. Chem 3 (2011) : 1234-1256.

[71] M.K. Jeon and M. Kang. “Synthesis and characterization of indium-tin-oxide particles prepared using sol-gel and solvothermal methods and their conductivities after fixation on polyethyleneterephthalate films.” Mater. Lett. 62 (2008) : 676-682.

[72] P. Wang, T. Xie, D. Wang, and S. Dong. “Facile synthesis of TiO_2(B) crystallites/nanopores structure: A highly efficient photocatalyst.” J. Colloid Interf. Sci. 350 (2010) : 417-420.

[73] G. Tian, Y. Chen, K. Pan, D. Wang, W. Zhou, Z. Ren, and H. Fu. “Efficient visible light-induced degradation of phenol on N-doped anatase TiO_2 with large surface area and high crystallinity.” Appl. Surf. Sci. 256 (2010) : 3740-3745.

[74] W.Y.Teoh, R.Amal, L. Madler, and S.E. Pratsinis. “Flame sparyed visible light-active Fe-TiO_2 for photomineralisation of oxalic acid.” Catal. Today 120 (2007) : 203-213.

[75] G.L. Chiarello, L. Forni, and E.Selli. “Photocatalytic hydrogen production by liquid- and gas-phase reforming of CH_2OH over flame-made TiO_2 and Au/TiO_2 .” Catal. Today 144 (2009) : 69-74.

[76] H. Chang, S.J. Kim, H.D. Jang, and J.W. Choi. “Synthetic routes for titania nanoparticles in the flame spray pyrolysis.” Colloid Surf. 313-314 (2008) : 282-287.

[77] O. Mekasuwandumrong, S. Phothakwanpracha, B.Jongsomjit, A. Shotipruk, and J.Panpranot, Powd. “Inflience of flame condition on the dispersion of PD on the flame spray-derived PD/TiO_2 nanoparticles.” Technol. 210 (2011) : 328-331.

[78] V.R. Gonzalez, R. Zanella, G.D. Angel, and R. Gomez. “MTBE visible-light photocatalytic decomposition over Au/TiO_2 and Au/TiO_2-Al_2O_3 sol-gel prepared catalysts.” J. Mol. Catal. 281 (2008) : 93-98.

[79] T. Puangpetch, S. Chavadej, and T. Sreethawong. “Hydrogen production over Au-loaded mesoporous-assembled $SrTiO_3$ nanocrytal photocatalyst: Effects of molecular structure and chemical properties of hole scavengers.” Energy Convers. Manage. 52 (2011) : 2256-2261.

[80] X. Lin, F. Rong, D. Fu and C. Yuan. “Enhanced photocatalytic activity of fluorine doped TiO2 by loaded with Ag for degradation of organic pollutants.” Powder Techno. 219 (2012) : 173-178.

APPENDIX

APPENDIX A

CALCULATION FOR PHOTOCATALYST PREPARATION

Table A.1 Chemical Properties

Chemicals	Molecular weight	Purity (wt.%)	Density (g/cm^3)
TiO_2	79.87	100	3.83
Au	196.97	100	-
TIPT	284.25	98	0.96
$HAuCl_4.3H_2O$	393.83	49 (Au Basis)	-

A.1 Calculation of Au modified by incipient impregnation

Preparation of Au modified by incipient impregnation method is shown as follows:

Reagent: Au

Support: TiO_2

Example: Calculation for the preparation of $0.26Au/TiO_2$ photocatalyst with $HAuCl_4.3H_2O$ as Au precursor

For 2 g of TiO_2 based photocatalyst

Au required = $2 \times (0.26/100)$ = 5.2×10^{-3} g

Thus, Au 5.2×10^{-3} g was prepared from $HAuCl_4.3H_2O$

Au metal 49 g in $HAuCl_4.3H_2O$ 100 g

For 5.2×10^{-3} g of Au metal

$HAuCl_4.3H_2O$ = $5.2 \times 10^{-3} \times (100/49)$ = 0.0106 g

A.2 Calculation of TiO_2 based photocatalyst prepared by flame spray pyrolysis

0.3 M solution was used as precursor for TiO_2 preparation by flame spray pyrolysis is shown as follows:

Example: Calculation for the preparation of the TiO_2 photocatalysts, TIPT were used as precursor and diluted with xylene to a 0.3 M solution.

Based on 0.3 M solution of Ti concentration will be as follows:
Basis 500 ml precursor solution 0.3 M:

$$\text{mol Ti} = 500 \text{ ml l} \frac{0.3 \text{ mol Ti}}{1000 \text{ ml}} = 0.15 \text{ mol Ti}$$

$$\text{TIPT} = 0.15 \text{ mol Ti} \times \frac{1 \text{ mol TIPT}}{1 \text{ mol Ti}} \times \frac{284.25 \text{ g TIPT}}{1 \text{ mol TIPT}} \times \frac{1 \text{ ml TIPT}}{0.96 \text{ g TIPT}} = 44.41 \text{ ml TIPT}$$

APPENDIX B

APPENDIX B

CALCULATION OF THE CRYSTALLITE SIZE

Calculation of the crystallite size by Debye-Scherrer equation

The crystallite size was calculated from the half-height width of the diffraction peak of XRD pattern using the Debye-Scherrer equation.

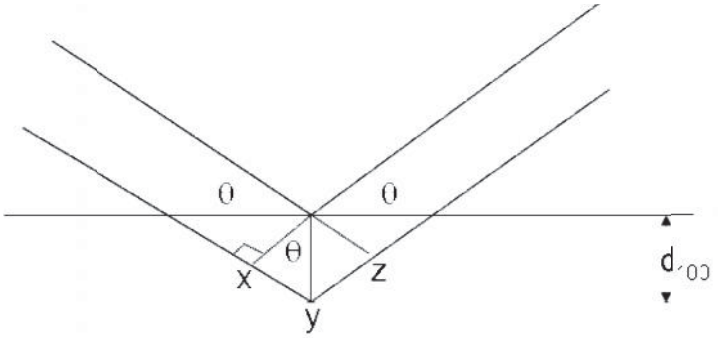

Figure B.1 Derivation of Bragg's Law for X-ray diffraction

$$xy = yz = d\sin\theta$$

Thus $xyz = 2d\sin\theta$

But $xyz = n\lambda$

Therefore $2d\sin\theta = n\lambda$ *Bragg's Law*

$$d = \frac{n\lambda}{2\sin\theta}$$

The Bragg's Law was derived to B.1

From Scherrer equation:

$$D = \frac{K\lambda}{\beta\cos\theta}$$

Where D = Crystallite size, Å

K = Crystallite-shape factor = 0.89

λ = X-ray wavelength, 1.5418 Å for CuKα

θ = Observed peak angle, degree

β = Full-Width at Half-Maximum (FWHM), radian

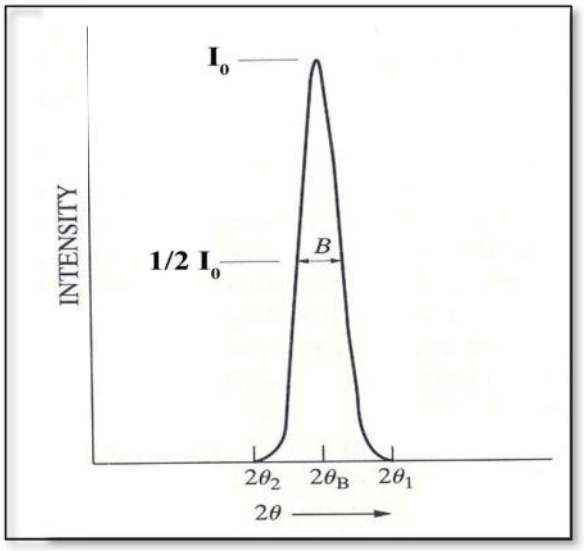

Figure B.2 The determining of the FWHM value of XRD line broadening

APPENDIX C

APPENDIX C

CALCULATION FOR TOTAL H_2 CHEMISORPTION AND DISPERSION

Calculation of the total H_2 chemisorption and metal dispersion of the catalyst, a stoischiometry of H_2 : Au = 1 : 2, is assumed. The calculation procedure is as follows:

Let the weight of photocatalyst used	=	W	g
Let the wt% of Au in photocatalyst used	=	X	g
Integral area of H_2 peak after adsorption	=	A	unit
Integral area of 100 µl of standard H_2 peak	=	B	unit
Amounts of H_2 adsorbed on photocatalyst	=	B-A	unit
Concentration of Au	=	0.26	wt.%
Volume of H_2 adsorbed on photocatalyst	=	100 × [(B-A)/B]	µl
Volume of 1 µmole of H_2 at 30 °C	=	24.88	µl
Mole of H_2 adsorbed on photocatalyst	=	[(B-A)/B]×[100/24.88]	µmole
Total hydrogen chemisorption	=	[(B-A)/B]×[100/24.88]×[1/W]	µmole /$g_{catalyst}$
	=	N	µmole /$g_{catalyst}$

$$\%\text{Au dispersion} = \frac{\text{The amount of Au equirvalent to } H_2 \text{ adsorption}}{\text{Total amount of Au loading}}$$

Molecular weight of Au = 196.97 $g.mol^{-1}$

Metal dispersion (%) $= \frac{2\times N\times 10^{-6}\times 100}{(X\times W)/196.97}$

$= \frac{(3.94\times 10^{-2})N}{X\times W}$

APPENDIX D

APPENDIX D

CALCULATION OF PHOTOCATALYTIC H_2 PRODUCTION RATE

The photocatalytic performance was evaluated in terms of photocatalytic H_2 production rate.

Photocatalytic H_2 production rate was calculated as follows:

Let the weight of photocatalyst used = *W* *g*

Flow rate of Ar carrier = *30* *ml/min*

Volume of sample gas = *5* *ml*

Amount of H_2 was determined from calibration curve in figure D.1 = *A* *µmol*

Which area of H_2 obtained from computer program based plot on TCD (GC-14B).

∴ *H_2 production rate (µmol / h .g of catalyst)*

$$= \frac{A\ \mu mol}{W\ g_{catalyst}} \times \frac{30\ ml.min^{-1}}{5\ ml} \times \frac{60\ min}{1\ h}$$

$$= \frac{360 \times A}{W} \quad \mu mol\ H_2.h^{-1}.g^{-1}_{catalyst}$$

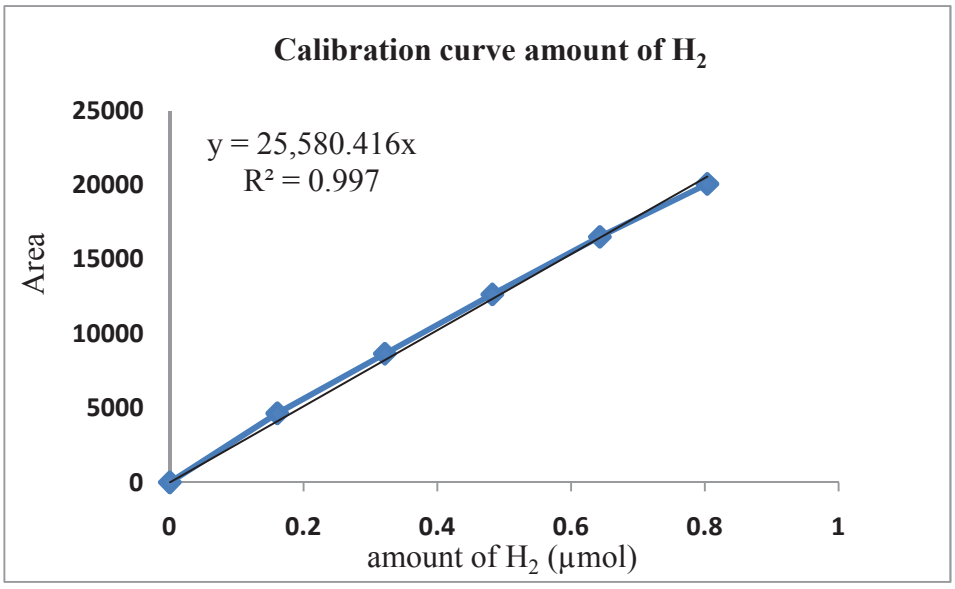

Figure D.1 Calibration curve of amount of H_2

APPENDIX E

APPENDIX E

INTERNATIONAL PROCEEDING

Karnanpus Dangsakol and Tarawipa Puangpetch

"Preparation method and characterization of Au modified TiO_2 for photocatalytic H_2 production with simulated solar energy", Paccon 2012, Pure and Applied Chemistry International Conference, Thailand, 11-13 Jan, 2012 (poster presentation)

BIOGRAPHY

Name-Family name	Mr. Karnnapus Dangsakol
Birthd	December 19, 1986 in Chumphon, Thailand.
Address	132 Subanan District, Thasae Amphur, Chumphon Province, Thailand, 86140.

Education Background

2009	received the bachelor degree of Chemical Engineering, Faculty of Engineering and Industrial Technology, Silpakorn University, Nakhon Phathom, Thailand.
2011	further studied in the master degree of Engineering, Department of Chemical Engineering, Graduate School, Silpakorn University, Thailand.

Special Interest Nanoparticle /Heterogeneous Catalysis/Renewable Energy